© Copyright 2017

Ryan J. Davis

Regulation of Substrate Degradation and Cancer Metabolism by the Fbw7 Ubiquitin Ligase

Ryan J. Davis

A dissertation

submitted in partial fulfillment of the

requirements for the degree of

Doctor of Philosophy

University of Washington

2017

Reading Committee:

Bruce E. Clurman, Chair

David M. Hockenbery

Sue Biggins

Program Authorized to Offer Degree:

Molecular and Cellular Biology

University of Washington

Abstract

Regulation of Substrate Degradation and Cancer Metabolism by the Fbw7 Ubiquitin Ligase

Ryan J. Davis

Chair of the Supervisory Committee:
Dr. Bruce E. Clurman, M.D., Ph.D.
Member, Divisions of Clinical Research and Human Biology
Fred Hutchinson Cancer Research Center
Professor of Medicine
University of Washington

Fbw7 is the substrate binding subunit of an SCF E3 ubiquitin ligase, which catalyzes the polyubiquitylation of substrates, initiating their recognition and degradation by the proteasome. The affinity of Fbw7 for its substrates is substantially increased following substrate phosphorylation at specific amino acids within short, linear sequences termed Cdc4 phosphodegrons (CPDs). Thus, regulation of substrate phosphorylation is a significant determinant of the contexts in which Fbw7 substrates will be degraded. Fbw7 is also a *bona-fide* tumor suppressor that is frequently mutated in human cancers; accordingly, many of Fbw7's substrates are potent oncoproteins. It is through the deregulation of substrate degradation that Fbw7 mutations exert their oncogenic effects. For my dissertation, I studied two aspects of Fbw7

biology: the regulation of substrate CPD phosphorylation and the biologic consequences of Fbw7 inactivation in colorectal cancers.

Cyclin E-CDK2 is an important regulator of the G1/S transition in the cell cycle, and cyclin E is also an Fbw7 substrate. Phosphorylation of cyclin E at serine 384 (S384) is the critical switch that enables high-affinity binding of Fbw7. Interestingly, S384 can only be autophosphorylated by the bound CDK2 molecule in *cis*; thus, cyclin E instigates its own degradation. We found that the PP2A-B56 phosphatase specifically opposes autophosphorylation of cyclin E at S384, and this dephosphorylation stabilizes catalytically active cyclin E-CDK2 complexes at the G1/S transition. siRNA-mediated depletion of PP2A-B56 is sufficient to decrease cyclin E kinase activity and shorten its half-life, which is consistent with the increased degradation of the catalytically active pool of cyclin E. Moreover, the phosphatase activity towards S384 is high in interphase but low in prometaphase. This likely provides a failsafe mechanism to ensure the complete degradation of cyclin E in mitosis, which is necessary for error-free chromosome segregation. Therefore, the dephosphorylation of cyclin E specifically at S384 is a critical regulator of its degradation by Fbw7 during the cell cycle.

A comprehensive understanding of the changes in cellular function that result from Fbw7 mutations in tumors is an ongoing area of investigation. This is due in part to Fbw7's large network of substrates that together regulate many biological functions. To better understand the consequences of Fbw7 mutations in human colorectal cancers, we applied novel computational approaches to analyze colorectal cancer gene expression datasets. These analyses identified altered cellular metabolism and mitochondrial function as important and conserved consequences of Fbw7 mutations. This computational prediction was validated using targeted gene expression assays and functional studies of cellular metabolism, and also revealed deregulated nucleotide

biosynthesis in Fbw7-mutant cells. Accordingly, $Fbw7^{-/-}$ cells were hypersensitive to both genetic and small-molecule inhibition of DHODH, an enzyme in the pyrimidine biosynthetic pathway. These experiments suggest that the metabolic deregulation present in Fbw7-mutant cancers could lead to specific vulnerabilities that can be therapeutically targeted.

Together, these studies have provided new and important insights into Fbw7 biology. Fbw7 has critical functions in normal cells, including organismal development, differentiation, and stem cell maintenance; conversely, inactivating mutations in Fbw7 are frequently selected for in neoplastic cells. A complete understanding of the Fbw7 pathway—from the regulation of its molecular interactions to the changes in cellular processes observed in cancers—will be critical to fully understand the importance of Fbw7 in cellular physiology, with the ultimate goal of developing new approaches to treating human disease.

TABLE OF CONTENTS

LIST OF FIGURES

LIST OF TABLES

ACKNOWLEDGEMENTS

To all of the people who have helped me along the way:

To Dr. Bruce Clurman, my graduate advisor and mentor. Your scientific rigor and motivation to tackle important questions—even when they are challenging to answer—has shaped my journey towards becoming an independent scientist. You provided me the freedom to pursue the offshoots I found interesting, even when it meant I got lost in the weeds. You have expanded my skills beyond the bench and helped me become a better scientific communicator and mentor. It has been a privilege to spend this time learning science from you.

To each member of my thesis committee: Drs. Sue Biggins, Jon Cooper, David Hockenbery, and Jim Roberts. You have challenged and supported me throughout my time here. I especially want to thank both Sue and David for reading my thesis, and David for all your scientific guidance.

To the scientists who shaped me before embarking on a PhD: Drs. Moses Lee and Jeff MacKeigan, and all of my professors at Hope College. You not only gave me an excellent foundation in science, but also challenged me to achieve things I otherwise never would have attempted.

To everyone I have worked alongside in the Clurman Lab, especially Drs. Markus Welcker, Jon Grim, and Bridget Hughes. You provided me daily support, knowledge, and feedback; helped me think through the challenging aspects of my work; and provided the encouragement to just keep pushing, even when things seemed most difficult.

To each of my MCB classmates, who are some of my best friends and were there for every step of this journey. And to all of the other friends—from Hope College to Seattle—that I

have found along the way. You have made my life so much richer and, in many ways, you have helped me to see the bigger picture of science and life.

To my family, without whom, none of this would have been possible. To my parents: James and Rosanne Davis. You have always given me encouragement, love, and guidance. You were my first teachers and mentors, and from my earliest days you modeled the value of hard work and the importance of not only setting goals, but also achieving them. I can't thank you enough for supporting me wherever I go. To my grandparents: Joyce and Lester Baker and Jim and Donna Doti. You helped provide the foundation for my life. I must especially acknowledge Nano—the first scientist I ever knew and the man who taught me perseverance in a way few others have. To my sister, Anna, for being a great friend and confidant at all times and Garrison, for being the best faux-bro I could hope for. Looking back, I can't imagine how I could have chosen anywhere but Seattle to earn my PhD. And to my new family: Mark and Debbie, and Dan, Jenny, and Bradley. Thank you for all of your love and support.

And finally to my wife, Sara. This journey has been your journey as much as mine, and through it all you have stood by my side and walked this road with me. I can't thank you enough for your love, encouragement, support, laughter, and inspiration. You truly are *fantastic*.

DEDICATION

To Sara

Chapter 1. Introduction

Portions of this chapter were adapted from a published manuscript.

Ryan J. Davis, Markus Welcker, and Bruce E. Clurman. Tumor Suppression by the Fbw7 Ubiquitin Ligase: Mechanisms and Opportunities. *Cancer Cell* (2014) 3;26(4):455-64.

1.1 Ubiquitin-Proteasome System

The ubiquitin-proteasome system (UPS) is a highly conserved cellular pathway that utilizes the covalent attachment of the small protein ubiquitin to earmark substrate proteins for various outcomes. This process, termed ubiquitylation, relies on a cascade of three classes of proteins to ubiquitylate substrates: E1 ubiquitin activating enzymes, E2 ubiquitin conjugating enzymes, and E3 ubiquitin ligases (Figure 1.1). Substrates can be either mono- or polyubiquitylated at specific lysine residues, and these two parallel pathways result in distinct functional consequences. Ubiquitin-mediated proteolysis, or protein destruction, is instigated by the attachment of K48 polyubiquitin chains to substrates, which provides a signal for recognition and degradation by the proteasome (1). Importantly, ubiquitin-mediated proteolysis is highly regulated, rapid, and irreversible, and has particularly important roles in cell division, growth, and differentiation. Thus, protein degradation by the UPS controls a broad array of cellular processes (2).

1.2 SCF^{Fbw7} E3 Ubiquitin Ligase

In most cases, E3 ubiquitin ligases are needed to recognize substrates and facilitate their ubiquitylation. SCFs (Skp1, Cullin-1, F box protein) are a class of E3s that use Cullin-1 as a scaffold and F box proteins as substrate receptors and have important roles in cancer biology (3-

5). F box proteins are thus adaptors that bring substrates into proximity with ubiquitylation enzymes.

Fbw7 is an evolutionarily conserved F box protein, and studies of its orthologs (Cdc4, *S. cerevisiae*; sel-10, *C. elegans*; Archipelago, *Drosophila*) have yielded fundamental insights into SCF^{Fbw7} function. The human FBXW7 gene resides on chromosome 4q32, a region commonly deleted in cancers, and produces three mRNAs, each under their own transcriptional control (6). The three Fbw7 mRNAs encode three protein isoforms that differ only by isoform-specific N-terminal exons that specify subcellular localization: Fbw7α is nucleoplasmic, Fbw7β is cytoplasmic, and Fbw7γ is nucleolar (Figure 1.2). All isoforms share three important functional domains: (1) the D domain mediates Fbw7 dimerization, which regulates substrate binding modes and ubiquitylation, (2) the F box binds Skp1 and links Fbw7 to the SCF complex, and (3) the WD40 domain forms a β propeller that binds phosphorylated substrates (Figures 1.2 and 1.3) (7-12). Fbw7α is thought to perform most Fbw7 functions, although specific roles for the other isoforms have also been described (13-18).

Substrate phosphorylation instigates Fbw7 binding to a conserved Cdc4 phosphodegron (CPD) motif (19-22). Mutational and structural studies have provided insights into the interactions between CPDs and Fbw7's β propeller (7-9). CPDs contain multiple residues that contact Fbw7 and typically include phosphorylated threonine or serine residues in the ''0'' and ''+4'' positions that interact with Fbw7 phosphate-binding pockets (23). CPD affinity varies among substrates; high-affinity CPDs contain two phosphorylations and other optimal residues, whereas low-affinity substrates may contain a negatively charged amino acid in lieu of a second phosphate or other unfavorable residues (Figure 1.3) (7,11,20). Importantly, three arginine residues in Fbw7's WD40 domain interact with CPD phosphates and are mutational hot spots in

cancers, as discussed below.

Ultimately, the signaling pathways that mediate CPD phosphorylation regulate substrate degradation. The presence of two phosphorylation sites in most CPDs provides a mechanism through which multiple signals can control substrate degradation. Most substrates have multiple turnover pathways; therefore, the regulation of CPD phosphorylation determines the context of their degradation by SCF^{Fbw7}. Glycogen synthase kinase 3 (GSK3) phosphorylates the central position of many CPDs, and this is opposed by mitogen stimulation of the PI3K-AKT pathway, which inactivates GSK3 (23,24). It is likely that by coupling Fbw7-mediated degradation with GSK3 activity, mitogenic signaling can coordinately stabilize substrates with key roles in cell proliferation (e.g., Myc, cyclin E, and Jun). The abnormal AKT and PTEN activity commonly found in cancers might similarly allow oncogenic Fbw7 substrates to accumulate.

Fbw7 dimerization provides another important level of regulation. Because each protomer of an Fbw7 dimer contains a substrate-binding domain, dimers can simultaneously bind two CPDs, which is particularly important for substrates with degrons that are too weak to drive Fbw7 binding without cooperating CPDs (11). The combinatorial impact of multiple CPDs allows highly specific control of substrate ubiquitylation. Additionally, dimerization promotes substrate degradation by expanding the number of substrate lysine residues that are accessible for ubiquitin conjugation (7,9,11).

1.3 Fbw7 Substrates

SCF^{Fbw7} targets approximately two-dozen proteins with key roles in proliferation, differentiation, apoptosis, and metabolism (Figure 1.2). With few exceptions (e.g., cyclin E and MCL1), Fbw7 substrates are transcription factors (TFs) or transcriptional regulators that control complex gene-

expression programs; this extends Fbw7's impact far beyond its direct substrates. Below, we highlight only those substrates that are known oncoproteins or have emerging roles in tumorigenesis.

1.3.1 *Cyclin E*

Cyclin E, in conjunction with its catalytic partner cyclin-dependent kinase 2 (CDK2), regulates cell-cycle entry and progression. Cyclin E has long been implicated in carcinogenesis, and The Cancer Genome Atlas (TCGA) studies demonstrating frequent cyclin E amplifications in solid tumors (e.g., ovarian and breast) confirm its role as an oncogenic driver (25,26). Multisite phosphorylation of two well-defined CPDs regulates cyclin E stability and periodicity (6,15,19,21,22,27-29), and this is discussed more extensively in Chapter 2. Genome instability is a critical consequence of constitutive cyclin E-CDK2 activity during the cell cycle caused by its impaired degradation (14,30-35). This appears to be a central mechanism through which cyclin E drives carcinogenesis and is opposed by p53 activation (33).

1.3.2 *c-Myc*

c-Myc (hereafter called Myc) sustains gain-of-function mutations, including amplifications in solid tumors and translocations in hematologic malignancies. Myc deregulation promotes tumorigenesis largely through its transcriptional regulation of proliferation, protein synthesis, apoptosis, metabolism, and differentiation. Fbw7α mediates Myc ubiquitylation in the nucleoplasm, whereas Fbw7γ ubiquitylates Myc in the nucleolus, which inhibits Myc's ability to promote cell growth (13,15,18,36,37). Early work found that phosphorylation of the threonine 58 (T58) CPD stimulates Myc degradation (38,39), and this is now known to be mediated by Fbw7. The T58 region is targeted by missense mutations in lymphomas, suggesting a crucial role for

impaired Myc degradation by Fbw7 (40,41). This has been confirmed in mouse models (see below). N-Myc also contains the T58 CPD and is commonly amplified in cancers (e.g., neuroblastoma), but the significance of its degradation by Fbw7 is less well understood.

1.3.3 *Notch*

Notch proteins are transcriptional regulators of cell fate and differentiation that are broadly implicated in human cancers; they are typically dominant oncogenes, although they can be tumor suppressive in some cancers. All four Notch paralogs contain motifs homologous with the Notch1 CPD, but most studies have focused on Notch1 (42-47). Notch1 is processed by a series of proteolytic cleavages, and the transcriptionally active Notch1 intracellular domain (NICD) is ubiquitylated by SCF^{Fbw7}. Activating Notch1 mutations occur in approximately 50% of T cell acute lymphoblastic lymphomas (T-ALLs) and often target the PEST domain, which contains the Fbw7 CPD (48). Fbw7 mutations are also common in T-ALL and are mutually exclusive with Notch PEST mutations, underscoring the importance of Fbw7-dependent Notch degradation in this disease (44,46,49,50). Furthermore, Fbw7 mutations in T-ALL may confer resistance to Notch inhibition by γ-secretase inhibitors, which prevent Notch processing (44).

1.3.4 *Additional Fbw7 substrates*

In addition to Myc, Notch, and cyclin E, additional Fbw7 with important roles in both normal cell biology and tumorigenesis have been described. c-Jun (hereafter called Jun) is a component of the AP-1 TF and has essential roles in mitogen-stimulated cell proliferation. Jun overexpression is common in cancers and is thought to drive oncogenesis; this is supported by the finding of Jun amplifications in some human cancers, such as liposarcomas. Two different Jun CPDs have been described, one of which is mutated in the v-Jun retroviral oncogene

(51,52). Myeloid Cell Leukemia 1 (MCL1) is an antiapoptotic protein that is overexpressed in cancers, and its stabilization in tumors with Fbw7 mutations causes resistance to chemotherapy (53,54). MED13/13L is the component of the Mediator transcriptional coactivator complex that recruits CDK8, an oncogene amplified in colorectal cancer (55). Because Mediator is required for all transcription and CDK8 regulates specific oncogenic transcriptional programs, MED13 degradation may greatly expand Fbw7's role in global transcriptional control. PPARγ Coactivator-1α (PGC-1α) is a transcriptional coactivator that coordinates mitochondrial biogenesis and cellular energetics and has an expanding role in tumorigenesis (56). Similar to Notch, Kruppel-Like Factor 5 (KLF5) and CCAAT/Enhancer Binding Protein Delta (C/EBPδ) have either oncogenic or tumor-suppressive functions in different cancers (57-59). TGIF1 is a transcriptional repressor that inhibits transforming growth factor β signaling, a crucial oncogenic pathway (60). Additional oncoproteins have been reported to be Fbw7 substrates, but either they lack consensus CPDs or the contexts of their regulation by Fbw7 requires further confirmation (e.g., Hif1α, mTOR, Aurora kinase A, and Myb) (61).

1.4 Fbw7 and Tumorigenesis

1.4.1 *Fbw7 mutations in human cancers*

Because many of Fbw7's first reported substrates were potent oncoproteins, its role as a tumor suppressor was quickly evaluated and confirmed. Early studies showed that 6%–10% of colorectal carcinomas contain Fbw7 mutations, and subsequent work revealed Fbw7 mutations in a wide range of organ sites, including a high prevalence in T-ALL and cholangiocarcinoma (23,62). These studies revealed a high frequency of heterozygous missense mutations of the three

Fbw7 arginine residues that bind CPD phosphates (R465, R479, and R505), hereafter called Fbw7^{ARG}. Because these residues make the most critical contacts with the CPD phosphates and are absolutely required for high-affinity Fbw7-substrate interactions (7-9), Fbw7^{ARG} mutations have a uniquely profound impact on substrate-binding affinity compared with other missense mutations. Moreover, Fbw7 dimers, which have increased substrate affinity, tolerate many missense mutations that disable monomers. Fbw7 dimerization thus greatly restricts the repertoire of deleterious Fbw7 missense mutations to only these most stringent positions (11). There are many possible mutations that could produce either Fbw7 null alleles or truncated proteins, but they occur much less commonly than Fbw7^{ARG} mutations. The strong biologic selection of Fbw7^{ARG} mutations suggests that they are not simple loss-of-function alleles and is most consistent with dominant-negative alleles, which has been confirmed in mouse models, as discussed below.

TCGA studies have provided a wealth of mutational and expression data for different cancers (63-65). Although large-scale studies of T-ALL are still in progress, previous work indicates that T-ALL represents a special example of Fbw7-associated cancer with mutations in up to 30% of cases (Table 1.1) (44,46,49,50). Fbw7 is significantly mutated (>10% of samples) in at least five tumor types: T-ALL, colorectal adenocarcinoma, uterine carcinosarcoma, uterine endometrial carcinoma, and bladder carcinoma. Other cancers with somewhat less frequent Fbw7 mutations include stomach adenocarcinoma, lung squamous cell carcinoma, cervical squamous cell carcinoma, and head and neck squamous cell carcinoma (Table 1.2). In contrast, Fbw7 mutations are not found in some cancers, such as acute myeloid leukemia (AML) and multiple myeloma. One possibility is that Fbw7 substrate stabilization is detrimental in these neoplasms. For example, the Fbw7 substrate C/EBPα suppresses AML (66), and multiple

myelomas require constitutive NF-κB signaling; therefore, disruption of Fbw7-mediated NF-κB2 ubiquitylation in these tumors results in cell death (67). Despite extensive studies, the prognostic significance of Fbw7 mutations in cancer remains uncertain. For example, whereas TCGA Pan-Cancer analyses found Fbw7 mutations to be detrimental across multiple tissue types (65), the colorectal-specific TCGA study found no overlap between Fbw7 mutations and distant metastases, suggesting that mutations could be beneficial. Analogous studies of Fbw7 mutations in T-ALL have similarly yielded conflicting results.

We performed a meta-analysis of TCGA data using the cBioPortal for Cancer Genomics online interface to compare and contrast Fbw7 mutations across cancer types (68,69). These results are based upon data generated in whole by the TCGA Research Network (http://cancergenome.nih.gov/) and confirm the striking skewing toward $Fbw7^{ARG}$ mutations, particularly in organ sites where Fbw7 is most frequently mutated (Table 1.2). Importantly, most tumors with $Fbw7^{ARG}$ mutations retain a normal second Fbw7 allele. This notably contrasts with the ‘‘two-hit’’ mutation pattern of some tumor suppressors. However, nonsense mutations (sometimes in combination with allelic loss) and homozygous null mutations are found in some tumors; thus, Fbw7 exhibits classic tumor-suppressor features in these cases. The frequency and types of Fbw7 mutations vary among organ sites. For example, colorectal cancers contain the entire spectrum of Fbw7 mutations (deletions and missense and nonsense mutations), whereas others, such as T-ALLs, exhibit nearly 100% heterozygous $Fbw7^{ARG}$ mutations. This suggests that distinct Fbw7 mutations produce unique biologic outcomes, presumably through differential effects on specific substrates (see below).

Instead of mutations in Fbw7 itself, some cancers contain substrate CPD mutations that prevent their ubiquitylation, including Myc CPD mutations in Burkitt’s lymphoma, Notch PEST

mutations in T-ALL, and a KLF5 CPD mutation in colon cancer (40,41,48,70). This suggests particularly important roles for these substrates in specific tumors. However, the paucity of single-substrate CPD mutations compared with Fbw7 mutations suggests that in most cases, Fbw7-associated tumorigenesis requires the concurrent deregulation of multiple oncoproteins.

1.4.2 *Additional mechanisms of Fbw7 disruption in cancer*

Mechanisms other than mutations and allelic loss also impair Fbw7 function in cancers. Fbw7 is targeted by oncogenic micro-RNAs such as miR-27, miR-92, and miR-223 in numerous cancers (71,72). Promoter hypermethylation downregulates Fbw7β expression in breast cancers and thymomas (73,74), and Fbw7 mRNA is also repressed in melanomas and gliomas, although the underlying mechanisms are not known (75,76). Fbw7β is a p53 target gene; therefore, p53 mutations may reduce Fbw7 expression (77). Two Fbw7 substrates feed back to control Fbw7 mRNA expression: C/EBPδ, which may contribute to mammary tumor metastasis (57), and Hes5 (a Notch target gene) (78). Many studies have examined low Fbw7 mRNA expression in tumors as a biomarker, which generally appears to be a high-risk feature.

Fbw7 protein stability is another regulatory mechanism that has been examined in tumors. One example is Fbw7β degradation by Parkin, which subsequently inhibits MCL-1 degradation (14). It has also been suggested that Pin1 overexpression in cancers destabilizes Fbw7 by directly generating Fbw7 monomers that are targeted for degradation through enhanced autoubiquitylation (79). However, two other studies have disputed these findings (11,80).

1.5 Mouse Models of Fbw7-Associated Cancer

Germline Fbw7 deletion in mice causes embryonic lethality (81,82). Therefore, conditional

strains have been used to study Fbw7 in normal tissues and during tumorigenesis. Mice with knockin mutations that ablate the cyclin E degrons (hereafter termed cyclin $E^{\Delta CPD}$) have also been used to specifically study impaired cyclin E degradation. These models have convincingly demonstrated that (1) FBXW7 is a bona fide tumor suppressor gene, (2) $Fbw7^{ARG}$ mutations have unique functional consequences, (3) specific Fbw7 substrates contribute to tumorigenesis, and (4) multiple oncogenic pathways cooperate with Fbw7 mutations.

1.5.1 *Fbw7 regulates stem cells, differentiation, and genome stability*

Studies of normal tissues have provided valuable insights into pathways that are also important for tumorigenesis. Fbw7 loss profoundly affects differentiation and proliferation in stem and progenitor cell types, often through similar mechanisms. For example, in neural stem cells and intestinal crypt progenitor cells, loss of Fbw7 leads to increased proliferation and differentiation defects through the combined actions of Jun and Notch, respectively (83-85). Similarly, aberrant Notch activity causes differentiation defects in hepatocytes (86). Novel TF substrates may mediate differentiation phenotypes in other tissues. For example, Fbw7 loss reprograms pancreatic ductal cells toward endocrine lineages by stabilizing Ngn3 (85).

Fbw7 also controls hematopoietic stem cell (HSC) quiescence and self-renewal (87,88). HSCs are quickly exhausted after Fbw7 deletion, largely because of the detrimental effects of Myc overexpression on proliferation and apoptosis, although impaired cyclin E degradation also causes defective HSC self-renewal after hematologic stress (89,90). Importantly, $Fbw7^{ARG/+}$ HSCs have intermediate Myc abundance compared with $Fbw7^{-/-}$ and $Fbw7^{+/+}$ HSCs, and they do not exhibit these phenotypes—suggesting a unique role for heterozygous $Fbw7^{ARG}$ alleles and dose-dependent Myc effects in preserving HSC function (91).

These phenotypes have also been studied in cyclin $E^{\Delta CPD}$ mice to isolate cyclin E from

other substrates affected by Fbw7 mutations. Impaired cyclin E degradation causes epithelial cell hyperproliferation, abnormal cell-cycle control, impaired erythroid differentiation, and genome instability (28,31).

1.5.2 *Colorectal cancer*

Although Fbw7 mutations are found in early stage human colon adenomas (35), its deletion from the mouse gut is not sufficient to cause neoplasia. However, loss of Fbw7 in mice collaborates with other mutations commonly found in human colorectal cancer (CRC), including APC^{Min} alleles (which mimic the WNT pathway activation seen in nearly all human CRC) and p53 loss. When combined with APC^{Min}, both $Fbw7^{-/-}$ and $Fbw7^{ARG/+}$ mutations decreased tumor latency and increased tumor burden (92-94). However, these neoplasms did not progress beyond the adenoma stage and were neither invasive nor metastatic. $Fbw7^{ARG/+}$ mice exhibited increased tumorigenesis compared with $Fbw7^{+/-}$ animals, confirming that $Fbw7^{ARG}$ is not simply a null allele (93). TGIF1 and KLF5 were elevated in $Fbw7^{ARG/+}$, but not $Fbw7^{+/-}$, tumors (93); thus, these proteins may similarly contribute to Fbw7-associated human CRC and could represent examples of substrate-specific consequences of $Fbw7^{ARG/+}$ mutations. In $Fbw7^{-/-}$ tumors, Jun and Notch abundance was increased, and concurrent Jun deletion decreased tumor size (94).

In a second approach, p53 and Fbw7 were codeleted from the mouse gut, which caused advanced adenocarcinomas that were highly invasive and metastatic (83). In accordance with the findings that p53 suppresses cyclin-E-induced genomic instability caused by Fbw7 loss, these adenocarcinomas exhibited a chromosomal instability (CIN) phenotype, which is the most common form of genome instability in human CRC but is rare in mouse tumors.

1.5.3 *Hematologic cancers*

Unlike CRC, Fbw7 deletion in either T cells or HSCs is sufficient to cause T-ALL, and this is accelerated by concurrent p53 loss, PTEN loss, or Notch activation (87,88,91,95,96). The specific roles of $Fbw7^{ARG}$ alleles in leukemogenesis and leukemia-initiating cells (LICs), rare cells with stem-cell-like properties (e.g., self-renewal and quiescence) and important roles in disease propagation and resistance to therapy, have also been studied (91). $Fbw7^{ARG/+}$ mice did not develop spontaneous T-ALL, demonstrating another example of the differences between Fbw7 missense and homozygous null mutations. However, the $Fbw7^{ARG/+}$ mutation strongly cooperated with Notch deregulation to drive T-ALL and resulted in LIC expansion that is largely attributable to increased Myc abundance. Genetic or pharmacologic Myc inhibition depleted LICs in this model, demonstrating an essential role for Myc, although this occurs independently of Fbw7 mutational status. These data suggest that Myc abundance in $Fbw7^{ARG/+}$ cells is finely tuned such that it does not affect HSC maintenance while still being sufficiently elevated to achieve tumorigenic effects in LICs. This may, in part, explain the high prevalence of $Fbw7^{ARG}$ mutations in T-ALL. While Myc and Notch are clearly key players in Fbw7-associated T-ALL, cyclin $E^{\Delta CPD}$ mice also developed T cell malignancies that exhibited CIN (90), which is not seen in $Fbw7^{ARG/+}$ T-ALL. Different lesions in the Fbw7 pathway may thus lead to T-ALL through different mechanisms. In addition to Fbw7-associated malignancies, mouse models have also shown that Fbw7 depletion induced apoptosis of chronic myeloid leukemia (CML) LICs and B cell lymphomas (71,97,98).

1.5.4 *Consequences of $Fbw7^{ARG}$ mutations in cancers*

Fbw7's mutational spectrum strongly suggests that $Fbw7^{ARG}$ alleles have dominant-negative activity. The mouse models described above confirm this idea and demonstrate that heterozygous

Fbw7^{ARG} mutations impact Fbw7 function intermediate to that caused by single allele loss and homozygous null mutations. The concept that this intermediate Fbw7 inactivation favors tumorigenesis has been termed the ‘‘just-enough’’ hypothesis (99), and the stabilization of Myc in Fbw7$^{ARG/+}$ HSCs to levels that favor leukemogenesis, but not apoptosis, most likely represents this mechanism (91). Two important aspects of Fbw7^{ARG} mutations remain poorly understood: (1) how do they produce dominant-negative effects, and (2) why are they so frequently selected for in tumors compared with nonsense and homozygous null mutations? To understand these issues, we believe it is crucial to consider Fbw7's mode of action as a dimer, which enhances substrate binding affinity by engaging multiple CPDs simultaneously (Figure 1.4A) (11). Because Fbw7^{ARG} can dimerize with wild-type Fbw7 and potentially produce impaired Fbw7^{WT}-Fbw7^{ARG} heterodimers (that contain only a single intact WD40 domain), we suggest that Fbw7^{ARG} proteins dominantly inhibit wild-type Fbw7 (Figure 1.4B). Fbw7^{WT}-Fbw7^{ARG} heterodimers may also have special properties that produce substrate-specific effects (23). While the ubiquitylation of low-affinity substrates depends upon both substrate-binding domains of an Fbw7^{WT}-Fbw7^{WT} dimer, other substrates may have enough binding affinity to be ubiquitylated by Fbw7^{WT}-Fbw7^{ARG} heterodimers that contain only a single substrate-binding domain (Figure 1.4B). Therefore, dimer-dependent substrate interactions might account for the selection of heterozygous Fbw7^{ARG} mutations in cancers by allowing Fbw7^{WT}-Fbw7^{ARG} heterodimers to target substrates whose degradation is permissive or advantageous for tumorigenesis, while sparing the oncoproteins that drive tumor formation. Finally, although truncated Fbw7 proteins that can dimerize with Fbw7^{WT} might similarly act as dominant negatives, these types of mutations are less common. We suggest that the selection for mutations that produce full-length Fbw7^{ARG} protein reflects important, yet undefined, roles for continued interactions between

substrates and a mutated, but full-length, Fbw7 protein (Figure 1.4C).

1.6 Thesis Goals

Fbw7 is frequently mutated in a number of human cancers; therefore, a more complete understanding of its biology could lead to mechanistic insights into tumorigenesis and potentially novel therapeutic strategies. This is challenging for a number of reasons, including the large number of Fbw7 substrates, the diverse biological processes that Fbw7 substrates cumulatively regulate, and an incomplete understanding of the mechanisms that control Fbw7-substrate interactions. To begin to address some of these gaps in knowledge, my thesis had two overarching goals. First, I wanted to better understand the mechanisms controlling how and when Fbw7 recognizes substrates for ubiquitylation. Second, the majority of Fbw7 substrates are transcription factors; therefore, I wanted to determine whether conserved patterns of transcriptional deregulation in Fbw7-mutant cancers could predict the biological phenotypes of these cells. Chapter 2 addresses the first question, where I present my work investigating the dephosphorylation of cyclin E CPDs by the PP2A-B56 phosphatase. The second aim, which addresses the biological consequences of Fbw7 mutations in tumors is discussed in Chapter 3. Here, we utilized novel computational analyses of TCGA datasets to discover that Fbw7-mutant colorectal cells are have altered cellular metabolism and are shifted towards oxidative metabolism. Together, these studies have reveled new understandings of Fbw7 biology and relevance to human disease.

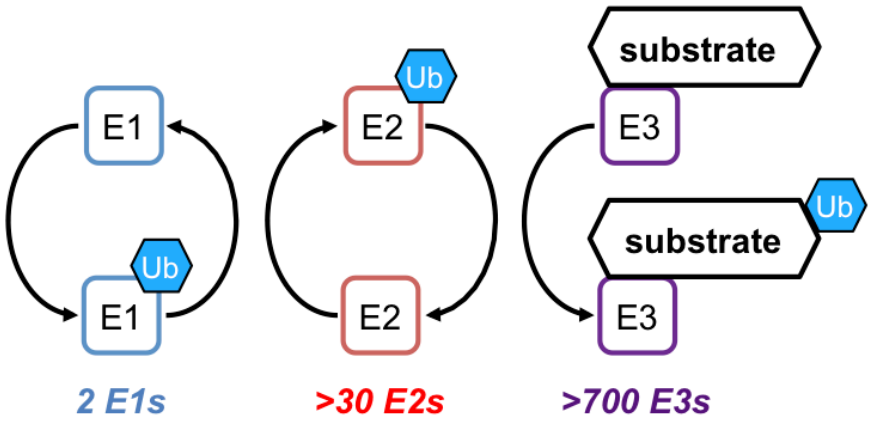

Figure 1.1. Overview of the ubiquitin-proteasome system.
The ubiquitin-proteasome system relies on a cascade of three enzymes to covalently link ubiquitin to target substrates. E1 enzymes are ubiquitin activating enzymes and serve to charge the ubiquitin that will be added to substrates. The charged ubiquitin is then transferred to an E2 ubiquitin conjugating enzyme that will covalently attach the ubiquitin to the substrate. Finally, E3 ubiquitin ligases serve as substrate specificity factors by binding directly to target proteins and bringing them in proximity to the rest of the ubiquitylation machinery. While the human genome encodes for only two E2s and approximately 30 E2 enzymes, there are more than 700 E3 enzymes, providing further evidence for these enzymes in the regulation of the UPS.

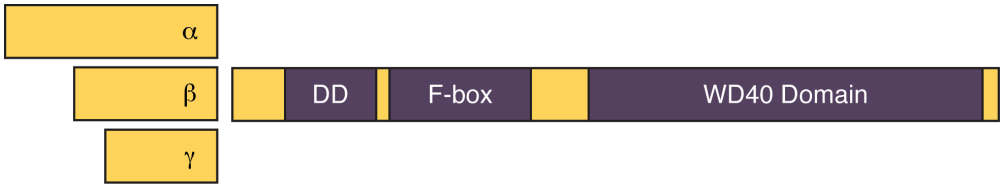

Figure 1.2. Conserved motifs of Fbw7 isoforms.
Fbw7 exists as three protein isoforms (α, β, and γ) that differ only by their N-terminal exons. All isoforms share three functional domains that are critical to their function as ubiquitin ligases: (1) the dimerization domain (‘‘DD’’) mediates Fbw7 dimerization, (2) the F box binds to the rest of the SCF complex via Skp1 (see Figure 1.3), and (3) the WD40 domain binds to phosphorylated substrates and includes the three arginine residues that are mutational hot spots in cancers.

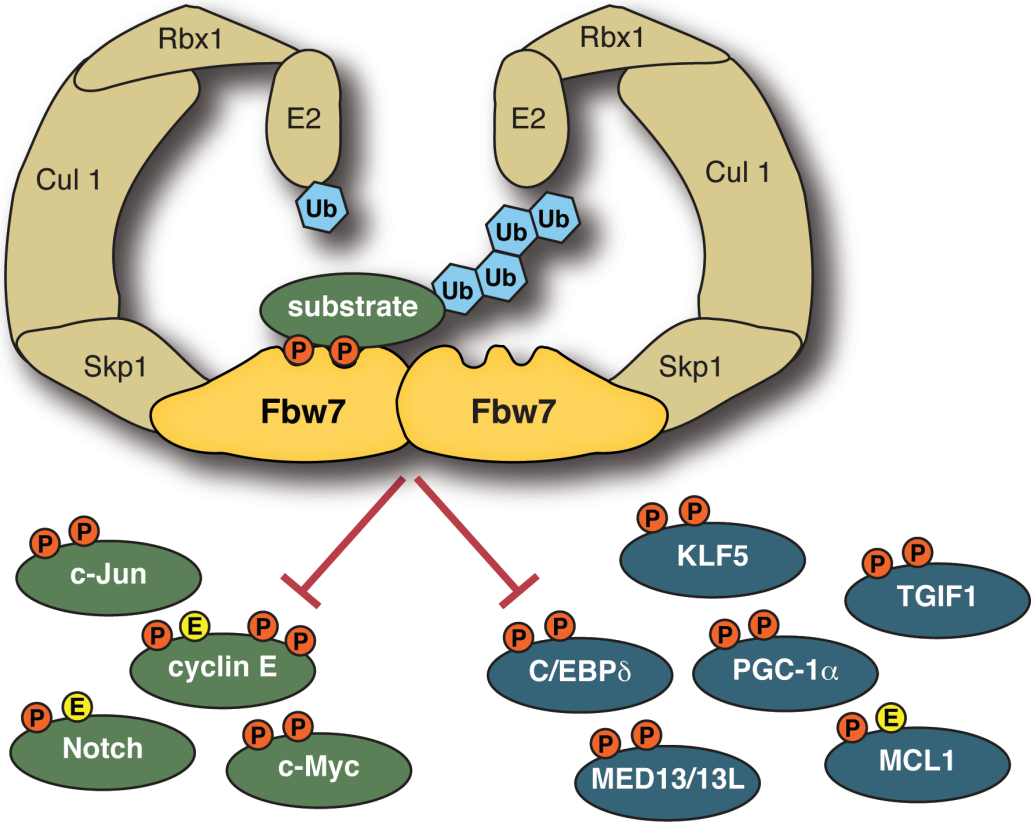

Figure 1.3. The SCF^{Fbw7} complex degrades numerous substrates implicated in cancer.
Fbw7 binds to both phosphorylated substrates and the rest of the SCF complex (comprised of Skp1, Cullin-1, Rbx1, and an E2 enzyme), resulting in substrate polyubiquitylation and degradation by the proteasome. The network of Fbw7 substrates contains proteins with clear roles in carcinogenesis (shown in green) and others with emerging roles in Fbw7-associated tumors (shown in blue). Optimal (high-affinity) substrates have recognition signals termed CPDs that contain two phosphorylated residues (orange ‘‘P’’); other, lower-affinity CPDs contain a negatively charged amino acid (yellow ‘‘E’’) in place of the second phosphate.

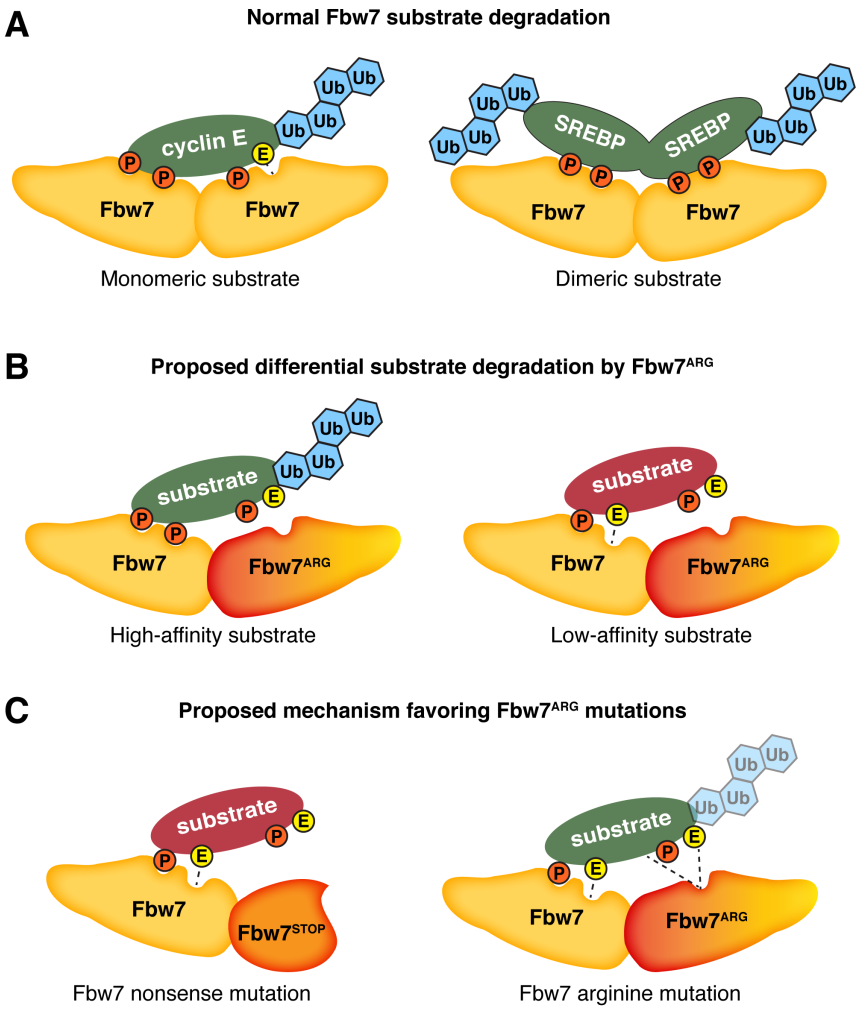

Figure 1.4. Possible mechanisms of Fbw7^{ARG} missense mutations in cancers.
(**A**) Normal interactions of Fbw7 dimers with monomeric (left) or dimeric (right) substrates. Each protomer within an Fbw7 dimer can interact with a separate substrate CPD, leading to greatly increased binding affinity between substrates and Fbw7. The two substrate CPDs can be present within a monomeric substrate (e.g., cyclin E; left) or separated onto two interacting proteins (e.g., SREBP; right). The reduced number of contacts made by suboptimal degrons is indicated by a dashed line. (**B**) Model of heterozygous Fbw7^{ARG} dominant-negative activity in cancers resulting from the formation of impaired Fbw7^{WT}-Fbw7^{ARG} heterodimers. We speculate that Fbw7^{WT}-Fbw7^{ARG} heterodimers differentially affect substrates, depending on CPD affinity. The degradation of high-affinity substrates may still be driven by the normal protomer of an Fbw7^{WT}-Fbw7^{ARG} heterodimer (left), whereas suboptimal substrates (depicted by glutamate instead of a second CPD phosphate) rely on the concerted binding of two CPDs to an Fbw7 dimer and will not be ubiquitylated by Fbw7^{WT}-Fbw7^{ARG} heterodimers (right). (**C**) Fbw7 truncation mutants may also generate heterodimers with Fbw7^{WT} but are not nearly as frequent in tumors as Fbw7^{ARG}. We therefore speculate that a full-length Fbw7 protein is critical for the dominant-negative effect of Fbw7^{ARG}, perhaps by retaining sufficient residual binding affinity (depicted by dashed line) for substrates with intermediate affinity.

Table 1.1. Fbw7 mutational frequency in T-ALL cell lines and patient samples

Study Reference	No. Samples	Source of cells	Fbw7 Mutations (%)	Arginine hotspot mutations/total point mutations
O'Neil et al., 2007	20	Cell lines	35%	85.7%
	7	Primary samples	100%	100%
Maser et al., 2007	23	Cell lines	48%	81.8%
	38	Primary samples	29%	72.7%
Thompson et al., 2007	89	Primary samples	16.8%	100%
Malyukova et al., 2007	15	Cell lines	33.3%	100%
	26	Primary samples	30.8%	87.5%

Table 1.2. Fbw7 mutational frequency in selected human cancers

Tumor Type	No. Samples	Arginine hotspot mutations	Nonsense mutations	Other missense mutations	All point mutations	Arginine hotspot mutations/total point mutations	Homozy-gous deletions
Uterine Cacinosarcoma	56	23.2%	3.6%	14.3%	39.3%	59.1%	0.0%
Colon and rectal adenocarcinoma	212	8.0%	3.3%	6.1%	16.5%	48.6%	0.0%
Uterine corpus endometrial carcinoma	240	5.8%	3.3%	7.9%	15.8%	36.8%	0.0%
Stomach adenocarcinoma	219	4.6%	1.8%	2.3%	8.7%	58.8%	0.5%
Urothelial bladder carcinoma	127	3.1%	4.7%	3.9%	9.4%	33.3%	2.4%
Lung squamous cell carcinoma	178	2.2%	2.2%	1.7%	6.2%	36.4%	0.6%
Head and neck squamous cell carcinoma	302	1.7%	0.7%	3.0%	5.0%	33.3%	1.3%
Cutaneous melanoma	262	0.4%	1.1%	2.7%	4.2%	9.1%	0.8%
Breast cancer	962	0.3%	0.2%	1.0%	1.6%	20%	0.6%
Cervical squamous adenocarcinoma	36	0.0%	2.8%	2.8%	5.6%	0%	0.0%
Lung adenocarcinoma	230	0.0%	1.3%	0.4%	1.7%	0%	0.0%
Glioblastoma multiforme	281	0.0%	0.4%	0.0%	0.4%	0%	0.4%

Chapter 2. The PP2A-B56 Phosphatase Opposes Cyclin E Autocatalytic Degradation via Site-Specific Dephosphorylation

This chapter was adapted from a manuscript published in *Molecular and Cellular Biology*.

Ryan J. Davis[1, 2], Jherek Swanger[1], Bridget T. Hughes[1], and Bruce E. Clurman[1]

[1]Divisions of Human Biology and Clinical Research, Fred Hutchinson Cancer Research Center, Seattle, WA, 98109, USA
[2]Molecular and Cellular Biology Program, University of Washington, Seattle, WA, 98195, USA

2.1 Abstract

Multiple mechanisms control cyclin E–CDK2 activity during the cell cycle, including phosphorylation-dependent cyclin E ubiquitylation by the SCF^{Fbw7} ubiquitin ligase. Serine 384 (S384) is the critical cyclin E phosphorylation site that stimulates Fbw7 binding and subsequent cyclin E degradation. Because S384 is autophosphorylated by CDK2, cyclin E therefore instigates its own degradation in an autocatalytic manner. This presents a paradox as to how cyclin E-CDK2 is able to phosphorylate its numerous substrates prior to cyclin E autophosphorylation-catalyzed degradation. Here we find that the PP2A-B56 phosphatase specifically dephosphorylates cyclin E at S384, thereby uncoupling cyclin E degradation from cyclin E-CDK2 activity. Furthermore, the rate of S384 dephosphorylation is high in interphase and low in mitosis, allowing PP2A-B56 to oppose autocatalytic cyclin E degradation and maintain cyclin E-CDK2 activity at the G1/S transition.

2.2 Introduction

The mammalian cell cycle is regulated by cyclin-dependent kinases (CDKs) and their associated cyclin regulatory subunits. Cyclin E-CDK2 has essential roles as cells exit quiescence

and during endoreduplication cycles, and also regulates numerous processes during the G1 and S-phases of the cell cycle including S-phase entry, DNA replication, and centrosome duplication. Cyclin E-CDK2 phosphorylates a large and diverse network of substrates and non-catalytic functions for cyclin E in DNA replication have also been described (100-104).

Cells must tightly regulate cyclin E-CDK2 activity to ensure normal cell cycle progression. This is accomplished through a variety of mechanisms including E2F-dependent cyclin E transcription, binding of CDK inhibitor proteins (p27Kip1 and p21Cip1), activating and inhibitory phosphorylation of CDK2, and cyclin E degradation by the ubiquitin-proteasome system (100,101). Deregulation of cyclin E-CDK2 activity disrupts normal G1/S control and causes genomic instability (30,33,34,105-107). Importantly, cyclin E is oncogenic in multiple contexts: the cyclin E gene is amplified in human serous ovarian and basal breast cancers, and its increased activity promotes tumorigenesis in mouse models (25,26,31,108).

The F-box protein Fbw7 is the substrate recognition component of an SCF ubiquitin ligase that targets cyclin E for degradation after it becomes phosphorylated within conserved motifs called Cdc4 phosphodegrons (CPDs) (19,21,22,27,109). Fbw7 substrate CPDs typically contain two negative charges: a p-Thr/Ser in the 0 position followed by a second p-Thr/Ser or an acidic amino acid in the +4 position (20,110). Cyclin E is somewhat unique because it contains two CPDs: a high-affinity C-terminal degron that is doubly phosphorylated at T380 and S384 and is the primary determinant of Fbw7 binding, and a low-affinity N-terminal degron that is only phosphorylated at T62 (Figure 2.1A). Phosphorylation of S384 is the critical signal that initiates cyclin E degradation, as Fbw7's affinity towards the doubly phosphorylated form of cyclin E (T380/S384) is more than 1000-fold higher than mono-phosphorylated T380 (7). Ubiquitylation of cyclin E by SCF^{Fbw7} is essential for cyclin E periodicity, and impaired cyclin E

degradation causes constitutive cyclin E-CDK2 activity throughout the cell cycle, hyperproliferation in epithelial and hematopoietic cells, and accelerates tumorigenesis (15,30,31,90,111,112).

Importantly, while T380 is phosphorylated by multiple kinases and its phosphorylation is largely constitutive, S384 can only be autophosphorylated by CDK2 in *cis* (Figure 2.1A) (22). Cyclin E binding to Fbw7 is therefore stimulated by a phosphorylation that is predicted to occur almost simultaneously with the formation of an active cyclin E-CDK2 complex. Autocatalytic-stimulated cyclin E degradation thus presents a significant paradox: How can a cyclin E-CDK2 complex persist in cells long enough to phosphorylate substrates prior to priming itself for recognition and ubiquitylation by SCF^{Fbw7}? We hypothesized that there must be a mechanism that counteracts this autocatalytic degradation; one possibility is that a phosphatase dephosphorylates cyclin E's CPDs in order to prevent Fbw7 binding. Indeed, degron dephosphorylation has been shown to be important for c-Myc, another Fbw7 substrate (113,114), as well as the cyclin E orthologue Cln2 in budding yeast (115). Therefore, there is biological precedence for dephosphorylation of degrons as a mechanism that controls substrate recognition by E3 ubiquitin ligases.

PP2A is a member of the phosphoprotein phosphatase (PPP) family of serine/threonine phosphatases, which includes PP1-PP7. These enzymes share a conserved core catalytic domain and together contribute much of the total cellular serine/threonine phosphatase activity (116). PP2A regulates diverse signaling pathways and cellular processes, including cell division (117,118). The active PP2A holoenzyme is typically a heterotrimer consisting of a catalytic (C) subunit, a scaffold (A) subunit, and a variable regulatory (B) subunit that dictates substrate specificity. The catalytic (PPP2CA/B) and scaffold (PPP2R1A/B) subunits are each encoded by

two genes that produce nearly identical α and β isoforms of the proteins, which are thought to be largely functionally redundant. In contrast, PP2A B subunits are divided into at least four distinct families: B/B55, B'/B56, B'', and B'''/Striatins. The structural and functional distinctions between these families alter how PP2A holoenzymes interact with substrates and achieve substrate specificity (119,120).

In this study, we determined the importance of cyclin E CPD dephosphorylation as a regulatory mechanism controlling autocatalytic cyclin E degradation. We have found that PP2A specifically dephosphorylates cyclin E at S384, and the activity of this pathway is higher in interphase than in mitosis. Moreover, while both PP2A-B55 and PP2A-B56 holoenzymes can dephosphorylate S384 *in vitro*, only PP2A-B56 complexes regulate S384 phosphorylation *in vivo*. By opposing S384 phosphorylation in active cyclin E-CDK2 complexes, PP2A-B56 positively regulates cyclin E activity and protein stability. Thus, cell cycle-specific PP2A-mediated S384 dephosphorylation uncouples cyclin E activity from its degradation in the portion of the cell cycle where cyclin E function is most important.

2.3 Materials and Methods

2.3.1 *Cell Lines, plasmids, and drug treatments*

All cells were maintained in DMEM supplemented with 10% FBS and Penicillin/Streptomycin. Myc-cyclin E and HA-CDK2 have been described previously (121). All PP2A B subunits were PCR amplified from either a collection of GFP-tagged expression constructs (a gift from T. Kapoor, Rockefeller University, as previously described (122)) or HEK293A cDNA, cloned into pCS2-3xFLAG vectors, and verified by Sanger sequencing. Transient transfections of plasmids were performed using the calcium phosphate precipitation method. Tautomycetin (Tocris) and

okadaic acid (Santa Cruz Biotechnology) were used at 10 nM, roscovitine (Sigma) was used at 25 μM or 10 μM (Figure 2.5), and calyculin A was used at 50 nM.

2.3.2 *RNAi*

FBXW7 shRNA was obtained from Open Biosystems (pGIPZ backbone; sense strand 5'-CAGAGAAATTGCTTGCTTT-3'). Lentiviral particles were produced in HEK293T cells by contransfection of pGIPZ, psPAX, and pMD2.G (obtained from Addgene). The following siRNAs were purchased from Qiagen: Allstar negative control, PPP2CA_1 (sense strand: 5'-GGAACUUGACGAUACUCUATT-3'), PPP2CA_2 (sense strand: 5'-CAAACAAUCAUUGGAGCUUAATT-3'), and PPP2CB_1 (sense strand: 5'-GGAAUUAGAUGACACUUUATT-3'), PPP2CB_2 (sense strand: 5'-CCGACAAAUUACCCAAGUAUATT-3'). siRNAs used in the siB55 pool were purchased from Qiagen: PPP2R2A (sense strand: 5'-CUGCAGAUGAUUUGCGGAUUATT-3'), PPP2R2B (sense strand: 5'- CCGGAAGAUCCAAGCAACAGATT-3'), PPP2R2C (sense strand: 5'-CGCUCAUUCUUCUCGGAAATT-3'), and PPP2R2D (sense strand: 5'-UUCAUCCAUAUCCGAUGUAAATT-3'). siB56 pools were described previously (122) and ordered from IDT. siRNAs used for PPP-family catalytic subunit and PP2A-B subunit *in vitro* screens were comprised of pools of four independent siRNAs targeting each gene (Qiagen). Sequences are provided in Table 2.1. All siRNA transfections were performed using Lipofectamine RNAiMax (Life Technologies) using the manufacturer's protocol.

2.3.3 *Western blotting*

Cells were harvested in NP-40 lysis buffer (50 mM Tris pH 8.0, 150 mM NaCl, 0.5% NP-40, 1 mM DTT) supplemented with protease and phosphatase inhibitor cocktail, with the following

exceptions. Lysates collected for *in vitro* dephosphorylation assays were harvested in lysis buffer containing only protease inhibitors. Cells harvested for PP2A complex purification were lysed in Tween-20 lysis buffer (50 mM Tris pH 7.5, 150 mM NaCl, 0.1% Tween-20, 10% glycerol, 1 mM EDTA, 2.5 mM EGTA, and 1 mM DTT) supplemented with a protease inhibitor cocktail. All lysates for western blotting were prepared in Laemmli sample buffer, boiled, and resolved on polyacrylamide gels before semi-dry transfer to PVDF membranes. All membranes were blocked in 5% milk/TBST and probed with primary antibodies from one hour at room temperature to overnight at 4°C. HRP-conjugated secondary antibodies were prepared in blocking solution at 1:10,000.

2.3.4 *In vitro dephosphorylation assays*

In vitro dephosphorylation assays using whole cell lysates were performed by incubating cell extracts with either recombinant GST-cyclin E-CDK2 (Figures 2.1F, 2.2A-C, and 2.3B) or immunoprecipitated Myc-cyclin E/HA-CDK2 complexes (Figure 2.3A) at 30°C for up to 60 minutes, with agitation. Assays testing the activity of specific PP2A complexes were performed by immunoprecipitating PP2A holoenzymes from cell lysates transfected with FLAG-tagged B subunits. These immunoprecipitates were washed two times in lysis buffer and once in phosphatase reaction buffer (50 mM Tris pH 7.4, 150 mM NaCl, 1 mM MnCl2, and 5 mM $MgCl_2$, supplemented with a protease inhibitor cocktail) and then incubated with recombinant GST-cyclin E-CDK2 in phosphatase reaction buffer at 30°C for up to 60 minutes. All reactions were quenched with the addition of 4X Laemmli sample buffer, boiled, and assayed by western blotting.

2.3.5 *Quantitative RT-PCR*

Total RNA was extracted from cells using TRIzol and purified with an RNA miniprep kit (Zymo Research). RNA was quantified and equal amounts were DNased before reverse transcription using a High Capacity cDNA Reverse Transcription kit (Applied Biosystems). qRT-PCR reactions were performed using transcript-specific primer probe sets (Figure 2.4D; Applied Biosystems) or transcript-specific SYBR primer sets (Figure 2.7; IDT) and 2X Taq Universal PCR Master Mix (Applied Biosystems) on a QuantStudio 5 instrument. Transcripts were normalized using ACTB as an endogenous control. Primer sequences for Figure 2.7 are as follows: PPP2R2B (Fwd: 5'- AGGACATTGATACCCGCAAA; Rev: 5'-AATTCTCCCGTGTGGTTGAA), PPP2R2D (Fwd: 5'-TGCGACAGACACTCCAAGTT; Rev: 5'-CGCCCACTATGACTGAATTT), and ACTB (Fwd: 5'- GCACAGAGCCTCGCCTT; Rev: 5'-GTTGTCGACGACGAGCG).

2.3.6 *Cyclin E kinase assays, and ^{35}S-Met pulse-chase*

Kinase assays were performed by immunoprecipitating endogenous cyclin E from cell lysates for two hours at 4°C. IPs were washed two times in lysis buffer and once in kinase assay buffer (50 mM HEPES pH 7.4, 10 mM $MgCl_2$, 1 mM DTT), and incubated at 30°C for 30 minutes in a 20 μl reaction containing 30 μM ATP, 2 μCi γ-^{32}P ATP, and Histone H1 as a substrate. Reactions were quenched by the addition of sample buffer, boiled, resolved on polyacrylamide gels, and exposed to film. Endogenous cyclin E half-life was measured by ^{35}S-Met pulse-chase as previously described (123).

2.3.7 *Flow cytometry*

For cell cycle flow cytometry analysis, cells were fixed in 90% ethanol before staining with a propidium iodide/RNase A solution and processed on a CANTO II flow cytometer (Becton Dickinson). Data were analyzed using FlowJo.

2.3.8 *Antibodies*

Antibodies were purchased from suppliers as follows. Santa Cruz Biotechnology: cyclin E IP (HE111, mouse monoclonal), cyclin E WB (HE12, mouse monoclonal, 1:1,000), CDK2 (M2, rabbit polyclonal, 1:1,000), p27 (C-19, rabbit polyclonal, 1:500), and γ-tubulin (C-20, goat polyclonal, 1:1,000). BD Biosciences: PP2A-C (610555, mouse monoclonal, 1:20,000). Calbiochem: CDK1/2 pY15 (219440; rabbit polyclonal; 1:1,000). Sigma: FLAG (M2, mouse monoclonal, 1:4,000) and α-tubulin (DM1A, mouse monoclonal, 1:1,000). Bethyl Antibodies: PP1α (A300-904A, rabbit polyclonal, 1:1,000), PP1β (A300-905A, rabbit polyclonal, 1:1,000), PP1γ (A300-906A, rabbit polyclonal, 1:1,000), PP4 (A300-835A, rabbit polyclonal, 1:1,000), PP5C (A300-909A, rabbit polyclonal, 1:1,000), and PP6C (A300-844A, rabbit polyclonal, 1:1,000). Cyclin E phospho-specific rabbit polyclonal antibodies for T62, T380, and S384 were developed by PhosphoSolutions as described previously (15,22,121). 9E10 hybridoma supernatant was used at 1:5.

2.4 Results

2.4.1 *Cyclin E is specifically dephosphorylated at S384*

To determine the potential role of phosphatases in regulating cyclin E phosphorylation, we first treated cells with the serine/threonine phosphatase inhibitor calyculin A and examined the three regulatory cyclin E CPD phosphorylation sites (T62, T380, and S384) using phospho-specific antibodies. Endogenous cyclin E is inherently unstable when phosphorylated at S384 and can only be readily detected when cyclin E turnover is disabled (15). We therefore studied both HeLa cells stably expressing an shRNA against FBXW7 (the gene name for Fbw7) and Hct116 cells in which FBXW7 was deleted by gene targeting (15). Calyculin A treatment rapidly increased S384 phosphorylation in both cell types, whereas neither T62 nor T380 phosphorylation changed appreciably (Figures 2.1B and 2.1C). The rapidity of S384 dephosphorylation was further shown by treating cells with the CDK1/2 inhibitor roscovitine to prevent S384 autophosphorylation. CDK2 inhibition led to the complete loss of S384 phosphorylation within minutes, whereas pT62 and pT380 were unaffected, although this may partially reflect continued phosphorylation of these sites by other kinases during roscovitine treatment (Figures 2.1B and 2.1D). To ensure these effects were not an indirect consequence of inactivating Fbw7, we overexpressed cyclin E-CDK2 in 293A cells, which exceeds the ubiquitylation capacity of the endogenous Fbw7 pathway. Again, S384 was completely dephosphorylated within minutes of adding roscovitine to the cells (Figure 2.1E).

To study cyclin E dephosphorylation independently of broadly acting phosphatase inhibitors, we performed an *in vitro* dephosphorylation assay by incubating recombinant GST-cyclin E-CDK2 with whole cell lysates in order to measure the relative phosphatase activity against each cyclin E CPD phosphosite (recombinant cyclin E-CDK2 isolated from baculovirus

SF9 cells is highly phosphorylated at T62, T380, and S384). Cell lysates contained robust phosphatase activity against S384 but had little activity against either T62 or T380 (Figure 2.1F). Together, these experiments indicate that S384 phosphorylation is highly labile in a number of different cell types, suggesting that dephosphorylation could represent a conserved cyclin E regulatory mechanism.

2.4.2 *PP2A dephosphorylates cyclin E at S384*

Calyculin A is a broad-spectrum inhibitor of the PPP phosphatases, with activity against PP1, PP2A, PP4, PP5, and PP6 (124). To identify the specific phosphatase catalytic subunit catalyzing S384 dephosphorylation, we first performed an *in vitro* dephosphorylation assay using lysates pretreated with either okadaic acid, which also targets many of the PPP family members, or tautomycetin, which is specific for PP1 (125). Consistent with our *in vivo* calyculin A results (Figures 2.1B and 2.1C), the reactions containing okadaic acid had no detectable phosphatase activity against S384. However, we found no difference in activity between control lysates and those treated with tautomycetin, suggesting that PP1 complexes do not dephosphorylate S384 (Figure 2.2A).

Because pharmacologic phosphatase inhibitors can have pleiotropic effects, we modified the *in vitro* dephosphorylation assay to screen candidate phosphatases using a genetic approach. 293A cells were transfected with siRNA pools targeting each of the PPP family catalytic subunits, and lysates from these cells were used to dephosphorylate recombinant cyclin E-CDK2. While each targeted phosphatase was similarly depleted, only the PP2A-depleted lysates had decreased S384 dephosphorylation activity (Figure 2.2B). To ensure this was not an off-target effect of the PP2A siRNA pool used for screening, we repeated this experiment using two additional PP2A siRNA pools (siPP2A-C_1/2, Figure 2.2C). In each case, PP2A catalytic

subunit knockdown prevented S384 dephosphorylation compared to lysates harvested from control siRNA cells. These data implicate PP2A as the phosphatase that dephosphorylates cyclin E at S384.

2.4.3 *PP2A-B56 dephosphorylates S384*

To identify the specific PP2A complex catalyzing S384 dephosphorylation, we performed another *in vitro* dephosphorylation assay, this time using pools of siRNAs targeting 12 different PP2A regulatory B subunits. Depletion of three different B subunits—PPP2R2A (B55α), PPP2R5C (B56γ), and PPP2R5D (B56δ)—partially decreased S384 phosphatase activity; however, none were as efficient as depletion of the PP2A catalytic subunit (Figure 2.3A). This could reflect functional redundancy among the individual B subunits, which would cause depletion of any single B subunit to confer only a partial phenotype.

We next determined if purified PP2A complexes directly dephosphorylate S384 *in vitro*. We expressed FLAG-tagged B subunits in 293A cells and purified intact PP2A holoenzymes via anti-FLAG immunoprecipiations. These complexes were subsequently incubated with recombinant cyclin E-CDK2 to test for direct phosphatase activity against S384. Intact PP2A complexes were obtained for each B subunit except PPP2R3C (B"γ), as determined by the amount of co-precipitating PP2A-C (Figure 2.3B). Multiple PP2A complexes directly dephosphorylated S384 *in vitro*, including all four B55 family members (to various extents), and two B56 family subunits: B56γ and B56ε (Figure 2.3B).

In vitro approaches reveal direct phosphatase activities but cannot model determinants of *in vivo* phosphatase specificity, such as subcellular localization or additional binding partners that facilitate protein-protein interactions. We therefore complemented these *in vitro* approaches

by determining whether B55 or B56 complexes could alter S384 phosphorylation *in vivo* by co-transfecting Myc-cyclin E and HA-CDK2 with B55 and B56 family subunits. In contrast with the *in vitro* assays, B55 subunit overexpression had no effect on pS384, whereas overexpression of the B56α, B56β, B56γ, and B56ε subunits decreased pS384 (Figure 2.3C). Importantly, B56 overexpression did not alter CDK2 binding to cyclin E (with the exception of B56β) or CAK-mediated activating phosphorylation of CDK2 (visualized by the lower migrating band of CDK2). Thus, while both B55 and B56 PP2A holoenzymes display activity towards S384 *in vitro*, only B56 complexes appear to regulate S384 phosphorylation *in vivo*.

2.4.4 *PP2A-B56 regulates cyclin E kinase activity and stability*

A substantial fraction of cyclin E cannot be targeted SCF^{Fbw7} because it is sequestered in inactive CDK2 complexes, due to the binding of Cip/Kip CDK inhibitor proteins or CDK2 inhibitory phosphorylation. Because S384 can only be phosphorylated when cyclin E is in a catalytically active complex, the predicted consequence of inhibiting its dephosphorylation is increased turnover of the active pool of cyclin E. To test this directly, we targeted the B55 and B56 subunit families in their entirety to reduce the effects of subunit redundancy, as suggested by both our results (Figure 2.3) and a previous study (122). Both the PP2A-B55 and PP2A-B56 complexes are essential regulators of mitotic exit and their inhibition causes mitotic arrest (126-128); therefore, we synchronized cells at the G1/S transition using the double thymidine protocol shown in Figure 2.4A to specifically study cyclin E within its most relevant cell cycle context. PP2A-B56 knockdown greatly decreased cyclin E-associated kinase activity and modestly decreased cyclin E abundance, whereas knockdown of the B55 subunits slightly increased kinase activity and did not affect cyclin E abundance (Figure 2.4B). Importantly, knockdown of PP2A-

B56 did not change the amount of CDK2 bound to cyclin E, the amount of CDK2 inhibitory phosphorylation (pY15), or the amount of bound p27 in cyclin E immunoprecipitates that were normalized for the different amounts of cyclin E in the input. We also assessed the cell cycle distributions of each of these populations and found the G1/S synchrony to be similar for all three populations, with the exception of a small percentage (~10%) of G2/M cells in the siB56 pool cells (Figure 2.4C). However, this is insufficient to account for the observed changes in cyclin E abundance and likely reflects the necessity of PP2A-B56 for exit from mitosis. We also examined transcriptional changes as an alternative explanation for decreased cyclin E abundance. CCNE1 mRNA was reduced by 35% in the siB55 pool cells and 25% in the siB56 pool cells (Figure 2.4D). While the mechanism underlying the decrease in mRNA in the siB55 pool cells is unclear, the change in siB56 pool cells may largely reflect the fact that cyclin E-CDK2 stimulates cyclin E transcription by E2F (129), and these cells have decreased cyclin E kinase activity. Finally, we used a ^{35}S-Met metabolic pulse-chase assay to determine the effect of B56 depletion on endogenous cyclin E stability. As predicted, inhibition of PP2A-B56 decreased cyclin E half-life, from 6.7 hours in control cells to 3.6 hours in siB56 pool cells (Figure 2.4E). Importantly, because this half-life reflects the stability of both active and inactive cyclin E complexes, it underrepresents the full impact of PP2A-B56 on Fbw7-mediated cyclin E degradation.

2.4.5 *S384 phosphatase activity varies throughout the cell cycle*

PP2A-B56 complexes are inhibited at the start of mitosis before being reactivated by the PP1 phosphatase to initiate mitotic exit (128). To test for differential S384 phosphatase activity at different points of the cell cycle, we treated both asynchronous and nocodazole-arrested Hct116 Fbw7$^{-/-}$ cells with roscovitine and analyzed changes in S384 phosphorylation over a short

period of time (Figure 2.5). As we observed previously (Figures 2.1B, 2.1D, and 2.1E), asynchronous cells rapidly dephosphorylated S384 upon inhibition of CDK2. However, we found almost no dephosphorylation of S384 in the nocodazole-arrested cells, indicating that the phosphatase activity of PP2A-B56 towards S384 is markedly lower in prometaphase than in interphase. Thus, S384 dephosphorylation—which protects cyclin E from autocatalytically-stimulated degradation—is highest in the portions of the cell cycle where cyclin E-CDK2 activity is needed, and lowest in mitosis.

2.5 Discussion

In this study, we have shown that PP2A-B56 specifically dephosphorylates cyclin E at S384, thereby opposing its recognition and ubiquitylation by SCF^{Fbw7}. Accordingly, disrupting S384 dephosphorylation by inactivation of B56 regulatory subunits is sufficient to decrease cyclin E kinase activity and shorten its half-life, consistent with the increased degradation of catalytically active cyclin E. Dephosphorylation thus provides a solution to the paradox of how cyclin E can both earmark itself for destruction via autophosphorylation at S384 and persist in cells long enough to phosphorylate its substrates and drive cell cycle progression.

Our finding that mitotic cells have low S384 phosphatase activity is consistent with the observation that the PP2A-B56 phosphatases are repressed during most of mitosis (128). Additionally, we have previously shown that Fbw7-null cells have extremely high cyclin E-CDK2 activity in mitosis due to decreased inhibitory phosphorylation of CDK2 (15). Together, the combined effects of maximal S384 autophosphorylation by CDK2 and decreased S384 dephosphorylation by PP2A-B56 may synergistically protect mitotic cells against inappropriate cyclin E-CDK2 activity, which causes chromosome segregation failures and aneuploidy by

inhibiting the activity of the anaphase-promoting complex/cyclosome (APC/C) ubiquitin ligase (30). A model depicting the relationship between PP2A-B56 activity and cyclin E abundance throughout the cell cycle is shown in Figure 2.5B.

In contrast with our work, a previous study found that a different PP2A holoenzyme, PP2A-B55β, dephosphorylates all three cyclin E CPD phosphosites (T62, T380, and S384) and stabilizes cyclin E (130). While we did detect phosphatase activity of PP2A-B55 towards S384 *in vitro*, we found that only B56 regulatory subunits affected S384 phosphorylation and cyclin E-CDK2 kinase activity *in vivo* (Figures 2.3C and 2.4B). Moreover, Hct116 cells contain robust S384 phosphatase activity (Figures 2.1C and 2.1D) but have been reported to not express the B55β isoform due to promoter hypermethylation at the PPP2R2B gene (131). We confirmed this experimentally (Figure 2.7) and therefore conclude that another phosphatase(s) must regulate S384 phosphorylation in Hct116 cells. However, the reasons underlying the discrepancies between our studies remain unclear and we cannot preclude roles for PP2A-B55β in cyclin E regulation in other contexts. Finally, while S384 is only autophosphorylated by CDK2, T62 and T380 are phosphorylated by multiple cellular kinases, and can therefore be phosphorylated when cyclin E is in an inactive complex (22). Thus, the distinction between general cyclin E CPD dephosphorylation and specific S384 dephosphorylation suggests that PP2A-B56 functions to specifically stabilize cyclin E within active CDK2 complexes.

The cyclin E gene (CCNE1) is commonly amplified in human cancers, including serous ovarian adenocarcinomas and basal breast cancers (25,26,132). Because overexpression of B56 regulatory subunits might be expected to phenocopy cyclin E overexpression in tumorigenesis, we used cBioportal to examine TCGA ovarian and breast cancer datasets for amplifications of CCNE1 and the B56 subunits (25,26,68,69). As shown in Figure 2.6, B56 subunits are amplified

in both organ sites, and the amplifications of the various B56 subunits are nearly mutually exclusive of one another. This suggests that they may, in part, be functioning redundantly. Intriguingly, there is also a strong tendency towards mutual exclusivity of B56 subunit amplifications with CCNE1 amplifications. While these data are merely correlative, they do raise the possibility that amplifications of B56 subunits contribute to tumorigenesis through cyclin E deregulation, which will need to be addressed in future work. PP2A is frequently considered a tumor suppressor gene due to a variety of evidence including its opposition of many pro-growth signaling pathways, inactivation by the SV40 small T viral oncoprotein, and mutations of the A scaffold subunit in cancer (133-138). The finding that PP2A-B56 complexes promote cyclin E activity at the G1/S transition and are amplified in primary human tumors suggests that in some contexts, a subset of PP2A complexes may also function as oncogenes. Thus, to fully understand the multi-faceted roles of PP2A in tumorigenesis, it will be necessary to continue to characterize the molecular pathways regulated by the large number of unique PP2A complexes.

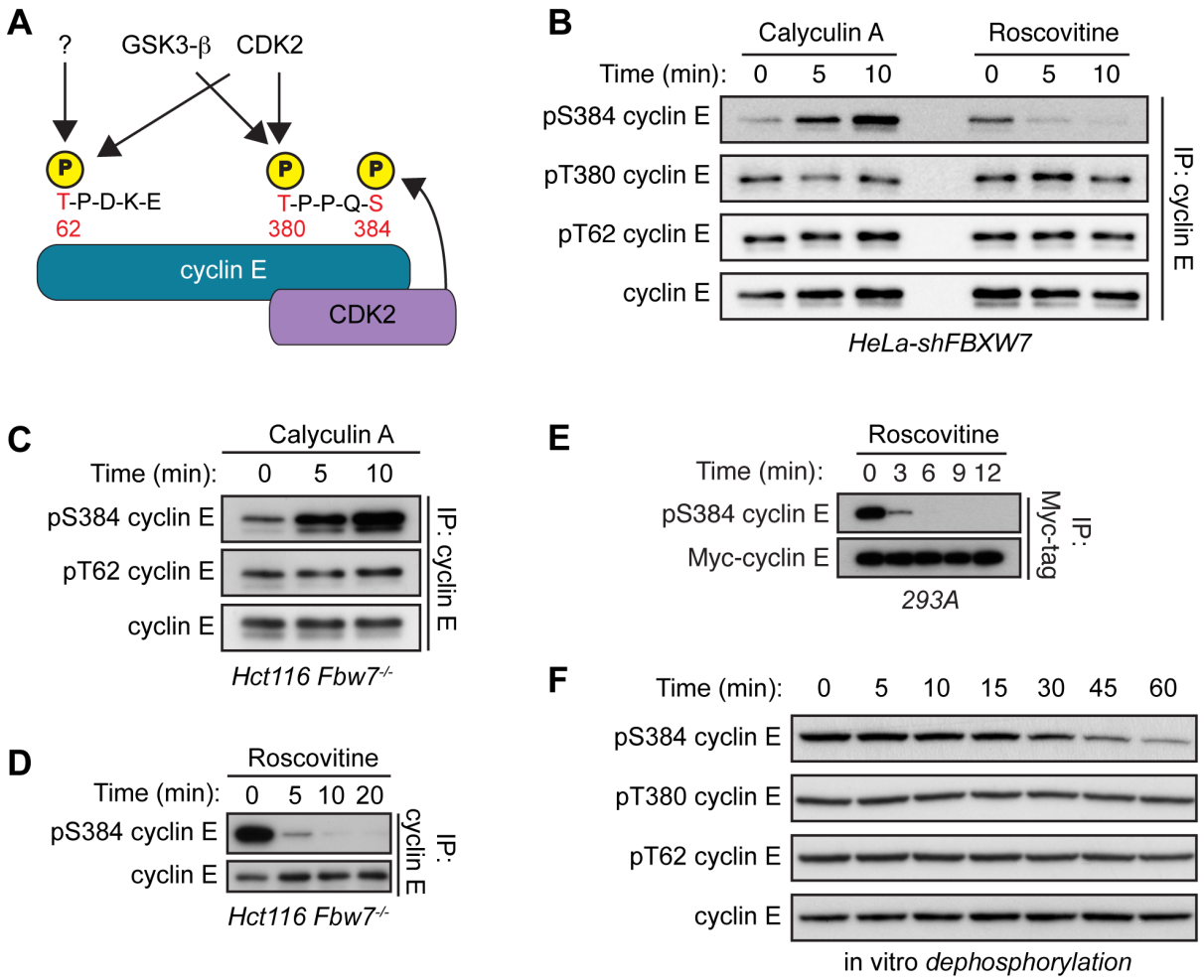

Figure 2.1. Cyclin E is dephosphorylated specifically at S384 both *in vivo* and *in vitro*.
(**A**) A schematic depicting cyclin E CPDs and the relevant kinases phosphorylating each residue. Cyclin E contains two CPDs: a low-affinity N-terminal degron centered at T62 that contains only one phosphosite (T62) and a high-affinity C-terminal degron centered at T380 that contains two phosphosites (T380 and S384). All three cyclin E CPD phosphosites can be phosphorylated by CDK2. T62 can also be phosphorylated by an unknown kinase, while T380 can also phosphorylated by GSK3-β. Importantly, S384 can only be phosphorylated by CDK2 in *cis*, as depicted. (**B**) HeLa cells stably expressing an shRNA against FBXW7 were treated with either the serine/threonine phosphatase inhibitor calyculin A, or the CDK1/2 inhibitor roscovitine for up to 10 minutes. Endogenous cyclin E was immunoprecipitated from whole cell lysates and changes in phosphorylation of T62, T380, and S384 (all three cyclin E CPD phosphosites) were determined by western blotting. (**C**) Hct116 Fbw7$^{-/-}$ cells were treated with calyculin A for up to 10 minutes and processed as in *B*. (**D**) Hct116 Fbw7$^{-/-}$ cells were treated with the CDK1/2 inhibitor roscovitine for up to 20 minutes and processed as in *B*. (**E**) 293A cells were co-transfected with Myc-cyclin E and HA-CDK2 and then treated with roscovitine for up to 12 minutes. Myc-cyclin E was immunoprecipitated from whole cell lysates and changes in S384 phosphorylation were assayed by western blotting. (**F**) 293A cells were lysed in buffer lacking phosphatase inhibitors and incubated with recombinant cyclin E for 0-60 minutes in an *in vitro* dephosphorylation assay. Changes in CPD dephosphorylation over time were measured by western blotting.

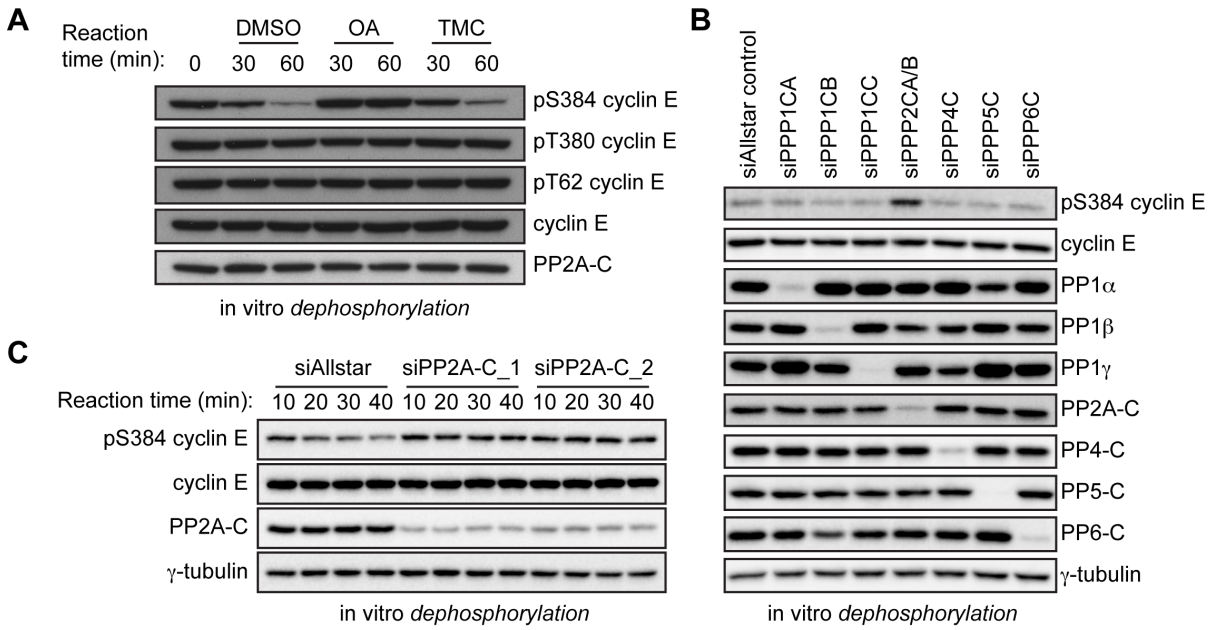

Figure 2.2. The serine/threonine phosphatase PP2A dephosphorylates cyclin E at S384.
(**A**) An *in vitro* dephosphorylation assay of recombinant cyclin E-CDK2 using cell lysates pre-treated with either DMSO, the PPP-family phosphatase inhibitor okadaic acid (10 nM), or the PP1-specific inhibitor tautomycetin (10 nM). (**B**) 293A cells were transfected with pools of four distinct siRNAs against the PPP-family phosphatases PP1α (PPP1CA), PP1β (PPP1CB), PP1γ (PPP1CC), PP2A (PPP2CA/B), PP4 (PPP4C), PP5 (PPP5C), and PP6 (PPP6C), as well as a negative control siRNA (siAllstar control). Lysates collected from these cells were incubated with recombinant cyclin E-CDK2 in an *in vitro* dephosphorylation assay. The efficacy of catalytic subunit depletion was measured by western blotting using antibodies specific for each subunit. (**C**) Same as in *B*, but performed with two distinct pools of siRNAs targeting both PP2A catalytic subunits (PPP2CA and PPP2CB), siPP2A-C_1 and siPP2A-C_2, in comparison with a negative control siRNA (siAllstar).

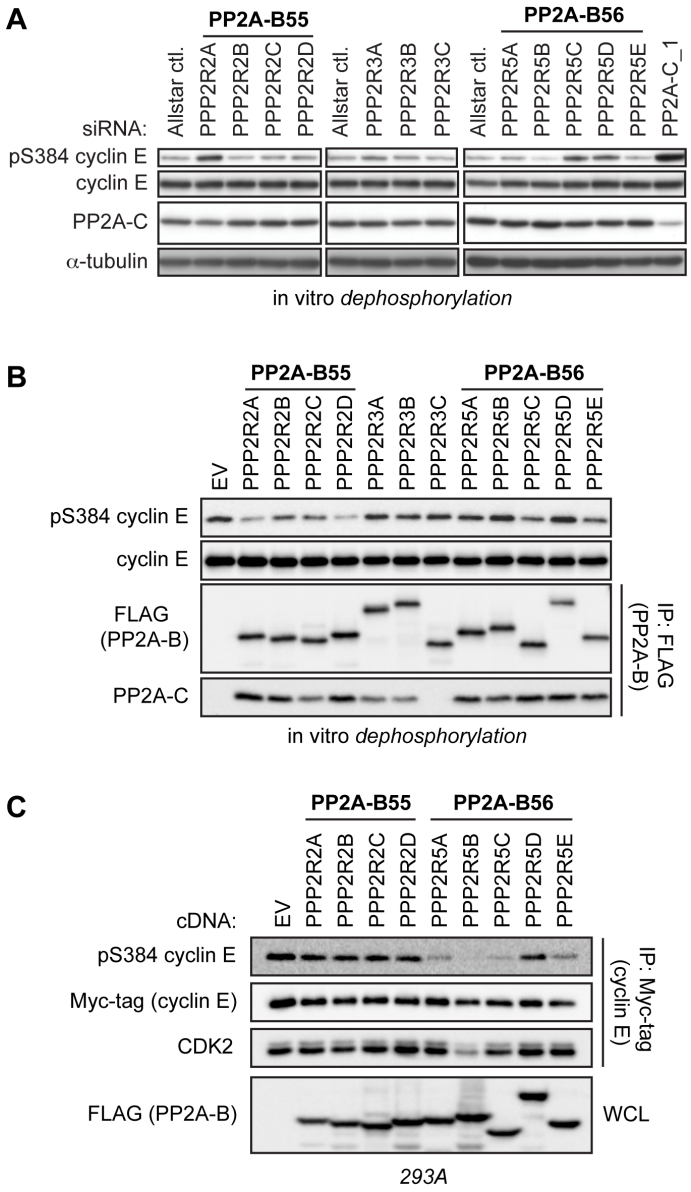

Figure 2.3. PP2A-B56 complexes regulate cyclin E S384 phosphorylation *in vitro* and *in vivo*.
(**A**) Specific PP2A B subunits were depleted by transfecting 293A cells with pools of siRNAs, as done in Figure 2B. Lysates harvested from these cells were incubated with purified cyclin E-CDK2 complexes in an *in vitro* dephosphorylation assay. Lysates depleted of the PP2A catalytic subunit were used as a positive control (siPP2A-C_1, far right lane). (**B**) 293A cells were transfected with FLAG-B subunits and then lysed in Tween-20 lysis buffer without phosphatase inhibitors. PP2A holoenzymes were purified via anti-FLAG immunoprecipitations, and then incubated with recombinant cyclin E-CDK2 complexes to test for direct dephosphorylation of S384 *in vitro*. IPs from cells transfected with empty vector (EV) served to control for non-specific co-precipitating phosphatase activity. The relative abundance of PP2A-C served to approximate the efficiency of purification of intact PP2A heterotrimers. (**C**) 293A cells were co-transfected with FLAG-B subunits. Myc-cyclin E, and HA-CDK2. Cells were lysed and exogenous cyclin E was immunoprecipitated and analyzed for pS384 and bound CDK2 by western blotting.

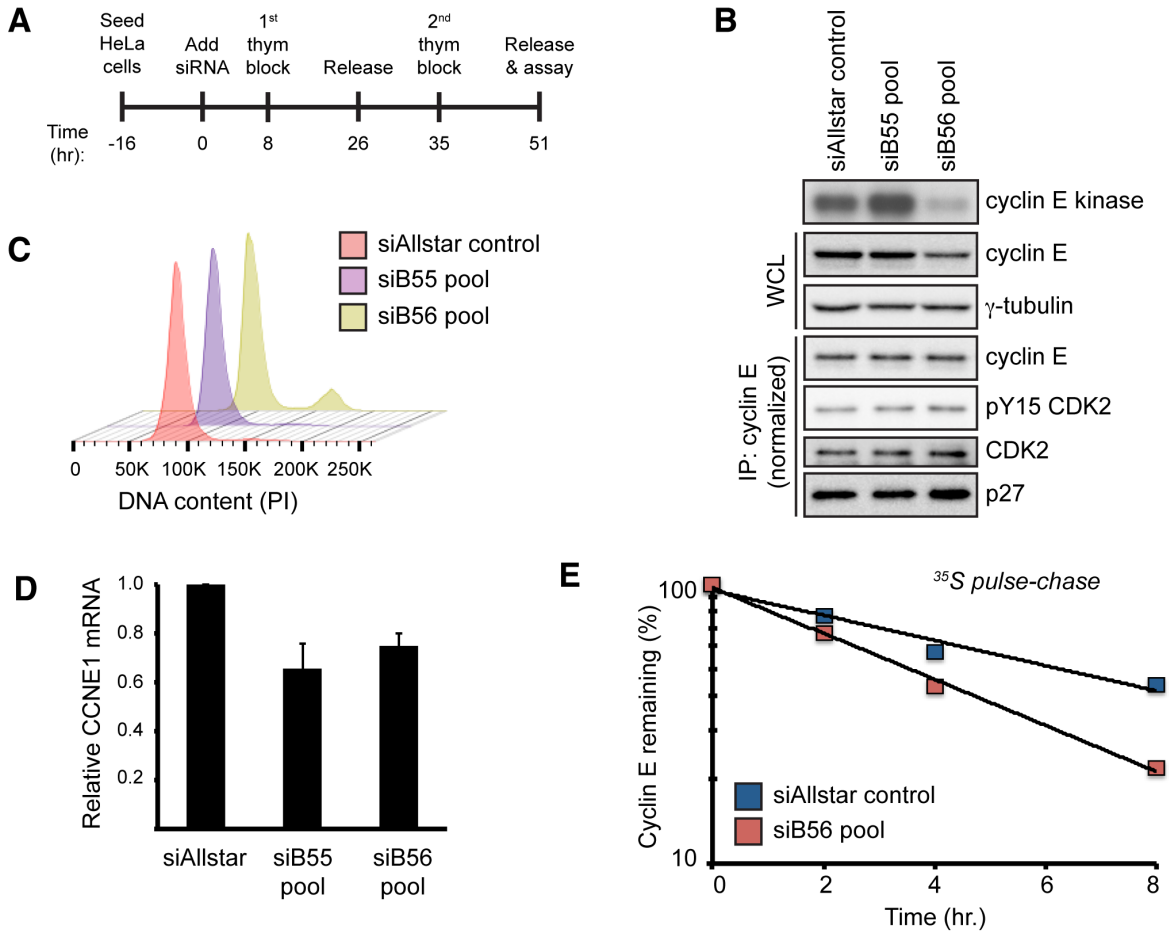

Figure 2.4. PP2A-B56 controls cyclin E kinase activity and protein stability.
(**A**) A schematic of the experimental protocol used in each panel of Figure 2.4. Cells were seeded and transfected with siRNAs on the next day (time 0). Cells were then synchronized at the G1/S transition using a double thymidine block and endpoint assays were conducted approximately 51 hours after siRNA transfection. (**B**) HeLa cells were transfected with siRNAs targeting all four PP2A-B55 regulatory subunits (siB55 pool), all five PP2A-B56 regulatory subunits (siB56 pool), or a negative control siRNA (siAllstar control). Following transfection, cells were synchronized as depicted in *A*, released for two hours, and assayed for cyclin E protein abundance and kinase activity. To assay for changes in the amount of bound CDK2, CDK2 inhibitory phosphorylation, and bound p27, we performed cyclin E immunoprecipitations after normalizing the input for the amount of cyclin E present in the whole cell extract. (**C**) Cell cycle FACS analysis of samples treated as in *B*. DNA was stained using propidium iodide (PI). (**D**) Analysis of CCNE1 transcript levels in cells treated as in *B*. Transcripts were normalized to ACTB expression. Data presented are means ± s.e.m. of two independent biological replicates. (**E**) Endogenous cyclin E half-life was measured using a ^{35}S-Met pulse-chase in cells synchronized at G1/S, as depicted in *A*.

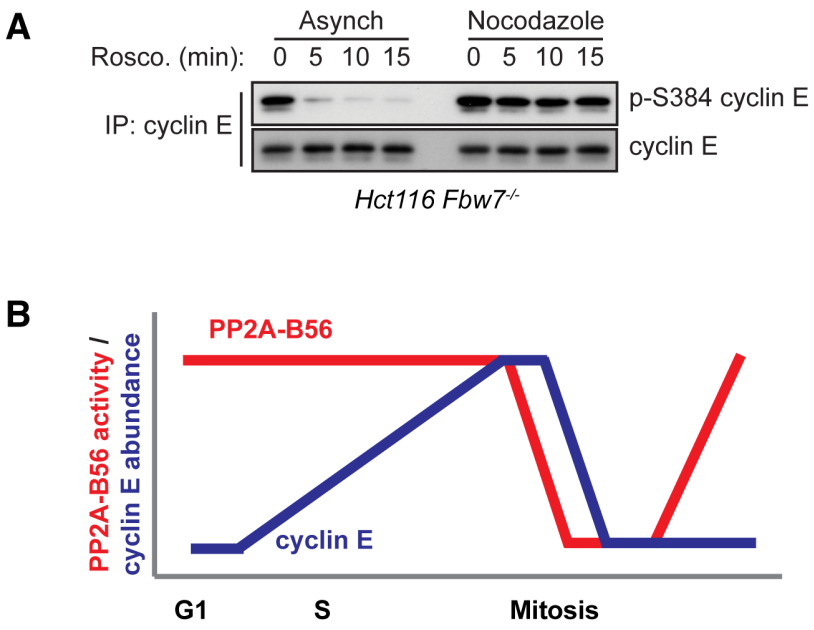

Figure 2.5. PP2A-B56 phosphatase activity towards S384 is decreased in mitosis.
(**A**) Hct116 Fbw7$^{-/-}$ cells were grown as asynchronous cultures or arrested in prometaphase by adding nocodazole for 18 hours. The CDK1/2 inhibitor roscovitine was then added for up to 15 minutes before harvesting the cells. Endogenous cyclin E was immunoprecipitated, and changes in pS384 were analyzed by western blotting. (**B**) A model depicting the cell cycle-regulation of PP2A-B56 and cyclin E. PP2A-B56 phosphatase activity is high during interphase before declining at the start of mitosis. It is then reactivated at the end of mitosis due to a dephosphorylation cascade. Cyclin E abundance is low at the beginning of G1 and increases as cells progress through the cell cycle, due to increasing transcription. Cyclin E abundance then declines in late S phase and mitosis due to increased ubiquitylation by the SCF^{Fbw7} ubiquitin ligase, and subsequent destruction by the proteasome.

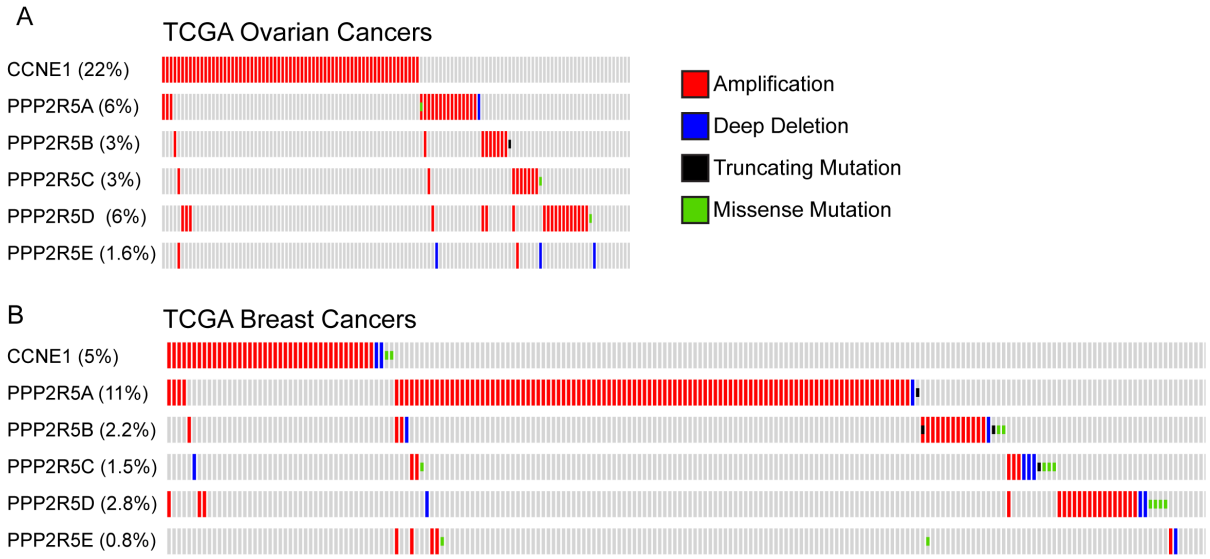

Figure 2.6. CCNE1 and B56 subunits are amplified in breast and ovarian cancers.
(**A**) The cBioPortal online interface (68,69) was used to analyze amplifications of CCNE1 and PP2A-B56 subunits in the TCGA ovarian cancer dataset (26). Individual patient samples are presented in columns. (**B**) Same analysis as *A*, except for the TCGA breast cancer dataset (25).

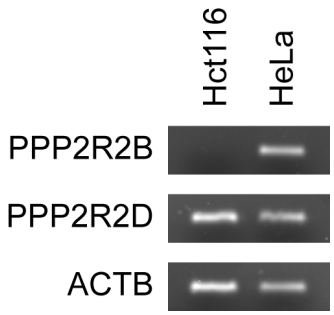

Figure 2.7. PPP2R2B is not expressed in Hct116 cells.
Semi-quantitative RT-PCR analysis of PPP2R2B (B55β), PPP2R2D (B55δ), and ACTB mRNA expression in Hct116 and HeLa cells. As previously published (131), Hct116 cells do not express detectable levels of PPP2R2B mRNA

Table 2.1. siRNA sequences used for *in vitro* activity screens.

Gene	siRNA #	Target sequence	Qiagen Cat. No.
PPP1CA	1	ATGGATTGATTGTACAGAAAT	SI04436390
PPP1CA	2	TACGACCTTCTGCGACTATTT	SI04897655
PPP1CA	3	CGGCTACGAGTTCTTTGCCAA	SI04436397
PPP1CA	4	AAGAGACGCTACAACATCAAA	SI02225755
PPP1CB	1	TACGAGGATGTCGTCCAGGAA	SI02225762
PPP1CB	2	AAGCGTTGAGTCATCAGGTAT	SI03033737
PPP1CB	3	ATTGGTTGACTTAGACCGTAA	SI03052490
PPP1CB	4	AACAGCTAATCCGCCGAAGAA	SI03027724
PPP1CC	1	CGGGACTTGTAACATAGAGTA	SI00041706
PPP1CC	2	TTCGGCGAATTATGCGACCAA	SI04436411
PPP1CC	3	GAGGAGTAAGTGTACAATTGA	SI02759211
PPP1CC	4	AACATCGACAGCATTATCCAA	SI02225776
PPP2CA	1	ACACCTCGTGAATACAATTTA	SI00041853
PPP2CA	2	ATGGAACTTGACGATACTCTA	SI02225783
PPP2CA	3	TACAAAGCCTCTTGTCATCAA	SI04436467
PPP2CA	4	TAAGACGATGTGACTGCACAA	SI04436453
PPP2CB	1	CACCGGATACAAACTACTTAT	SI00060277
PPP2CB	2	TGCGTTATCCAGAACGCATTA	SI04436481
PPP2CB	3	AAGAGGTTCGTTGCCCTGTTA	SI04436474
PPP2CB	4	CAGGCTGCTATCATGGAATTA	SI04436488
PPP4C	1	CGGACAATCGACCGAAAGCAA	SI02658698
PPP4C	2	CTGCACTGAGATCTTTGACTA	SI04436586
PPP4C	3	TGCGGCGACATCCATGGACAA	SI04713555
PPP4C	4	TCGCCAGATCACGCAGGTCTA	SI02658705
PPP5C	1	CTCGTGGAAACCACACTCAAA	SI02225853
PPP5C	2	CCCAAGCTTGAAGACGGCAAA	SI04897788
PPP5C	3	CACGGAGGCCTGTTCAGTGAA	SI00086317
PPP5C	4	CAGATTCTGGTACAGGTCAAA	SI03065041
PPP6C	1	CACAAATGAGTTTGTTCATAT	SI02225860
PPP6C	2	TTCCAGATTCAGAACGTGTTA	SI04436600
PPP6C	3	ACAGCTTACATTGTTAGCGTA	SI04897795
PPP6C	4	ACCATCGAACGGAATCAGGAA	SI04436607
PPP2R2A	1	AAGCGAGACATAACCCTAGAA	SI00041909
PPP2R2A	2	CTGCAGATGATTTGCGGATTA	SI02225825
PPP2R2A	3	CCCGGTCTTGGTGGTGGTATA	SI04436516
PPP2R2A	4	ATGGAAGGTATAGAGATCCTA	SI02225832
PPP2R2B	1	CCGGAAGATCCAAGCAACAGA	SI02658901
PPP2R2B	2	AGCAGTGGCGGCTACAAATAA	SI04897711
PPP2R2B	3	CAGGGACTACTTGACCGTCAA	SI02633582
PPP2R2B	4	CACCGTTTACTCTTAGACAAA	SI00065408
PPP2R2C	1	TACTGTCACATCATAGATTTA	SI00126434
PPP2R2C	2	AAGATTACCGAACGAGATAAA	SI03032498
PPP2R2C	3	ACCGCTCATTCTTCTCGGAAA	SI02659237
PPP2R2C	4	GAGGTTATTCTCAGTGGATTA	SI00126427
PPP2R2D	1	TTCATCCATATCCGATGTAAA	SI02759148
PPP2R2D	2	CAGAGACTACCTGTCGGTGAA	SI00691523
PPP2R2D	3	CCAGTGCAACGTGTTCGTCTA	SI04901785
PPP2R2D	4	CCGCTCCATTAAGAACAGTGA	SI00691530
PPP2R3A	1	CTGCCGGTGTCTACAATGAAA	SI04897732
PPP2R3A	2	CAGGAGGATTTCATCCCTCTA	SI02649717

PPP2R3A	3	CAGAAGGATGTTGAGAACGAT	SI04897725
PPP2R3A	4	CACCACGGTTATTCAGAGAAT	SI04897718
PPP2R3B	1	TACCTCGACCACGAGCAGAAA	SI03109155
PPP2R3B	2	CTGGTCAAGCCGAGGACTGAA	SI04887890
PPP2R3B	3	CGCCGTGGACCTGTACGAGTA	SI04887904
PPP2R3B	4	GTGCGTTTGTACGGAATGATA	SI04887897
PPP2R3C	1	AAGCGATGATCAATTACGAAA	SI04306869
PPP2R3C	2	ACGCGCCAAAGGCACACGATA	SI04345705
PPP2R3C	3	CGGGCTTATCGTGGCCTTTAA	SI00318115
PPP2R3C	4	TAGGGCCATACAGGAACTAAT	SI04201309
PPP2R5A	1	CACCCGGAAATCGGTCCGCAA	SI04436544
PPP2R5A	2	CTGTATCATGGCCATAGTATA	SI02225839
PPP2R5A	3	TTCGATGACCTTACTAGCTCA	SI03022782
PPP2R5A	4	CAGAGTGGTAACAGATGGGTA	SI04436551
PPP2R5B	1	AACCATCGTATCACTGATCTA	SI04897746
PPP2R5B	2	AAGGGCAAGCTTGACCAGGAA	SI04897739
PPP2R5B	3	CCGCATGATCTCAGTGAATAT	SI02659034
PPP2R5B	4	CCGGTTCATCTATGAATTCGA	SI00086212
PPP2R5C	1	ATGGTAGAATATATCACCCAT	SI03051986
PPP2R5C	2	GAGGAAGATGAACCAACGTTA	SI04897760
PPP2R5C	3	CCCGTGGTCCTTCTCCATATT	SI04897753
PPP2R5C	4	CCAACCTAATATAGCGAAGAA	SI03074253
PPP2R5D	1	CAGGAGATTATTCTCACCAAA	SI02653350
PPP2R5D	2	GAAGTTGTTTATGGAAATGAA	SI02653812
PPP2R5D	3	ACGGGCCGAGATGCCCTATAA	SI00086240
PPP2R5D	4	CTCGTGTATGAGTTCTTCTTA	SI00086254
PPP2R5E	1	CCGGTGATATTGACAATAGGA	SI02659048
PPP2R5E	2	CACCGGGATTGCAAATCTAAT	SI02659041
PPP2R5E	3	AAGGACTTCAATCCAAAGTTT	SI00086282
PPP2R5E	4	CTCGTTCTATATCTCATCACA	SI00086289

Chapter 3. Computational Analyses of Colorectal TCGA Datasets Identifies Altered Cellular Metabolism as a Hallmark of Fbw7-Mutant Tumors

This chapter was adapted from a manuscript in preparation.

Ryan J. Davis[1,2,3], Mehmet Gonen[4,5], Daciana H. Margineantu[1,2], Ken J. Lindsay[1,2], Jonathan E. Grim[2], Haiwei Gu[4], Danijel Djukovic[4], Sonali Arora[1], Patrick J. Paddison[1], Daniel Raftery[4], David M. Hockenbery[1,2], Adam Margolin[4,7], and Bruce E. Clurman[1,2]

[1]Division of Human Biology, Fred Hutchinson Cancer Research Center, Seattle, WA, 98109, USA
[2]Division of Clinical Research, Fred Hutchinson Cancer Research Center, Seattle, WA, 98109, USA
[3]Molecular and Cellular Biology Program, University of Washington, Seattle, WA, 98195, USA
[4]Oregon Health & Science University, Portland, OR 97239, USA
[5]Koc University, Istanbul, Turkey
[6]Northwest Metabolomics Research Center, University of Washington, Seattle, WA 98109-8057, USA; Division of Public Health Sciences, Fred Hutchinson Cancer Research Center, Seattle, WA 98109, USA.
[7]Sage Bionetworks, Seattle, WA 98109, USA; Computational Biology Program,

3.1 Abstract

The majority of Fbw7 substrates are oncoprotein transcription factors; therefore, tumors that acquire loss-of-function mutations in Fbw7 are predicted to have widespread changes in gene expression. We hypothesized that we could leverage these transcriptional changes to identify conserved biological alterations in Fbw7-mutant colorectal tumors. To this end, we developed novel computational methods to analyze TCGA datasets for gene expression signatures that could predict a tumor's Fbw7 mutation status. Surprisingly, genes with roles in cellular metabolism, and specifically mitochondrial function, were highly enriched in the predictive gene expression signature, suggesting that altered metabolism could be a conserved feature of Fbw7-

mutant colorectal tumors. We validated these predictions at the level of both gene expression and functional assays and found that Fbw7-mutant cells are shifted towards oxidative metabolism. Moreover, upregulation of pyrimidine biosynthesis is a significant contributor to the increased oxygen consumption in cells with Fbw7 mutations, and could represent a therapeutic opportunity for the treatment of Fbw7-mutant cancers.

3.2 Introduction

Alterations in cell metabolism are emerging as drivers of tumorigenesis, due largely to the requirements of anabolic processes to support increased cell growth and proliferation. Less obvious aspects of metabolism, such as redox homeostasis and altered host-tumor interactions, have also been recognized to be important (139,140). A significant emphasis towards understanding cancer metabolism has focused on the altered utilization of glutamine and glucose (141,142). The latter is classically referred to as the Warburg Effect, or aerobic glycolysis, and represents the trend in tumors to upregulate the conversion of glucose to lactate instead of fueling the citric acid cycle (TCA cycle). Alterations in other metabolic pathways, such as amino acid and lipid biosynthesis, can also drive cellular transformation (143,144).

Many metabolic changes are attributable to deregulation of specific oncogenes, including glutamine addiction in Myc-overexpressing tumors and upregulation of Warburg metabolism in KRAS mutant-cancer cells (140,145-147). Therefore, there is substantial interest in better understanding the ways in which tumors differentially utilize and generate metabolites, and the genetic alterations that underlie these changes. Ultimately, the hope is that rewired cellular metabolism will present metabolic vulnerabilities that could be targeted in patients.

Fbw7 is a tumor suppressor that is mutated in a number of cancers, including frequent mutations in up to 30% of T-cell acute lymphoblastic lymphoma (T-ALL), a significant fraction of colorectal cancers (CRC), and lower mutation rates in other organ sites including endometrium, stomach, and bladder (110). Fbw7's molecular function is as a substrate receptor for the Skp1-Cullin 1-F box (SCF) ubiquitin ligase (SCF^{Fbw7}), where it binds to target substrates once they become phosphorylated at short, conserved regions termed Cdc4 phosphodegrons (110). An overwhelming number of the loss-of-function mutations sustained by Fbw7 in cancer are heterozygous missense mutations of one of three specific arginine residues (R465, R479, and R505; termed $Fbw7^{ARG}$) that coordinate Fbw7's interaction with phosphorylated substrates. These mutations therefore result in the stabilization of oncoprotein substrates such as c-Myc, cyclin E, Notch, and PGC-1α, among others. In fact, the majority of Fbw7 substrates are either transcription factors or transcriptional regulators; therefore, the tumors that contain Fbw7 mutations are predicted to have widespread changes in the transcriptional output of the cell. Adding further complexity to trying to understand the consequences of Fbw7 mutations is that they are predicted to simultaneously deregulate the function of multiple substrates, making the attribution of specific phenotypes to specific substrates enormously challenging.

Increasing amounts of cancer genomic and gene expression data are becoming available through The Cancer Genome Atlas (TCGA) and other high-throughput sequencing studies. However, it is not always clear how to best utilize these data to better understand the biology of these tumors. It is therefore of significant importance to generate novel approaches for data analysis in order to uncover new insights into tumorigenesis, and guide follow-up investigations.

Towards this end, we developed a novel computational method to identify gene expression signatures that were predictive of a tumor's Fbw7 mutational status. We first

analyzed the TCGA colorectal cancer dataset (63), as this is both a very common cancer and contains a substantial proportion of Fbw7 mutations (Table 1.2). Interestingly, the biological process that was most enriched in the predictive gene expression signature was for mitochondrial-associated genes, suggesting that altered mitochondrial function, and cellular metabolism, could be a hallmark of Fbw7-mutant CRC. While a number of Fbw7 substrates control various metabolic processes (111,148-152), the specific contribution of impaired Fbw7 function on cancer cell metabolism is poorly understood. We validated this prediction in Fbw7-mutant CRC cells using both gene expression and phenotypic assays. During the course of these studies, we also identified additional metabolic alterations in amino acid and lipid metabolism. Furthermore, the upregulation of oxidative metabolism in Fbw7-mutant cells is being partially driven by changes in pyrimidine biosynthesis and this pathway could represent a targetable vulnerability in Fbw7-mutant colorectal cancer.

3.3 Materials and Methods

3.3.1 *Computational methods*

We analyzed 10 different solid tumor collections from TCGA PanCancer collection and identified five cancers with FBXW7 mutation rates higher than 4%: Bladder Urothelial Carcinoma (BLCA), Colon Adenocarcinoma/Rectum Adenocarcinoma (COADREAD), Head and Neck Squamous Cell Carcinoma (HNSC), Lung Squamous Cell Carcinoma (LUSC), Uterine Corpus Endometrioid Carcinoma (UCEC). We turned the problem of finding a transcriptional signature for FBXW7 mutations into a two-step algorithm, which can be summarized as (i) using a binary classifier that predicts FBXW7 mutation status of each tumor using its gene expression

data and (ii) identifying important gene expression features using the classification parameters to extract a transcriptional signature.

We evaluated two possible scenarios: (i) modeling each cancer as a separate problem and (ii) modeling the five cancers conjointly. In the first scenario, we trained a binary classifier that predicts the class label (i.e., FBXW7 mutation status) using input features (i.e., gene expression profile) for each cancer separately. We used the relevance vector machine (153) as our binary classifier. We then identified the top 500 genes out of 20530 that are positively correlated (i.e., overexpressed in mutated tumors) with FBXW7 mutation using the model parameters. We fed these genes into DAVID Bioinformatics Resources 6.7 (154,155) to find functionally related gene sets.

In the second scenario, we trained a conjoint binary classifier that solves related but distinct classification problems together to benefit from additional data, which is known as transfer learning. Instead of modeling each cancer cohort, we modeled them together to obtain more robust results. We used the kernelized Bayesian transfer learning algorithm (156) as our transfer learning classifier. Like the first scenario, after training the classifier, we identified the top 500 positively correlated genes for each cancer using the model parameters and fed these gene sets into DAVID Bioinformatics Resources 6.7.

To have stable results, we performed 50 replications of both scenarios using randomly picked 75% of tumors in training phase. We then used the average model parameter assigned to each gene when deciding to include this gene in the top 500 list. The following table provides the enrichment score and ranking of the gene set associated with mitochondrial functions for each cohort/scenario pair.

3.3.2 *Cell culture and RNAi*

All cells were maintained in DMEM supplemented with 10% FBS and penicillin/streptomycin. FBXW7 shRNA vector was obtained from Open Biosystems (pGIPZ backbone; sense strand 5'-CAGAGAAATTGCTTGCTTT-3'). Lentiviral particles were produced in HEK293T cells by contransfection of pGIPZ, psPAX, and pMD2.G (obtained from Addgene).

3.3.3 *Quantitative RT-PCR*

Total RNA was extracted from cells using TRIzol and purified with an RNA miniprep kit (Zymo Research). RNA was quantified and equal amounts were DNased before reverse transcription using a High Capacity cDNA Reverse Transcription kit (Applied Biosystems). Quantitative RT-PCR reactions were performed using 300 μM of F/R primers (purchased from IDT) and 2X SYBR Green PCR Master Mix (Applied Biosystems) on a QuantStudio 5 instrument. Primer sequences used are provided in Table 3.1.

3.3.4 *Seahorse extracellular flux assays*

Cells were seeded in Seahorse XF24 well plates the night before the assay. Extracellular Flux Assay cartridges were hydrated in XF Calibrant solution overnight at 37°C. The morning of the assays, cells were switched to unbuffered DMEM media lacking glucose, L-glutamine, sodium pyruvate, and sodium bicarbonate (Sigma D5030) that was then supplemented with 50 mM glucose, 2 mM L-glutamine, and 1 mM sodium pyruvate. Following the media change, cells were allowed to acclimate for at least one hour at 37°C prior to running the assay. Metabolic inhibitors (25 μM oligomycin; 5 μM FCCP; 5 nM rotenone/5 μM antimycin A) were sequentially added to each well to determine OCR and ECAR profiles. For assays testing the effect of DHODH inhibition on OCR, leflunomide was used at 30 μM. Following the assay, cell numbers were quantified using a Hoechst Assay as follows. The media was aspirated from each

well and the plate was frozen at -20°C. Next, the plate was thawed, 100 μL of 0.01% SDS was added to each well and then frozen at -80°C. The plate was then thawed, 100 μL of Hoechst Assay solution (4 μg/mL Hoechst 33342, 10 mM Tris pH 7.4, 1 mM EDTA, and 1 M NaCl) was added to each well, shaken at 37°C in the dark for one hour, and the fluorescence of each well was measured (Ex: 355 nM; Em: 460 nM).

3.3.5 *Gene targeting*

Hct116 Fbw7$^{-/-}$ cells have been previously described (15). Hct116 Fbw7$^{+/R505C}$ cells and LoVo Fbw7$^{+/+}$ cells were generated using adeno-associated virus (AAV) gene targeting, using a previously described protocol (15). Briefly, the targeting vector was designed such that a neomycin-resistance cassette was flanked by two homology arms with sequence homology to the genomic DNA at the FBXW7 locus, and the desired mutation was incorporated via PCR-mediated mutagenesis of the targeting vector (Hct116 changed amino acid 505 from an arginine to a cysteine (R505C); LoVo cells required the opposite substitution (C505R)). Targeted cells were enriched using neomycin selection, and resistant clones were screened by both PCR and genomic DNA sequencing to ensure they contained the mutation of interest. Floxed-neomycin resistance genes were excised from genomic DNA using RFP-Cre-Gessicles (Clontech), and removal of the cassette was confirmed by both PCR and restored sensitivity to neomycin. For CRISPR-Cas9 genetic knockout, sgRNAs were cloned into pLentiCRISPR_v2 (sgFBXW7: 5'-AAGAGCGGACCTCAGAACCA-3'; sgCtl: 5'-GTAGCGAACGTGTCCGGCGT-3'; vector provided by P. Paddison, FHCRC). Target cells were transduced with lentiviruses, selected with puromcin, and single clones were isolated by limiting dilution. Knockout of Fbw7 was confirmed by western blotting.

3.3.6 *Metabolite profiling*

For global metabolite profiling, cells were plated in six-well dishes and harvested 48 hours later (at ~80% confluency) by quickly washing twice with warm PBS, adding pre-chilled 90% methanol/10% chloroform (v/v) directly to cells, and immediately freezing at -80°C. Dishes were frozen for 30 minutes and then placed on dry-ice, scraped to harvest cells, and transferred to eppendorf tubes. To ensure complete capture of all cells and metabolites, a second round of extraction was performed and pooled with the first fraction. Extracts were centrifuged 14,000 RCF for 5 minutes at 4°C to separate the metabolites (in the supernatant) from the protein and cell debris in the pellet. The supernatant was transferred to a new tube and metabolites were dried down using a speed-vac. Dried metabolites were resuspended in 1% formic acid/dH_2O and analyzed by liquid chromatography-mass spectrometry (for global metabolite profiling) or gas chromatography-mass spectrometry (for U-^{13}C-glucose flux experiments). The residual protein pellet was resuspended in 200 μl 0.1M NaOH, quantified by Bradford Assay, and used to normalize metabolite abundances.

3.3.7 *CRISPR-Cas9 synthetic-lethal screen*

A sgRNA library specifically targeting genes with known roles in metabolism or metabolic regulation was used for screening. In total, 633 genes were represented in the library, each targeted by six unique sgRNAs (for a total of 3,798 sgRNAs). Target cells were transduced using pooled lentiviruses at a minimum of 1,000-fold library coverage and 30% transduction efficiency (to minimize the number of cells that were infected with multiple sgRNAs) in biological replicates and selected using puromycin for 72 hours. Following selection, half of the cells from each population were frozen as the day 0 timepoint and the remaining cells were passaged for an additional 18 days while maintaining at least 1,000-fold coverage of the library (i.e. > $4x10^6$

cells). Genomic DNA was extracted from each of the populations (QiAMP DNA Blood Mini Kit) and quantified by Nanodrop. To maintain 1,000-fold library coverage, sgRNAs were PCR amplified from at least 40 μg of total genomic DNA divided into separate PCR reactions each containing 1.5 μg DNA. PCRs were performed using 2X Phusion Flash PCR master mix (Thermo Fisher) and amplified for 12 cycles to maintain linear representation of sgRNAs. First-round PCR products were purified and a second amplification step was performed to add Illumina adapters and sample-specific barcodes using Heculase II Fusion DNA polymerase (Agilent). Amplicons from the second PCR step were column purified using PureLink PCR purification kit (Life Technologies) and MinElute PCR purification kit (Qiagen) to remove genomic DNA and first round PCR product. Purified products were quantified, mixed, and sequenced using HiSeq 2500 (Illumina). Bowtie was used to align the sequenced reads to the guides (157). The R/Bioconductor package edgeR (158,159) was used to assess changes across various groups. Guides having a fold change more than 1 and an adjusted FDR less than 0.05 were considered statistically significant.

3.3.8 *Drug viability assays*

Cells were seeded in black-walled 96 well plates at low density one day before drug addition. Serial dilutions of leflunomide were then added to the target cells for the four-day treatment period. To assay viability, alamar blue (resazurin) reagent was added to the cells and measured using a spectrophotometer.

3.4 Results

3.4.1 *Bioinformatic analyses of TCGA gene expression datasets*

TCGA gene expression datasets provide enormous opportunities to better understand mechanisms of tumorigenesis. However, a bottleneck can be the lack of robust computational methods that facilitate the generation of biologic hypotheses, which can subsequently be experimentally verified. To address this challenge, we developed a novel computational approach that utilizes machine-learning algorithms to rank genes by how well their expression predicts a specific alteration in a tumor. These alterations can be quite specific, such as a genomic deletion, amplification, or mutation, or more general, such as the tumors that have low expression of a specific gene. To identify specifically enriched biological processes or functions, the top 2.5% of the ranked-order list of predictive genes was analyzed using the online DAVID Bioinformatics Resource (154,155), as this is the subset of genes that presumably reflects the conserved biological changes elicited by the alteration being analyzed.

We leveraged this platform to identify the conserved functional consequences of Fbw7 mutations in human cancers. Fbw7 mutant cancers provided an excellent test case for several reasons. First, Fbw7 is most often disabled via single allele point mutations in its substrate interaction domain ($Fbw7^{ARG}$), thus tumors with impaired Fbw7 function are easily identified by a consistent mechanism of inactivation. Second, Fbw7 is frequently mutated in tumor types where there is sufficient data to power the computational analysis, including colorectal cancer. Finally, most Fbw7 substrates are transcription factors, therefore Fbw7 mutation that stabilize these oncogenic transcription factors should alter a tumor's transcriptional profile.

These methods were used to generate predictive gene expression scores for Fbw7 mutations in CRC (and other cancers, as described in the methods). DAVID analyses of this signature identified mitochondrial genes as the single most enriched functional category

(enrichment score: 5.378; p-value: $6.6x10^{-9}$). Interestingly, the same mitochondrial gene expression signature was also identified when we performed this analysis on other tumor types, including bladder cancers and glioblastomas where Fbw7 function is inhibited due to very low mRNA expression (data not shown). Together, this suggested that altered cellular metabolism could be a conserved feature of Fbw7 mutations in human cancers. To validate this prediction, we first analyzed the mRNA expression of the mitochondrial signature genes (MSGs) in multiple contexts of Fbw7 inhibition. First, the cBioPortal online interface contains gene expression data for the CRC cell lines indexed in the Cancer Cell Line Encyclopedia (CCLE) (68,69). Thus, the mean gene expression z-score in Fbw7 wild-type and $Fbw7^{ARG}$ cell lines was calculated for each of the 54 MSGs. This analysis found that 81% of all MSGs had elevated mRNA expression in $Fbw7^{ARG}$ cell lines compared to $Fbw7^{+/+}$ cells (Figure 3.1A). Given the significant amount of heterogeneity present in this collection of cell lines, this suggests that Fbw7 mutations can change MSG expression in a variety of genetic and mutational backgrounds.

Next, changes in MSG expression were assessed after direct manipulation of Fbw7 in isogenic cell systems. We have previously generated $Fbw7^{-/-}$ Hct116 cells (which are wild-type for Fbw7), using adeno-associated virus (AAV)-gene targeting (15), and have also generated Hct116 $Fbw7^{+/R505C}$ cells. On the contrary, LoVo cells naturally contain a heterozygous arginine mutation ($Fbw7^{+/R505C}$). Thus, AAV-gene targeting was used to correct the endogenous, mutant allele in these cells to restore wild-type Fbw7 function. Together, these cell lines provided two complementary isogenic systems—one in which Fbw7 function was acutely disabled and one in which Fbw7 mutations were a likely driving event in tumorigenesis—to query the specific effects of Fbw7 mutations. Quantitative RT-PCR assays were used to determine the expression of a subset of the MSGs in both sets of cells. Both Hct116 $Fbw7^{+/R505C}$ and $Fbw7^{-/-}$ cells, as well

as LoVo Fbw7$^{+/R505C}$ cells, had increased MSG expression in comparison to their respective Fbw7 wild-type controls (Figures 3.1B and 3.1C). Therefore, both CCLE CRC gene expression datasets and targeted gene expression analyses of isogenic cell lines recapitulated the computational prediction that Fbw7 mutations drive increased expression of mitochondrial-associated genes.

3.4.2 *Fbw7 mutations increase oxidative metabolism in CRC cells*

We next wanted to understand the effects of Fbw7 mutations on cellular metabolism. Real-time metabolic changes can be measured using a Seahorse Bioanalyzer, which determines both the extracellular acidification rate (ECAR; indicative of glycolytic metabolism) and oxygen consumption rate (OCR; indicative of oxidative metabolism). This assay also measures how cells dynamically change their utilization of glycolytic and oxidative pathways in response to various metabolic inhibitors. Because we were specifically interested in the impact of Fbw7 mutations on mitochondrial function, we used the Seahorse Bioanalyzer to perform a mitochondrial stress test. Here, OCR and ECAR are measured during (1) basal proliferative conditions, (2) periods of ATP synthase inhibition (to suppress respiration in coupled mitochondria), (3) after uncoupling maximal mitochondrial respiration from the electron transport chain (ETC), thereby revealing the mitochondrial reserve capacity, and (4) after full inhibition of mitochondrial respiration.

The mitochondrial stress test was first performed on isogenic Hct116 and LoVo cells. In the Hct116 cells, both Fbw7$^{+/R505C}$ and Fbw7$^{-/-}$ cells had moderately elevated basal OCR in comparison to wild-type cells, but greatly increased maximal OCR after addition of the mitochondrial uncoupler FCCP (Figure 3.2A). This same pattern was observed in isogenic LoVo cells. Both clones with restored wild-type Fbw7 function had slightly decreased basal OCR but dramatically decreased maximal OCR, suggestive of large differences in the mitochondrial

reserve (Figure 3.2B). Thus, in multiple isogenic cell systems, cells with impaired Fbw7 function had both increased basal mitochondrial respiration and a larger mitochondrial reserve than cells with wild-type Fbw7.

This shift towards oxidative metabolism (while suggested by the computational predictions) is notably different than the Warburg Effect, or aerobic glycolysis, which might be the expected metabolic phenotype of Fbw7-mutant cells as several of its substrates have been previously shown to dominantly drive Warburg metabolism in cancers (160,161). To analyze the relative usage of oxidative and glycolytic pathways in a broader collection of cell lines, we used the Seahorse Bioanalyzer to compare the OCR/ECAR ratios in CRC cell lines where Fbw7 was inactivated through a variety of mechanisms. In all cases analyzed, Fbw7-deficient cells had increased OCR/ECAR ratios under basal proliferative conditions, indicative of a shift from glycolysis towards oxidative metabolism. This included Hct116 and DLD1 Fbw7 knock-out cells (generated via AAV-mediated recombination) (Figure 3.2C), DLD1 and HT-29 cells with stable knockdown of Fbw7 expression using shRNA (Figure 3.2D), and three independently-derived Hct116 clones where Fbw7 was knocked-out using CRISPR-Cas9 technology (Hct116 sgFbw7) (Figure 3.2E). LoVo cell lines where the endogenous Fbw7 mutant allele was corrected back to wild-type also exhibited this same pattern (data not shown). Thus, CRC cell lines with impaired Fbw7 function do not upregulate aerobic glycolysis—as would be predicted if loss of Fbw7 was driving Warburg metabolism—but instead display shifts towards oxidative metabolism.

3.4.3 *Global metabolite profiling reveals alterations in nucleotide, amino acid, and central carbon metabolism*

To gain additional insights into the metabolic changes associated with loss of Fbw7, both AAV-targeted Hct116 $Fbw7^{+/+}$ and $Fbw7^{-/-}$ cells, and CRISPR-Cas9 generated Hct116 sgCtl and sgFbw7 cells, were profiled by mass spectrometry-based global metabolite profiling (Figures

3.3A and 3.3B). This assay measures the steady-state abundance of approximately 150 different metabolites in a number of metabolic pathways, including central carbon metabolism, amino acid metabolism, and nucleotide biosynthesis. One of the most striking changes in Fbw7-deficient cells was the significant increase in two amino acids: serine and aspartate (Figures 3.3A, 3.3B, 3.3C, and 3.3D). Both of these amino acids have emerging roles in tumorigenesis and cell proliferation. Increased flux through the serine synthesis pathway, which converts the glycolytic intermediate 3-phosphoglycerate (3-PG) to serine, is important for the pathogenesis of breast cancers that have amplifications of one of the enzymes in the pathway, PHGDH (162,163). Serine synthesis has also been recently shown to affect pancreatic cell proliferation and DNA/histone methylation (164). Aspartate synthesis is crucial to produce reducing equivalents via the electron transport chain in proliferating cells (165,166). Both aspartate and serine also have important functions in nucleotide biosynthesis. Orotate—a key intermediate in pyrimidine biosynthesis—was also specifically upregulated in both $Fbw7^{-/-}$ and sgFbw7 cells (Figure 3.3E). These changes in amino acid and pyrimidine metabolites suggested that Fbw7 mutations could be affecting nucleotide biosynthetic pathways, perhaps as a mechanism to support increased cell proliferation.

There are also important connections between glycolysis and TCA cycle metabolites to mitochondrial function. Interestingly, both $Fbw7^{-/-}$ and sgFbw7 cells had increased levels of glucose, but decreased abundance of glyceraldehyde-3-phosphate, 2-PG/3-PG, and phosphoenolpyruvate (Figure 3.3F). Moreover, there was no difference in the amount of lactate present in conditioned media harvested from $Fbw7^{-/-}$ or sgFbw7 cells (data not shown). These data are broadly consistent with the OCR/ECAR profiles of these cells and provides additional evidence that disabling Fbw7 function does not enhance aerobic glycolysis. The abundance of

TCA cycle metabolites was more variable. Both oxaloacetate (OAA) and α-ketoglutarate (α-KG) were specifically increased in Fbw7$^{-/-}$ and sgFbw7 cells (Figure 3.3G). However, the abundance of fumarate, succinate, and aconitate did not reliably track with Fbw7 status (Figure 3.3G). Thus, understanding the full effect of Fbw7 mutations on the TCA cycle requires additional functional assays, and could reflect complex anaplerotic reactions of TCA cycle metabolites in these cells.

3.4.4 *U-^{13}C-glucose flux experiments*

Changes in steady-state glycolytic metabolite abundance (Figure 3.3F) was suggestive of alterations in glucose utilization; these differences could be due to changes in the rate of metabolite production or consumption. We wanted to distinguish between these possibilities for glucose specifically in order to answer three questions regarding Fbw7-mediated metabolism. First, is there any evidence for aerobic glycolysis in Fbw7-null cells, as measured by the amount of glucose being converted to lactate? Second, is there a difference in the amount of glucose-derived acetyl-CoA that is being incorporated into the TCA cycle, thus suggesting a mechanism for increased mitochondrial respiration? Finally, is there evidence of upregulation of serine synthesis from 3-PG that could help explain the dramatically increased levels of serine in Fbw7-null cells?

To answer these questions, metabolic flux experiments were performed by labeling Hct116 Fbw7$^{+/+}$ and Fbw7$^{-/-}$ cells with U-^{13}C-glucose for 0, 3, 6, and 14 hours, and tracking the incorporation of the heavy carbon isotopes into downstream metabolites (Figure 3.4A depicts fractional isotope abundance at the three-hour timepoint). Pyruvate is the major endpoint of glycolysis and is an effective marker of flux through the pathway. Cells with decreased flux (i.e. decreased rate of synthesis), should have less m+3 labeled pyruvate, whereas cells with increased

rates of utilization should have equal or greater amounts of m+3 pyruvate. At the three-hour timepoint, there was 8% less m+3 pyruvate in the Fbw7$^{-/-}$ cells compared to Fbw7$^{+/+}$ cells; Similar trends were observed at the six- and fourteen-hour timepoints, indicating that Fbw7$^{-/-}$ cells do have slightly lower glycolytic flux.

Pyruvate is a central hub of metabolism because it has a number of metabolic fates, including conversion to lactate, alanine, and acetyl-CoA, each of which are shuttled into distinct pathways. At the three-hour timepoint, Fbw7$^{-/-}$ cells had 19% less m+3 lactate and 25% less m+3 alanine than wild-type cells (Figure 3.4A; acetyl-CoA could not be detected by the GC-MS methods used). This magnitude of change was larger than what was observed for pyruvate (i.e. the net flux through glycolysis) and definitively shows that impairing Fbw7 function in these cells does not increase Warburg metabolism. Moreover, it suggests that alanine is not a major endpoint for glucose-derived pyruvate in these cells.

To understand whether the higher rate of oxygen consumption in Fbw7$^{-/-}$ cells could be due to additional pyruvate fueling the ETC, the rate of glucose conversion to TCA cycle intermediates was also analyzed. Pyruvate that enters the mitochondria can be converted to acetyl-CoA, which subsequently combines with oxaloacetate to generate citrate. Thus, the citrate that is generated from glucose-derived acetyl-CoA is indicated by the m+2 isotope. Similar to what was observed for lactate, there was a 19% reduction in m+2-labeled citrate at the three-hour timepoint (Figure 3.4A). This suggests that glucose isn't driving the increased OCR of Fbw7$^{-/-}$ cells. Interestingly, both Fbw7$^{+/+}$ and Fbw7$^{-/-}$ cells had very low levels of m+2 labeled fumarate (Figure 3.4A). Thus, Hct116 cells may be generally less reliant on glucose for TCA cycle function, and could instead be utilizing alternative fuels such as glutamine.

Finally, the glucose flux assay was used to determine whether the increased serine observed in Fbw7$^{-/-}$ cells could be a result of increased synthesis from 3-PG (as indicated by the amount of m+3-labeled serine). While there was almost no difference at the three- or six-hour timepoints, there was a significant 21% increase in m+3 serine at 14 hours in Fbw7$^{-/-}$ cells (Figure 3.4B). It is relevant that even in breast cancers cells with amplifications of PHGDH (the first enzyme in the serine-synthesis pathway (SSP) from 3-PG), only 9-10% of glucose is diverted towards serine synthesis, compared to 1-2% in non-amplified cells (162). Thus, while the increase in serine derived from 3-PG in Fbw7$^{-/-}$ cells may not account for the entire increase in intracellular serine abundance, it is consistent with upregulation of the SSP. Additionally, both Fbw7$^{-/-}$ and sgFbw7 cells had increased steady-state abundance of α-KG (Figure 3.3G). NADH and α-KG are generated as a byproducts of serine synthesis; therefore, upregulation of this pathway could be relevant to the increased oxygen consumption of Fbw7$^{-/-}$ cells through generation of both TCA cycle intermediates (α-KG) and electron donors (NADH) for the ETC.

These glucose flux experiments did present an interesting question: If Fbw7$^{-/-}$ cells have only slightly reduced conversion of glucose to pyruvate, but the pyruvate is being converted at a slower rate to lactate, alanine, and citrate, what is its ultimate metabolic fate? One possibility is that it is being used for increased fatty acid synthesis from acetyl-CoA. As an initial test, Hct116 Fbw7$^{+/+}$ and Fbw7$^{-/-}$ cells were stained with Oil Red-O, which enables the visualization of lipid droplets (organelles that serve as a cellular storage compartment for lipids) (Figure 3.4C). Fbw7$^{-/-}$ cells had markedly stronger staining, suggesting that this could be the preferred metabolic fate of glucose in these cells, although this requires further validation.

3.4.5 *Metabolic CRISPR-Cas9 synthetic-lethal screen*

Ultimately, the goal of understanding the metabolic changes that result from loss of Fbw7 is to discover new potential treatments for these cancers. CRISPR-Cas9 technology provides a facile and robust method to interrogate the effects of genetic knockouts on cell proliferation in various genetic backgrounds (167,168). Therefore, a CRISPR-Cas9 sgRNA lentiviral library comprised of 633 metabolic genes was used to screen the isogenic Hct116 and LoVo Fbw7 cell lines for genes whose knockout was lethal only in an Fbw7-mutant background (Figure 3.5A). sgRNAs were scored as a candidate synthetic lethal hit if they were selectively depleted from Fbw7-mutant cells, but not the corresponding wild-type cell line, over the duration of the assay. This screen yielded a number of candidate genes across several different metabolic pathways. Surprisingly, no sgRNAs scored in both LoVo $Fbw7^{+/R505C}$ lines and Hct116 $Fbw7^{-/-}$ cell lines, although there were many cell-type specific hits (Figures 3.5B and 3.5C). The reason for this lack of overlap is unclear, but could be due to a number of factors. First, different Fbw7 alleles (heterozygous arginine mutations compared to homozygous null mutations) could have distinct functional consequences. Second, the different cancer-associated mutational backgrounds of Hct116 and LoVo cells could result in unique genetic interactions with the loss-of-function mutations in Fbw7. Finally, it is possible that cancer cells that arise in the context of an Fbw7 mutation—which is thought to be an early event in colon carcinogenesis (35)—may have different vulnerabilities than those that arose with wild-type Fbw7 function.

3.4.6 *$Fbw7^{-/-}$ cells are hypersensitive to DHODH inhibition*

Of the candidate genes identified in the sgRNA screen, one of the most interesting was dihydroorotate dehydrogenase (DHODH), which scored with three separate sgRNAs in the Hct116 $Fbw7^{-/-}$ cells (Figure 3.5C). Biochemically, DHODH catalyzes the conversion of

dihydroorotate to orotate in an upstream step of pyrimidine biosynthesis (Figure 3.6A). DHODH is localized in the inner mitochondria membrane and a byproduct of the reaction is the production of NADH, which transfers electrons to ubiquinone, thereby fueling the electron transport chain and oxidative metabolism (169). DHODH was also an interesting candidate gene due to corroborating metabolomic data that showed both Hct116 Fbw7$^{-/-}$ and Hct116 sgFbw7 cells have increased levels of both orotate and aspartate (Figures 3.3D and 3.3E), the latter of which is a precursor metabolite in the pathway, as shown in Figure 3.6A. There is also evidence that inhibition of DHODH could represent an effective treatment strategy for a number of cancers, including melanoma, acute myeloid leukemia, and B cell malignancies (170-172). Moreover, it is also a direct transcriptional target of the Fbw7 substrate Myc (173).

To validate that Fbw7$^{-/-}$ cells have increased sensitivity to DHODH inhibition, we took advantage of a commercially available inhibitor of the enzyme, leflunomide (174). Consistent with the CRISPR-Cas9 results, Hct116 Fbw7$^{-/-}$ cells were more sensitive to leflunomide than Fbw7$^{+/+}$ cells (Figure 3.6B). Importantly, Fbw7$^{-/-}$ cells were more sensitive over a range of drug concentrations, indicative of a robust dose-response relationship.

One of the predicted consequences of inhibiting DHODH is a reduction in the amount of NADH generated that can drive respiratory metabolism via the ETC (Figure 3.6A). Because Fbw7-deficient cells have increased oxygen consumption (Figure 3.2), we were interested in determining the specific contribution of the NADH generated by DHODH to this process. The Seahorse Bioanalyzer was used to test the effect leflunomide treatment on basal and maximal OCR in Fbw7 isogenic cells, using a similar mitochondrial stress. The only modification to the protocol was the addition of leflunomide or DMSO following measurements of basal respiration, before subsequent inhibitors were added. Due to the differences in normal respiration (Figure

3.2A), each cell line was normalized to its basal OCR to more easily visualize the effect of leflunomide treatment. Interestingly, leflunomide had a similar effect on basal respiration in both $Fbw7^{+/+}$ and $Fbw7^{-/-}$ cells, where the OCR was decreased by ~13% (Figure 3.6C). Therefore, under normal proliferation conditions, the NADH generated by DHODH is contributing a substantial pool of electrons to the ETC but this doesn't differ between Fbw7 genotypes. In contrast, inhibition of DHODH specifically decreased maximal OCR in $Fbw7^{-/-}$ cells, and this was sufficient to completely rescue the uncoupled respiration rate back to the levels observed in wild-type cells (Figure 3.6C, following FCCP addition). This suggests that $Fbw7^{-/-}$ cells do have increased flux through the pyrimidine biosynthetic pathway. Moreover, this finding mechanistically connects the increased maximal OCR of Fbw7-deficient cells to the increased abundance of aspartate and orotate, and provides a rationale for the hypersensitivity of $Fbw7^{-/-}$ cells to inhibitors of the pathway.

3.5 Discussion

Here, we report the use of novel computational approaches to further our understanding of the consequences of Fbw7 mutations in human CRC. This approach leveraged the fact that most Fbw7 substrates are transcription factors; therefore, the "signature" of these mutations could be determined by studying gene expression databases. Analyses of TCGA CRC datasets found that genes with roles in mitochondrial function were highly enriched in the subset of genes that were most predictive of Fbw7 mutations. This predicted functional outcome was validated by assays of mitochondrial metabolism (Figure 3.2). Furthermore, CRISPR-Cas9 functional genomic screens identified pyrimidine biosynthesis as a potential therapeutic vulnerability of Fbw7-mutant cells, which was validated using specific inhibitors against DHODH, an intermediate

enzyme in the pathway. Finally, the NADH generated from DHODH is a critical contributor to the increased respiration of Fbw7$^{-/-}$ cells (Figure 3.6C).

Many Fbw7 substrates have been reported to regulate cell metabolism and mitochondrial biogenesis, including Myc, Notch, PGC-1α, and even cyclin E (111,148,175,176). While there are some reports showing how Fbw7 influences metabolism, these focus on glucose metabolism (85,177,178). To our knowledge this is the first in-depth study of how Fbw7 mutations specifically rewire CRC cancer cell metabolism. Moreover, the mitochondrial gene expression signature was one of the most predictive features of Fbw7 mutations across multiple tumor types. Thus, metabolic deregulation could represent an under-recognized, but important, consequence of Fbw7 mutations in human cancers, although this will need to be confirmed in future studies.

It is interesting to note that the oxidative metabolism of Fbw7-impaired cells shown here is reminiscent of other cell types, including some cancer stem cells (179) as well as a subset of melanomas with high expression of PGC-1α (56,180). It was also somewhat surprising to find a lack of evidence showing that impairing Fbw7 function increases aerobic glycolysis, even though this is the described metabolic phenotype of many Fbw7 substrates, including Myc (149). One explanation could be that CRC cell lines have other alterations that drive glycolytic metabolism, such as mutations in the RAS/RAF/MAPK pathway (140,145). However, if loss of Fbw7 was dominantly driving Warburg metabolism, these effects should have been observed in LoVo cells that already contain Fbw7 mutations. On the contrary, the genetic reversion studies showed that Fbw7 mutations had either no effect, or were actually restraining, the ECAR of these cells. Similarly, the glucose flux experiments directly showed that Hct116 Fbw7$^{-/-}$ cells have less conversion of glucose to lactate than Fbw7$^{+/+}$ cells.

The glucose flux experiments also suggested that Fbw7-null cells might have increased lipid synthesis, as indicated by less conversion of glucose to lactate, alanine, or citrate, and increase in lipid droplets, in the Fbw7$^{-/-}$ cells (Figures 3.4A and 3.4C). Therefore, other Fbw7 substrates such as SREBP could have underappreciated roles in Fbw7-mediated tumorigenesis, and are likely important regulators of the metabolic state of an Fbw7-deficient cell.

Potentially the most important finding of this research was that nucleotide biosynthesis, and pyrimidine biosynthesis in particular, could be a therapeutic vulnerability of CRC cells with Fbw7 mutations. The antimetabolite 5-fluorouracil (5-FU), which similarly impairs nucleotide production, has long been recognized as an effective cancer treatment, and remains a front-line therapy for the treatment of CRC today (181). Given that CRC cells are thus generally sensitive to inhibitors of nucleotide synthesis, it is interesting to speculate what creates the therapeutic window for DHODH inhibition in Fbw7-mutant cells. One possibility is that Fbw7$^{-/-}$ cells simply have a faster rate of proliferation and therefore an increased demand for nucleotides. Additionally, these cells could be using the NADH generated by DHODH in other redox processes and not to power the ETC. This is supported by the fact that leflunomide did not have genotype-specific effects on basal respiration but did specifically impair the uncoupled respiration of Fbw7$^{-/-}$ cells, suggesting that the additional NADH generated might have other cellular fates. One other potential explanation for this difference is that cells with Fbw7 mutations have increased levels of cyclin E, which is an important regulator of DNA synthesis and S-phase progression (100,101). It is well established that deregulation of CDK2 activity can have detrimental effects during S-phase and sensitizes cells to DNA replication inhibitors (182). Thus, the increased sensitivity to leflunomide in Fbw7$^{-/-}$ cells could be due to the generation of unbalanced nucleotide pools, which subsequently initiates DNA replication stress that is

exacerbated by increased levels of cyclin E-CDK2 activity. If true, a natural extension of this work would be to determine if using both leflunomide and S-phase toxins results in a synergistic killing of Fbw7$^{-/-}$ cells.

In conclusion, we have shown the Fbw7 mutations bring about complex changes in cancer cell metabolism, including changes in oxidative and glycolytic metabolism; mitochondrial respiration reserve; and lipid, amino acid, and nucleotide biosynthetic pathways. Although individual Fbw7 substrates have been shown to play roles in each of these, we argue that it is the coordinate deregulation of a network of oncogenes that includes c-Myc, Notch, cyclin E, PGC-1α, SREBP, KLF5, and others, that together elicit these metabolic changes. While certain substrates likely player different sized roles in the regulation of each of these processes, it is their collective deregulation that determines the metabolic state of an Fbw7-mutant cancer cell.

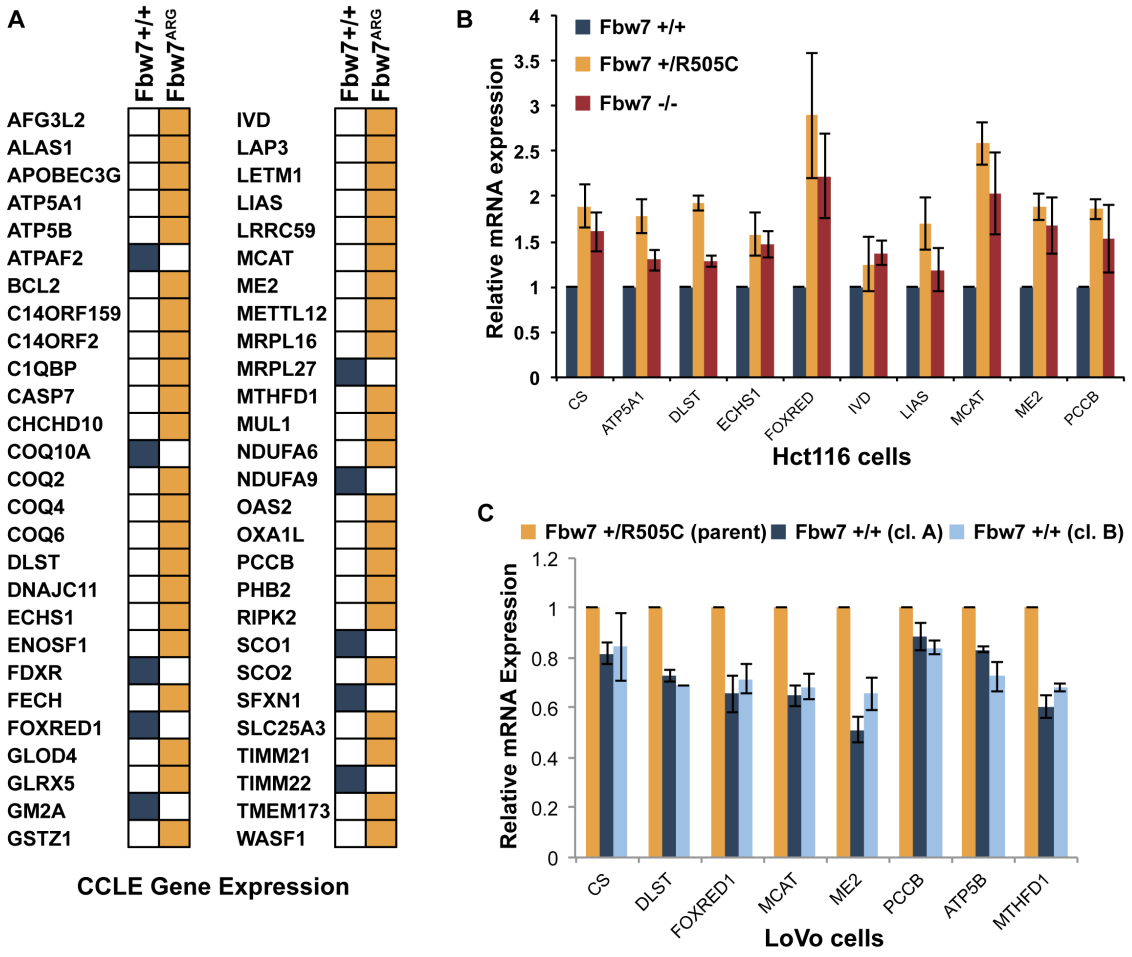

Figure 3.1. Fbw7 mutations increase gene expression of mitochondrial signature genes.
(**A**) cBioPortal (68,69) was used to determine the mean gene expression z-score from both $Fbw7^{+/+}$ (n = 38) and $Fbw7^{ARG}$ (n = 11) CRC cell lines indexed in the Cancer Cell Line Encyclopedia. Blue boxes indicate genes whose mean expression was found to be higher in $Fbw7^{+/+}$ cells; yellow boxes indicate genes whose mean expression was found to be higher in $Fbw7^{ARG}$ cells. (**B**) Quantitative RT-PCR analysis of gene expression of a subset of mitochondrial signature genes in isogenic Hct116 cells that were targeted at the endogenous locus to generate $Fbw7^{+/+}$, $Fbw7^{+/R505C}$, or $Fbw7^{-/-}$ cell lines. Data represent means ± s.e.m. of at least two biological replicates. (**C**) Quantitative RT-PCR analysis of a subset of mitochondrial signature genes in isogenic LoVo cell lines that were gene targeted at the endogenous locus to revert the naturally occurring heterozygous $Fbw7^{R505C}$ allele present in LoVo cells. Two independent Fbw7 wild type clones were isolated and profiled (cl. A and cl. B). Data represent means ± s.e.m. of at least two biological replicates.

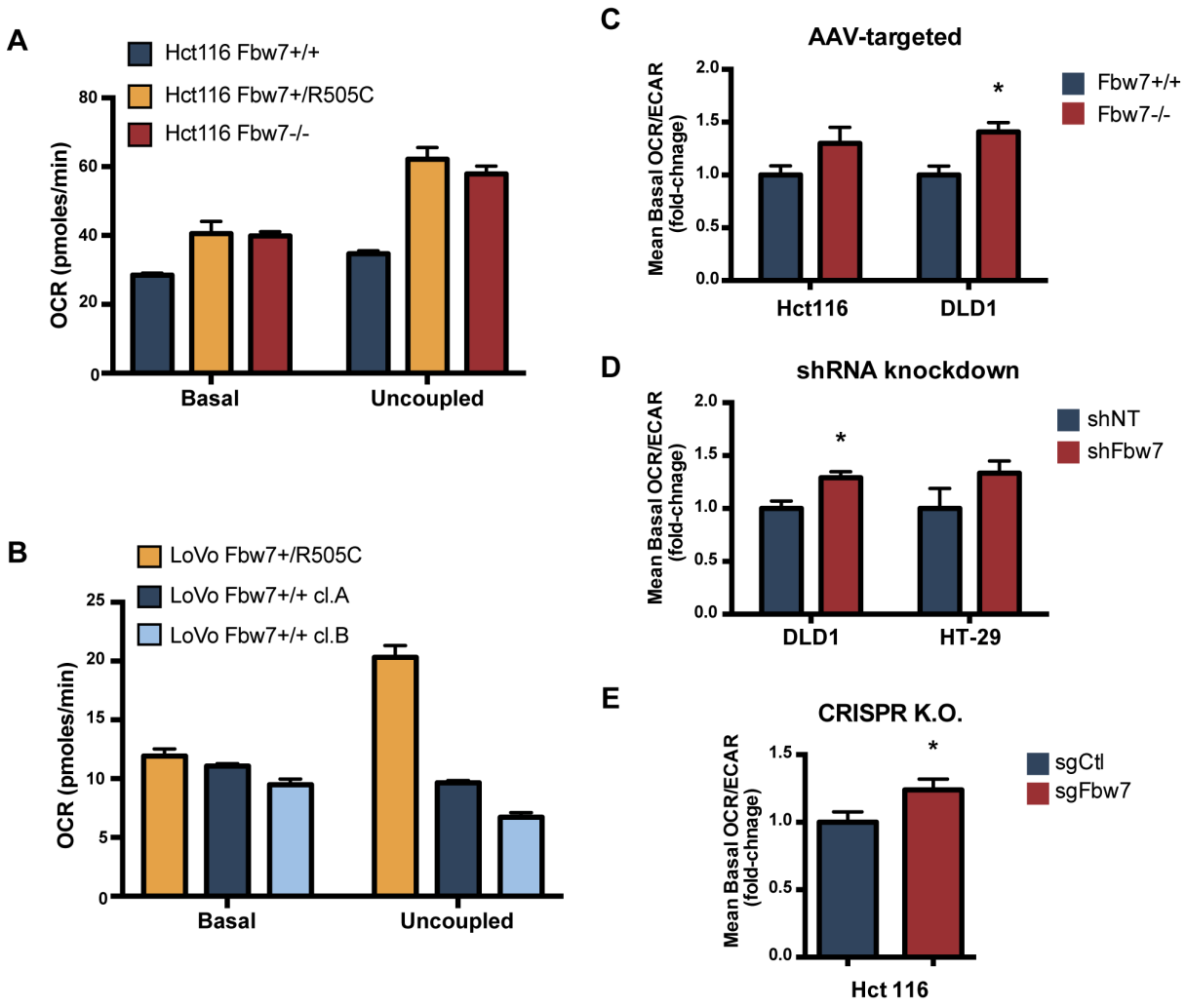

Figure 3.2. Impairing Fbw7 function increases oxidative metabolism in CRC cell lines.
(A) The metabolic profile of Hct116 heterozygous arginine ($Fbw7^{+/R505C}$) and homozygous null ($Fbw7^{-/-}$) knock-in cell lines was measured using the Seahorse Extracellular Flux analyzer to determine oxygen consumption rates (OCR) under both resting conditions (Basal) and following treatment with the mitochondrial uncoupling agent FCCP, thus revealing the maximal mitochondrial respiration (Uncoupled). OCR was normalized to total cell numbers. (**B**) LoVo cells, which naturally have a heterozygous mutation in Fbw7 (+/R505C) were reverted to wild-type using AAV-mediated gene targeting. Two independent wild-type reverted clones (cl.A and cl.B) were profiled for oxygen consumption rate, as described in (A). (**C**) Hct116 and DLD1 $Fbw7^{+/+}$ and $Fbw7^{-/-}$ cells were generated by AAV-mediated gene targeting. Basal OCR and extracellular acidification rates (ECAR) in proliferating cultures were measured using the Seahorse Extracellular Flux bioanalyzer and are presented as the ratio of OCR/ECAR. (**D**) DLD1 and HT-29 cells stably expressing either control or FBXW7 shRNA were analyzed as described in (C). (**E**) Hct116 Fbw7 knockout cells were generated by infecting cells with either control sgRNA (sgCtl) or FBXW7 sgRNA (sgFbw7) along with Cas9 endonuclease. Three independent clones for each sgRNA were isolated, and measured as described in (C). The mean OCR/ECAR ratio of pooled results from the three clones is presented. For all panels, error bars represent s.e.m.

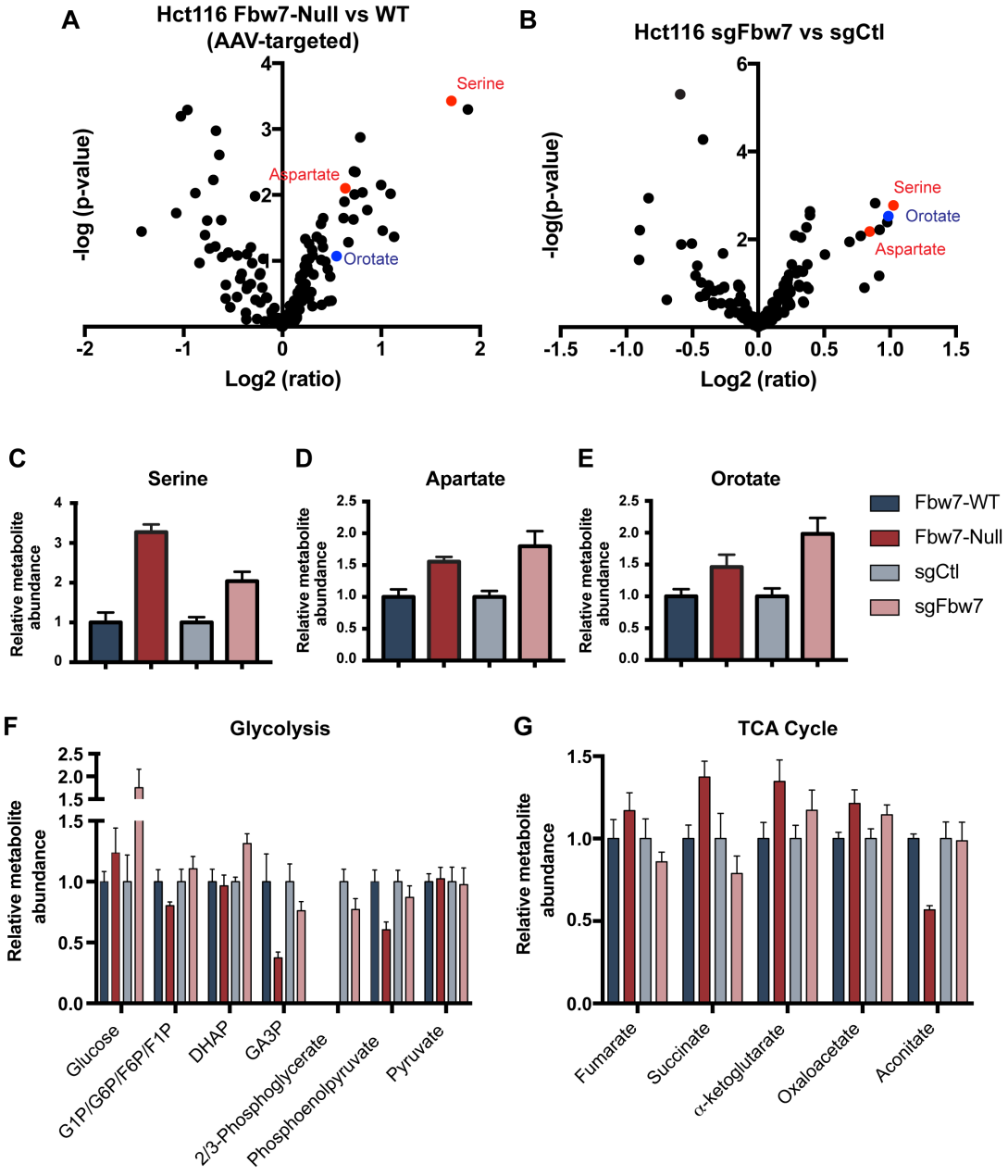

Figure 3.3. Fbw7 mutations change amino acid, orotate, glycolytic, and TCA cycle metabolite levels. Targeted LC-MS metabolomics was performed on Fbw7-deficient cells to determine altered metabolic pathways. (**A**) Volcano plots depicting –log(p-value) vs. Log2(ratio) of metabolite abundance in Hct116 Fbw7$^{-/-}$ cells compared to Hct116 Fbw7$^{+/+}$ cells. Three highly-upregulated metabolites—serine, aspartate, and orotate—are shown in red, red, and blue, respectively. Data were collected from four biological replicate samples and normalized to total protein abundance. (**B**) Same analysis as (A), except showing Hct116 sgFbw7 cells compared to Hct116 sgCtl cells. Data shown are pooled from three independent biological replicates of three separate sgCtl clones and three separate sgFbw7 clones (a total of nine replicates for each genotype). Normalized mean intracellular metabolite levels for (**C**) Serine, (**D**) Aspartate, and (**E**) Orotate in Hct116 Fbw7$^{+/+}$ and Fbw7$^{-/-}$ cells, and Hct116 sgCtl and sgFbw7 cells. Error bars represent s.e.m. (**F**) Same as (C), except presenting data for glycolytic metabolites. (**G**) Same as (C) except presenting data for TCA cycle metabolites.

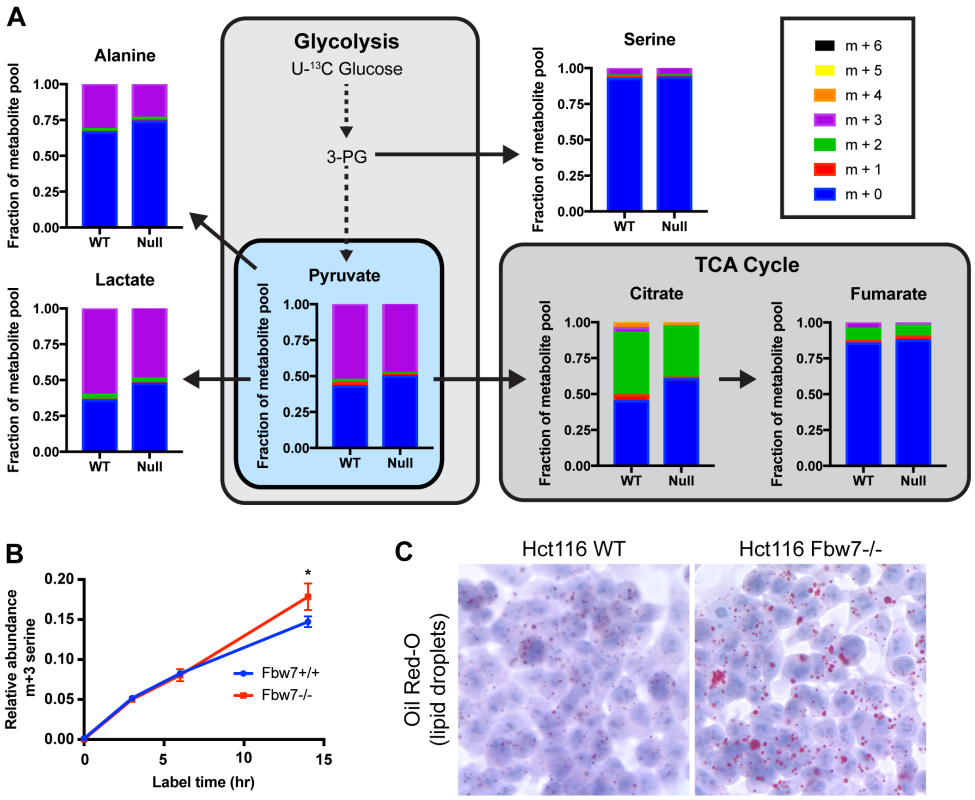

Figure 3.4. Altered glucose utilization in Fbw7$^{-/-}$ cells is revealed by U-^{13}C-glucose flux.
(**A**). Hct116 Fbw7$^{+/+}$ and Fbw7$^{-/-}$ cells were labeled with U-^{13}C-glucose for 3 hours and the incorporation of heavy carbon into downstream metabolites was measured using GC-MS. Direct metabolism of glucose carbons into pyruvate, alanine, lactate, and serine is indicated by the m+3 isotope. Direct incorporation of glucose-derived carbons into citrate and fumarate (TCA cycle intermediates) is depicted by the m+2 isotope, as these are derived from acetyl-CoA. Data presented are mean values from three independent biologic replicates. (**B**) The fractional abundance of m+3 labeled serine was measured as described in (A). m+3 peak represents the serine that is synthesized from glucose via 3-phosphoglycerate. (**C**) Hct116 Fbw7$^{+/+}$ and Fbw7$^{-/-}$ cells were stained with Oil Red-O, which is a marker of lipid droplets. Images shown are representative micrographs.

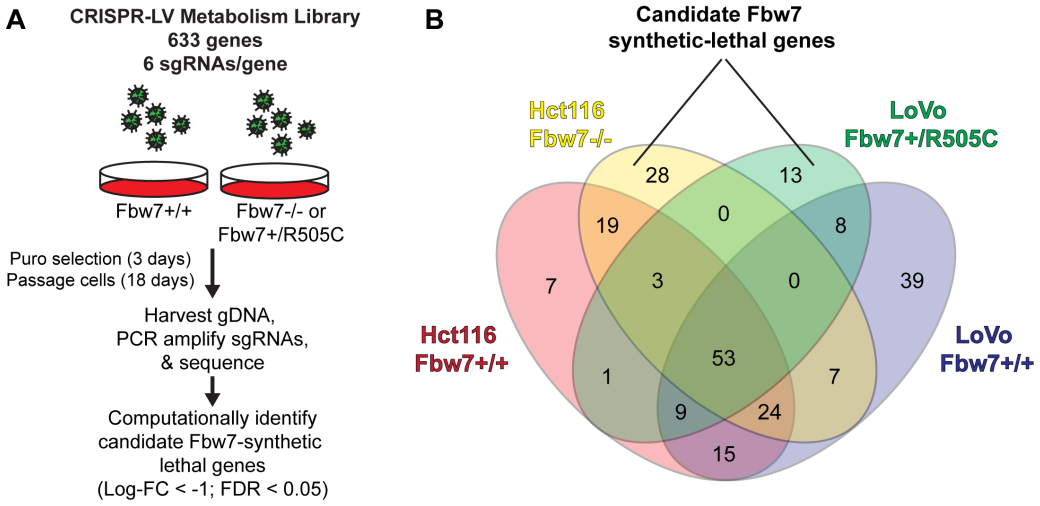

C

Hct116-specific sgRNAs	
ACAD9_6	IK_2
ATP6V0D1_5	IVD_4
ATP6V1B2_2	NDUFA2_5
CMAS_5	NDUFB9_4
COASY_1	NDUFS1_2
DARS_2	PDXDC1_2
DHODH_4	PTS_2
DHODH_5	SOD2_6
DHODH_6	TARS_3
EHMT1_5	TPI1_5
EPRS_5	UMPS_6
FPGS_5	YARS2_3
IARS2_1	ZNF259_2
IDI1_5	ZNF259_6

D

LoVo-specific sgRNAs
ADHFE1_5
AKR1C1_4
DPYD_5
ENPP2_2
GCDH_4
GLS_6
GPI_2
HNMT_6
NASP_6
SEPHS1_4
SLC1A3_3
SLC7A1_6
TRMT11_5

Figure 3.5. A targeted CRISPR-Cas9 screen identifies candidate synthetic lethal genes in Fbw7-mutant CRC cells.

(**A**) Schematic depicting the workflow for the CRISPR-Cas9 screen using a targeted sgRNA library of 633 genes with roles in cellular metabolism. Each gene was represented with six independent sgRNAs, for a total library size of 3,798 sgRNAs. sgRNAs and Cas9 were transduced into target cells (Hct116 $Fbw7^{+/+}$ and $Fbw7^{-/-}$; LoVo $Fbw7^{+/R505C}$ and $Fbw7^{+/+}$) using lentiviruses. Candidate synthetic lethal sgRNAs were defined computationally as those that were specifically lost from the Fbw7-mutant population of isogenic cells using defined criteria (Log-FC < -1; FDR < 0.05). (**B**) Venn diagram depicting the overlap of candidate lethal sgRNAs between each cell line. (**C**) List of candidate sgRNAs that are synthetic-lethal with Fbw7 mutations in corresponding cellular background.

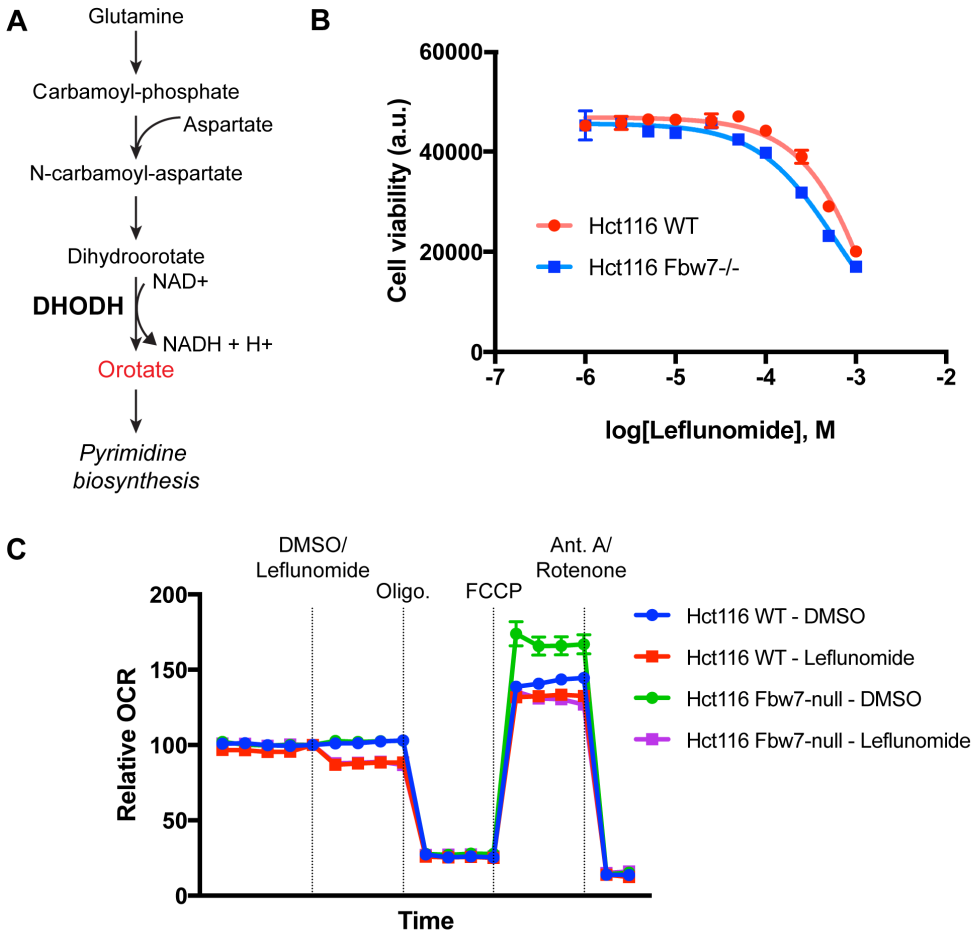

Figure 3.6. Hct116 Fbw7$^{-/-}$ cells are hypersensitive to DHODH inhibition.
(**A**) Overview of key reactions in pyrimidine biosynthesis. The enzyme dihydroorotate dehydrogenase (DHODH) converts dihydroorotate into orotate (shown in red) while also generating a NADH that is incorporated directly into the electron transport chain. (**B**) Hct116 Fbw7$^{+/+}$ and Fbw7$^{-/-}$ were treated with increasing doses of the DHODH inhibitor leflunomide for 96 hours and then assayed for viability using alamar blue. Data presented are means of replicate wells ± s.e.m. (**C**) The effect of the DHODH inhibitor leflunomide on the oxygen consumption ratio (OCR) of Hct116 Fbw7$^{+/+}$ and Fbw7$^{-/-}$ cells was measured using the Seahorse Bioanalyzer. To easily visualize the effect of leflunomide on OCR irrespective of starting respiration rate, all plots were normalized to basal respiration. Vertical lines on the plot indicate the addition of the indicated compound(s) to the assay plate. Oligomycin (Oligo.) inhibits ATP synthase; FCCP uncouples respiration from the ETC; Antimycin A (Ant. A) and Rotenone completely block respiration.

Table 3.1. Enrichment of mitochondrial genes in multiple human tumors identified using transfer learning across TCGA cohorts.

	Scenario 1: Separate Analysis	**Scenario 2: Joint Analysis**
Tumor Type	*Enrichment Score / Ranking*	*Enrichment Score / Ranking*
BLCA	0.3410 / 118	6.9312 / 3
COADREAD	1.6000 / 25	5.3781 / 1
HNSC	20.0874 / 1	4.0755 / 3
LUSC	NA / NA	0.0089 / 149
UCEC	6.3895 / 11	5.3919 / 5

Table 3.2. Quantitative RT-PCR primer sequences

Gene	Forward Primer	Reverse Primer
MTHFD1	5’-GCGCCAGCAGAAATCCTGA-3’	5’-GCGCCAGCAGAAATCCTGA-3’
CS	5’-ATGGCTTTACTTACTGCGGC-3’	5’-AATTCGTGGAGGAAGCACTG-3’
ATP5A1	5’-TTGGGTTCATCTTTCATTGC-3’	5’-GCTCCAAGAATACGCTCTTCA-3’
ATP5B	5’-AAACAATTTGCTCCCATTCATGC-3’	5’-GACAACCTTGATACCAGTCACC-3’
DLST	5’-TCTGAAGGAGGCCCAGAATA-3’	5’-AAAGCCTCTTTGTGCCGAG-3’
ECHS1	5’-CGTGTCCTGCTGTCCTGC-3’	5’-CCACGGTGTTATTCTTCCCT-3’
FOXRED1	5’-CGCAGAGGAGGCTTTTCTC-3’	5’-TGGCTGGTGTCTTGCAGTAG-3’
IVD	5’-AATTTTGGAAGCAGCTGGG-3’	5’-TATCTCCTCCATCACCAGCA-3’
LIAS	5’-CATTATACTGCAAGTGGCCC-3’	5’-TGTGATCTTGAAGGTCTTGTTGA-3’
MCAT	5’-AGCCATGGAATTTGCTGAAG-3’	5’-GAGGACAGACAGCATCCCAC-3’
ME2	5’-CGGGTGTACCTCCTGTCG-3’	5’-GCCAAAGTACAAGTGGTGGAA-3’
PCCB	5’-CACGGATCCAAGAAGGAGTG-3’	5’-GGCCCATGATCAGAGAAATC-3’
ACTB	5’-GCACAGAGCCTCGCCTT-3’	5’-GTTGTCGACGACGAGCG-3’
36B4	5’-CATGTTGCTGGCCAATAAGG-3’	5’-TGGTGATACCTAAAGCCTGGAA-3’

Chapter 4. Summary and Future Directions

4.1 Summary

Fbw7 is the substrate receptor of an SCF E3 ubiquitin ligase that has a large and diverse network of substrates. It is also a frequently mutated tumor suppressor in a number of human cancers, and genetically engineered mouse models (GEMMs) have confirmed Fbw7 to be a driver of tumorigenesis. Fbw7 also plays a role during normal development, and its function is particularly important for various stem cell compartments (183).

Attempts to understand how Fbw7 mutations contribute to cancer formation have largely focused on trying to connect either established or novel substrates to observed tumor phenotypes. The work described here expands the Fbw7 field in two critical ways. First, we have shown in Chapter 2 that identifying additional factors controlling Fbw7-substrate interactions is crucial to understanding the timing and regulation of substrate degradation. Future studies that detail these regulatory mechanisms will be essential to achieve a complete understanding of the Fbw7 pathway. Second, the work described in Chapter 3 identifies altered cellular metabolism as a key consequence of Fbw7 mutations in CRC. Furthermore, we suggest that while it can be conceptually useful to attribute specific cancer phenotypes to single substrates (and may be true in select cases, such as Notch in T-ALL), this likely underestimates the complex biologic changes associated with Fbw7 mutations, due to its large pool of transcription factor substrates with overlapping functions. It is provocative to consider that complex deregulation of cellular transcription due to the coordinate stabilization of multiple transcription factor substrates could be the net oncogenic effect of Fbw7 mutations in tumors.

4.1.1 *PP2A-B56 regulates cyclin E stability at the G1/S transition*

The identification of novel substrates is a dominant theme of the Fbw7 literature; less well studied are the other factors that control substrate recognition and ubiquitylation by SCF^{Fbw7}, such as regulators of CPD phosphorylation or substrate deubiquitylation. Indeed, altering the activities of either of these processes could have similar functional outcomes as Fbw7 inactivation, at least for the particular substrate on which they are acting. Furthermore, analyses of substrate CPD phosphorylation have primarily focused on the relevant kinases (22,36) while less attention has been given to the corresponding phosphatases, even though it is the net balance of these enzymes that determines whether a substrate can be bound by Fbw7. To our knowledge, Myc, Jun, and cyclin E are the only Fbw7 substrates where dephosphorylation of CPD phosphosites has been described (113,114,130,184). Therefore, understanding how phosphatases impact substrate recognition and ubiquitylation by SCF^{Fbw7} remains an understudied aspect of the field.

My work in this area focused on the dephosphorylation of cyclin E, which is a particularly interesting case because autophosphorylation at serine 384 by the bound molecule of CDK2 is the key event that triggers Fbw7 binding, a conundrum we termed the autocatalytic paradox. We found that the PP2A-B56 phosphatase specifically dephosphorylates cyclin E at S384 but not the other two CPD phosphosites, T62 or T380. This dephosphorylation is required to accumulate catalytically active cyclin E-CDK2 complexes at the G1-S transition, and RNAi-mediated knockdown of PP2A-B56 complexes results in the increased degradation of the active pool of cyclin E. Interestingly, the activity of PP2A-B56 towards S384 is high in interphase but low in prometaphase. Thus, changes in phosphatase activity enable the accumulation of active cyclin E-CDK2 complexes during the periods of the cell cycle when cyclin E activity is most required and the turnover of these same complexes at points in the cell cycle when cyclin E

activity is detrimental. B56 subunits are also amplified in the same human cancers where aberrant cyclin E activity is thought to be a driving event in tumor formation, including breast and ovarian cancers. Therefore, while PP2A complexes are commonly thought of as acting as tumor suppressors, these data suggest that they could have context-specific oncogenic functions as well.

4.1.2 *Fbw7 mutations shift CRC cells toward oxidative metabolism*

There is a significant appreciation for the fundamental role that metabolic alterations have in tumorigenesis. While metabolic functions have been described for a number of Fbw7 substrates, the consequences of impaired Fbw7 activity itself have not been thoroughly investigated, particularly in regards to carcinogenesis. Using novel computational methods to analyze TCGA gene expression datasets, we identified mitochondrial and metabolic dysregulation as a highly conserved feature of Fbw7 mutations in a number of different tumor types.

We studied the role of Fbw7 specifically in colorectal cancer metabolism. Interestingly, cells with impaired Fbw7 function were rewired towards oxidative metabolism and there was no evidence for increased aerobic glycolysis, or Warburg metabolism. While several Fbw7 substrates have been implicated in regulating either oxidative or glycolytic metabolism, or both, these data suggest that the net effect of Fbw7 mutations is to shift cells towards oxidative metabolism. Additional changes in other metabolic pathways, including amino acid and nucleotide biosynthesis, were also observed in $Fbw7^{-/-}$ cells, suggestive of widespread alterations in core metabolic pathways.

Metabolic changes often present therapeutic opportunities for the treatment of tumors harboring specific mutations. Utilizing a genetic knockout screen, we identified many genes whose activity may be required in cells with Fbw7 mutations, including dihydroorotate

dehydrogenase (DHODH), an enzyme in the pyrimidine biosynthetic pathway. This was validated using a specific inhibitor of DHODH, leflunomide, and Seahorse profiling showed that there was a specific effect of leflunomide on Fbw7$^{-/-}$ cells' mitochondrial reserve capacity. Moreover, steady-state metabolomics data identified upregulation of both upstream (aspartate) and downstream (orotate) metabolites as specifically upregulated in Fbw7$^{-/-}$ cells. Together, these data connect phenotypic profiles of oxidative metabolism, steady-state metabolites, and inhibitor sensitivity to Fbw7 mutations in CRC cells, and suggest that additional explorations of metabolic deregulation in Fbw7-mutant tumors could lead to new therapeutic strategies. Moreover, given the prominence of Fbw7 as a tumor suppressor, understanding the changes in cancer cell metabolism upon its inactivation is a largely understudied aspect of the Fbw7 field.

4.2 Future Directions

4.2.1 *Opposition of Fbw7 substrate degradation by dephosphorylation*

The finding that PP2A-B56 phosphatases oppose cyclin E degradation suggests numerous opportunities for future studies of the regulation of CPD phosphorylation. On a general level, it is interesting to speculate that degron dephosphorylation may be important for other Fbw7 substrates beyond cyclin E, Myc, and Jun. This could represent a general mechanism controlling substrate recognition by Fbw7, and would provide an additional level of regulation to fine-tune the timing of substrate degradation. Interestingly, substrate CPDs are regulated by a variety of phosphatases: Myc is dephosphorylated by PP2A-B56α (although this was reported to stabilize the protein), Jun by PP2A-B55α (although this did not change steady-state Jun abundance), and cyclin E by PP2A-B55β and/or PP2A-B56 complexes. If CPD dephosphorylation is shown for

other substrates, it will be particularly interesting to see whether additional PP2A complexes—or even other serine/threonine phosphatases—perform this regulation. It is intriguing to imagine a situation where phosphorylation by GSK3-β primes a large network of Fbw7 substrates for degradation, but the differential actions of distinct phosphatases (which themselves could be regulated in a cell cycle- or localization-specific manner) dictates the substrate pool that is accessible to Fbw7.

One of the more interesting findings from this work was that B56 subunits are amplified in a number of different cancers—including those for which aberrant cyclin E activity is thought to be driving tumorigenesis. This runs counter to the prevailing thinking that PP2A complexes are tumor suppressors and suggests that they could have oncogenic functions in certain contexts. Because CCNE1 and B56 amplifications are nearly mutually exclusive with one another, it is tempting to speculate that they are acting in the same pathway, and therefore performing similar functions during transformation. Future work will need to determine whether tumors or cell lines that harbor amplifications of B56 subunits have increased cyclin E activity and protein stability, thereby increasing the CDK activity of the cell. If true, it would further highlight the oncogenic role of cyclin E in those cancers, and could perhaps provide new ways of thinking about how to therapeutically target those tumors.

4.2.2 *Phenotypic consequences of Fbw7 mutations in tumors*

Colorectal cancer is both a common and relatively lethal cancer, with an estimated total of over 1,000,000 annual new cases and over 600,000 annual deaths worldwide (185). A significant proportion of these tumors contain Fbw7 mutations (Table 1.2); therefore, mechanistic insights leading to novel treatment strategies—such as our work with the DHODH inhibitor leflunomide—could have the opportunity to help a large number of patients. Moreover,

other cancers, including T-ALL, also contain a substantial fraction of Fbw7 mutations. Therefore, it will be important to perform similar studies of metabolic regulation in other tumor types to achieve a comprehensive, tissue-specific, understanding of the effects of Fbw7 mutations on cancer cell metabolism.

Perhaps the most important finding from this work was the increased sensitivity of Fbw7-mutant cells to leflunomide. The widespread metabolic changes in Fbw7-mutant CRC cells suggests that simultaneous targeting of other metabolic pathways could synergize with leflunomide treatment to specifically eliminate Fbw7-mutant cells. One obvious candidate for this approach is the serine biosynthetic pathway. Serine was specifically elevated in a number of Fbw7-deficient cells, also has roles in nucleotide biosynthesis, and small molecule inhibitors of PHGDH—the first enzyme in the serine synthesis pathway—have recently been described (186,187). A second possibility for combinational therapy is to determine if leflunomide synergizes with S-phase poisons, such as the DNA polymerase inhibitor aphidicolin or the ribonucleotide reductase inhibitor hydroxyurea. Our lab and others have shown that inappropriately high CDK2 activity during S-phase results in remarkable sensitization to these inhibitors, and Fbw7-mutant cells have elevated levels of cyclin E. Thus, unbalanced nucleotide pools created by low doses of leflunomide could generate enough replication stress that, in combination with elevated levels of cyclin E-associated kinase activity, could result in a larger therapeutic window when combined with S-phase poisons.

Finally, an important next step towards understanding the full effects of Fbw7 mutations on tumor metabolism will be to undertake *in vivo* studies in GEMMs. Tissue culture systems are able to provide important insights into the metabolic deregulation caused by Fbw7 mutations. However, they fail to model all of the *in vivo* constraints and demands of metabolism, including

limited oxygen and nutrient availability. Studying CRC *in vivo* also recapitulates the complex interplay of the gut epithelium with the intestinal microbiome, including the sharing of metabolic byproducts such as short-chain fatty acids (188). Thus, *in vivo* studies will likely be necessary to fully understand how Fbw7-mediated changes in metabolic regulation contribute to the development of CRC.

BIBLIOGRAPHY

1. Finley, D. (2009) Recognition and processing of ubiquitin-protein conjugates by the proteasome. *Annu Rev Biochem* **78**, 477-513
2. Hershko, A., and Ciechanover, A. (1998) The ubiquitin system. *Annu Rev Biochem* **67**, 425-479
3. Deshaies, R. J., and Joazeiro, C. A. (2009) RING domain E3 ubiquitin ligases. *Annu Rev Biochem* **78**, 399-434
4. Skaar, J. R., Pagan, J. K., and Pagano, M. (2013) Mechanisms and function of substrate recruitment by F-box proteins. *Nat Rev Mol Cell Biol* **14**, 369-381
5. Lee, E. K., and Diehl, J. A. (2014) SCFs in the new millennium. *Oncogene* **33**, 2011-2018
6. Spruck, C. H., Strohmaier, H., Sangfelt, O., Müller, H. M., Hubalek, M., Müller-Holzner, E., Marth, C., Widschwendter, M., and Reed, S. I. (2002) hCDC4 gene mutations in endometrial cancer. *Cancer Res* **62**, 4535-4539
7. Hao, B., Oehlmann, S., Sowa, M. E., Harper, J. W., and Pavletich, N. P. (2007) Structure of a Fbw7-Skp1-cyclin E complex: multisite-phosphorylated substrate recognition by SCF ubiquitin ligases. *Mol Cell* **26**, 131-143
8. Orlicky, S., Tang, X., Willems, A., Tyers, M., and Sicheri, F. (2003) Structural basis for phosphodependent substrate selection and orientation by the SCFCdc4 ubiquitin ligase. *Cell* **112**, 243-256
9. Tang, X., Orlicky, S., Lin, Z., Willems, A., Neculai, D., Ceccarelli, D., Mercurio, F., Shilton, B. H., Sicheri, F., and Tyers, M. (2007) Suprafacial orientation of the SCFCdc4 dimer accommodates multiple geometries for substrate ubiquitination. *Cell* **129**, 1165-1176
10. Welcker, M., and Clurman, B. E. (2007) Fbw7/hCDC4 dimerization regulates its substrate interactions. *Cell Div* **2**, 7
11. Welcker, M., Larimore, E. A., Swanger, J., Bengoechea-Alonso, M. T., Grim, J. E., Ericsson, J., Zheng, N., and Clurman, B. E. (2013) Fbw7 dimerization determines the specificity and robustness of substrate degradation. *Genes Dev* **27**, 2531-2536
12. Zhang, W., and Koepp, D. M. (2006) Fbw7 isoform interaction contributes to cyclin E proteolysis. *Mol Cancer Res* **4**, 935-943
13. Bonetti, P., Davoli, T., Sironi, C., Amati, B., Pelicci, P. G., and Colombo, E. (2008) Nucleophosmin and its AML-associated mutant regulate c-Myc turnover through Fbw7 gamma. *J Cell Biol* **182**, 19-26
14. Ekholm-Reed, S., Goldberg, M. S., Schlossmacher, M. G., and Reed, S. I. (2013) Parkin-dependent degradation of the F-box protein Fbw7β promotes neuronal survival in response to oxidative stress by stabilizing Mcl-1. *Mol Cell Biol* **33**, 3627-3643
15. Grim, J. E., Gustafson, M. P., Hirata, R. K., Hagar, A. C., Swanger, J., Welcker, M., Hwang, H. C., Ericsson, J., Russell, D. W., and Clurman, B. E. (2008) Isoform- and cell cycle-dependent substrate degradation by the Fbw7 ubiquitin ligase. *J Cell Biol* **181**, 913-920
16. Matsumoto, A., Tateishi, Y., Onoyama, I., Okita, Y., Nakayama, K., and Nakayama, K. I. (2011) Fbxw7β resides in the endoplasmic reticulum membrane and protects cells from oxidative stress. *Cancer Sci* **102**, 749-755

17. van Drogen, F., Sangfelt, O., Malyukova, A., Matskova, L., Yeh, E., Means, A. R., and Reed, S. I. (2006) Ubiquitylation of cyclin E requires the sequential function of SCF complexes containing distinct hCdc4 isoforms. *Mol Cell* **23**, 37-48
18. Welcker, M., Orian, A., Grim, J. E., Grim, J. A., Eisenman, R. N., and Clurman, B. E. (2004) A nucleolar isoform of the Fbw7 ubiquitin ligase regulates c-Myc and cell size. *Curr Biol* **14**, 1852-1857
19. Koepp, D. M., Schaefer, L. K., Ye, X., Keyomarsi, K., Chu, C., Harper, J. W., and Elledge, S. J. (2001) Phosphorylation-dependent ubiquitination of cyclin E by the SCFFbw7 ubiquitin ligase. *Science* **294**, 173-177
20. Nash, P., Tang, X., Orlicky, S., Chen, Q., Gertler, F. B., Mendenhall, M. D., Sicheri, F., Pawson, T., and Tyers, M. (2001) Multisite phosphorylation of a CDK inhibitor sets a threshold for the onset of DNA replication. *Nature* **414**, 514-521
21. Strohmaier, H., Spruck, C. H., Kaiser, P., Won, K. A., Sangfelt, O., and Reed, S. I. (2001) Human F-box protein hCdc4 targets cyclin E for proteolysis and is mutated in a breast cancer cell line. *Nature* **413**, 316-322
22. Welcker, M., Singer, J., Loeb, K. R., Grim, J., Bloecher, A., Gurien-West, M., Clurman, B. E., and Roberts, J. M. (2003) Multisite phosphorylation by Cdk2 and GSK3 controls cyclin E degradation. *Mol Cell* **12**, 381-392
23. Welcker, M., and Clurman, B. E. (2008) FBW7 ubiquitin ligase: a tumour suppressor at the crossroads of cell division, growth and differentiation. *Nat Rev Cancer* **8**, 83-93
24. Crusio, K. M., King, B., Reavie, L. B., and Aifantis, I. (2010) The ubiquitous nature of cancer: the role of the SCF(Fbw7) complex in development and transformation. *Oncogene* **29**, 4865-4873
25. Network, C. G. A. (2012) Comprehensive molecular portraits of human breast tumours. *Nature* **490**, 61-70
26. Network, C. G. A. R. (2011) Integrated genomic analyses of ovarian carcinoma. *Nature* **474**, 609-615
27. Clurman, B. E., Sheaff, R. J., Thress, K., Groudine, M., and Roberts, J. M. (1996) Turnover of cyclin E by the ubiquitin-proteasome pathway is regulated by cdk2 binding and cyclin phosphorylation. *Genes Dev* **10**, 1979-1990
28. Minella, A. C., Loeb, K. R., Knecht, A., Welcker, M., Varnum-Finney, B. J., Bernstein, I. D., Roberts, J. M., and Clurman, B. E. (2008) Cyclin E phosphorylation regulates cell proliferation in hematopoietic and epithelial lineages in vivo. *Genes Dev* **22**, 1677-1689
29. Won, K. A., and Reed, S. I. (1996) Activation of cyclin E/CDK2 is coupled to site-specific autophosphorylation and ubiquitin-dependent degradation of cyclin E. *EMBO J* **15**, 4182-4193
30. Keck, J. M., Summers, M. K., Tedesco, D., Ekholm-Reed, S., Chuang, L. C., Jackson, P. K., and Reed, S. I. (2007) Cyclin E overexpression impairs progression through mitosis by inhibiting APC(Cdh1). *J Cell Biol* **178**, 371-385
31. Loeb, K. R., Kostner, H., Firpo, E., Norwood, T., D Tsuchiya, K., Clurman, B. E., and Roberts, J. M. (2005) A mouse model for cyclin E-dependent genetic instability and tumorigenesis. *Cancer Cell* **8**, 35-47
32. Minella, A. C., Swanger, J., Bryant, E., Welcker, M., Hwang, H., and Clurman, B. E. (2002) p53 and p21 form an inducible barrier that protects cells against cyclin E-cdk2 deregulation. *Curr Biol* **12**, 1817-1827

33. Minella, A. C., Grim, J. E., Welcker, M., and Clurman, B. E. (2007) p53 and SCFFbw7 cooperatively restrain cyclin E-associated genome instability. *Oncogene* **26**, 6948-6953
34. Spruck, C. H., Won, K. A., and Reed, S. I. (1999) Deregulated cyclin E induces chromosome instability. *Nature* **401**, 297-300
35. Rajagopalan, H., Jallepalli, P. V., Rago, C., Velculescu, V. E., Kinzler, K. W., Vogelstein, B., and Lengauer, C. (2004) Inactivation of hCDC4 can cause chromosomal instability. *Nature* **428**, 77-81
36. Welcker, M., Orian, A., Jin, J., Grim, J. E., Grim, J. A., Harper, J. W., Eisenman, R. N., and Clurman, B. E. (2004) The Fbw7 tumor suppressor regulates glycogen synthase kinase 3 phosphorylation-dependent c-Myc protein degradation. *Proc Natl Acad Sci U S A* **101**, 9085-9090
37. Yada, M., Hatakeyama, S., Kamura, T., Nishiyama, M., Tsunematsu, R., Imaki, H., Ishida, N., Okumura, F., Nakayama, K., and Nakayama, K. I. (2004) Phosphorylation-dependent degradation of c-Myc is mediated by the F-box protein Fbw7. *EMBO J* **23**, 2116-2125
38. Gregory, M. A., Qi, Y., and Hann, S. R. (2003) Phosphorylation by glycogen synthase kinase-3 controls c-myc proteolysis and subnuclear localization. *J Biol Chem* **278**, 51606-51612
39. Sears, R., Nuckolls, F., Haura, E., Taya, Y., Tamai, K., and Nevins, J. R. (2000) Multiple Ras-dependent phosphorylation pathways regulate Myc protein stability. *Genes Dev* **14**, 2501-2514
40. Bahram, F., von der Lehr, N., Cetinkaya, C., and Larsson, L. G. (2000) c-Myc hot spot mutations in lymphomas result in inefficient ubiquitination and decreased proteasome-mediated turnover. *Blood* **95**, 2104-2110
41. Bhatia, K., Huppi, K., Spangler, G., Siwarski, D., Iyer, R., and Magrath, I. (1993) Point mutations in the c-Myc transactivation domain are common in Burkitt's lymphoma and mouse plasmacytomas. *Nat Genet* **5**, 56-61
42. Fryer, C. J., White, J. B., and Jones, K. A. (2004) Mastermind recruits CycC:CDK8 to phosphorylate the Notch ICD and coordinate activation with turnover. *Mol Cell* **16**, 509-520
43. Gupta-Rossi, N., Le Bail, O., Gonen, H., Brou, C., Logeat, F., Six, E., Ciechanover, A., and Israël, A. (2001) Functional interaction between SEL-10, an F-box protein, and the nuclear form of activated Notch1 receptor. *J Biol Chem* **276**, 34371-34378
44. O'Neil, J., Grim, J., Strack, P., Rao, S., Tibbitts, D., Winter, C., Hardwick, J., Welcker, M., Meijerink, J. P., Pieters, R., Draetta, G., Sears, R., Clurman, B. E., and Look, A. T. (2007) FBW7 mutations in leukemic cells mediate NOTCH pathway activation and resistance to gamma-secretase inhibitors. *J Exp Med* **204**, 1813-1824
45. Wu, G., Lyapina, S., Das, I., Li, J., Gurney, M., Pauley, A., Chui, I., Deshaies, R. J., and Kitajewski, J. (2001) SEL-10 is an inhibitor of notch signaling that targets notch for ubiquitin-mediated protein degradation. *Mol Cell Biol* **21**, 7403-7415
46. Thompson, B. J., Buonamici, S., Sulis, M. L., Palomero, T., Vilimas, T., Basso, G., Ferrando, A., and Aifantis, I. (2007) The SCFFBW7 ubiquitin ligase complex as a tumor suppressor in T cell leukemia. *J Exp Med* **204**, 1825-1835
47. Oberg, C., Li, J., Pauley, A., Wolf, E., Gurney, M., and Lendahl, U. (2001) The Notch intracellular domain is ubiquitinated and negatively regulated by the mammalian Sel-10 homolog. *J Biol Chem* **276**, 35847-35853

48. Weng, A. P., Ferrando, A. A., Lee, W., Morris, J. P., Silverman, L. B., Sanchez-Irizarry, C., Blacklow, S. C., Look, A. T., and Aster, J. C. (2004) Activating mutations of NOTCH1 in human T cell acute lymphoblastic leukemia. *Science* **306**, 269-271
49. Malyukova, A., Dohda, T., von der Lehr, N., Akhoondi, S., Akhondi, S., Corcoran, M., Heyman, M., Spruck, C., Grandér, D., Lendahl, U., and Sangfelt, O. (2007) The tumor suppressor gene hCDC4 is frequently mutated in human T-cell acute lymphoblastic leukemia with functional consequences for Notch signaling. *Cancer Res* **67**, 5611-5616
50. Maser, R. S., Choudhury, B., Campbell, P. J., Feng, B., Wong, K. K., Protopopov, A., O'Neil, J., Gutierrez, A., Ivanova, E., Perna, I., Lin, E., Mani, V., Jiang, S., McNamara, K., Zaghlul, S., Edkins, S., Stevens, C., Brennan, C., Martin, E. S., Wiedemeyer, R., Kabbarah, O., Nogueira, C., Histen, G., Aster, J., Mansour, M., Duke, V., Foroni, L., Fielding, A. K., Goldstone, A. H., Rowe, J. M., Wang, Y. A., Look, A. T., Stratton, M. R., Chin, L., Futreal, P. A., and DePinho, R. A. (2007) Chromosomally unstable mouse tumours have genomic alterations similar to diverse human cancers. *Nature* **447**, 966-971
51. Wei, W., Jin, J., Schlisio, S., Harper, J. W., and Kaelin, W. G. (2005) The v-Jun point mutation allows c-Jun to escape GSK3-dependent recognition and destruction by the Fbw7 ubiquitin ligase. *Cancer Cell* **8**, 25-33
52. Nateri, A. S., Riera-Sans, L., Da Costa, C., and Behrens, A. (2004) The ubiquitin ligase SCFFbw7 antagonizes apoptotic JNK signaling. *Science* **303**, 1374-1378
53. Inuzuka, H., Shaik, S., Onoyama, I., Gao, D., Tseng, A., Maser, R. S., Zhai, B., Wan, L., Gutierrez, A., Lau, A. W., Xiao, Y., Christie, A. L., Aster, J., Settleman, J., Gygi, S. P., Kung, A. L., Look, T., Nakayama, K. I., DePinho, R. A., and Wei, W. (2011) SCF(FBW7) regulates cellular apoptosis by targeting MCL1 for ubiquitylation and destruction. *Nature* **471**, 104-109
54. Wertz, I. E., Kusam, S., Lam, C., Okamoto, T., Sandoval, W., Anderson, D. J., Helgason, E., Ernst, J. A., Eby, M., Liu, J., Belmont, L. D., Kaminker, J. S., O'Rourke, K. M., Pujara, K., Kohli, P. B., Johnson, A. R., Chiu, M. L., Lill, J. R., Jackson, P. K., Fairbrother, W. J., Seshagiri, S., Ludlam, M. J., Leong, K. G., Dueber, E. C., Maecker, H., Huang, D. C., and Dixit, V. M. (2011) Sensitivity to antitubulin chemotherapeutics is regulated by MCL1 and FBW7. *Nature* **471**, 110-114
55. Davis, M. A., Larimore, E. A., Fissel, B. M., Swanger, J., Taatjes, D. J., and Clurman, B. E. (2013) The SCF-Fbw7 ubiquitin ligase degrades MED13 and MED13L and regulates CDK8 module association with Mediator. *Genes Dev* **27**, 151-156
56. Olson, B. L., Hock, M. B., Ekholm-Reed, S., Wohlschlegel, J. A., Dev, K. K., Kralli, A., and Reed, S. I. (2008) SCFCdc4 acts antagonistically to the PGC-1alpha transcriptional coactivator by targeting it for ubiquitin-mediated proteolysis. *Genes Dev* **22**, 252-264
57. Balamurugan, K., Sharan, S., Klarmann, K. D., Zhang, Y., Coppola, V., Summers, G. H., Roger, T., Morrison, D. K., Keller, J. R., and Sterneck, E. (2013) FBXW7α attenuates inflammatory signalling by downregulating C/EBPδ and its target gene Tlr4. *Nat Commun* **4**, 1662
58. Liu, N., Li, H., Li, S., Shen, M., Xiao, N., Chen, Y., Wang, Y., Wang, W., Wang, R., Wang, Q., Sun, J., and Wang, P. (2010) The Fbw7/human CDC4 tumor suppressor targets proproliferative factor KLF5 for ubiquitination and degradation through multiple phosphodegron motifs. *J Biol Chem* **285**, 18858-18867

59. Zhao, D., Zheng, H. Q., Zhou, Z., and Chen, C. (2010) The Fbw7 tumor suppressor targets KLF5 for ubiquitin-mediated degradation and suppresses breast cell proliferation. *Cancer Res* **70**, 4728-4738
60. Bengoechea-Alonso, M. T., and Ericsson, J. (2010) Tumor suppressor Fbxw7 regulates TGFβ signaling by targeting TGIF1 for degradation. *Oncogene* **29**, 5322-5328
61. Wang, Z., Inuzuka, H., Zhong, J., Wan, L., Fukushima, H., Sarkar, F. H., and Wei, W. (2012) Tumor suppressor functions of FBW7 in cancer development and progression. *FEBS Lett* **586**, 1409-1418
62. Akhoondi, S., Sun, D., von der Lehr, N., Apostolidou, S., Klotz, K., Maljukova, A., Cepeda, D., Fiegl, H., Dafou, D., Dofou, D., Marth, C., Mueller-Holzner, E., Corcoran, M., Dagnell, M., Nejad, S. Z., Nayer, B. N., Zali, M. R., Hansson, J., Egyhazi, S., Petersson, F., Sangfelt, P., Nordgren, H., Grander, D., Reed, S. I., Widschwendter, M., Sangfelt, O., and Spruck, C. (2007) FBXW7/hCDC4 is a general tumor suppressor in human cancer. *Cancer Res* **67**, 9006-9012
63. Network, C. G. A. (2012) Comprehensive molecular characterization of human colon and rectal cancer. *Nature* **487**, 330-337
64. Kandoth, C., Schultz, N., Cherniack, A. D., Akbani, R., Liu, Y., Shen, H., Robertson, A. G., Pashtan, I., Shen, R., Benz, C. C., Yau, C., Laird, P. W., Ding, L., Zhang, W., Mills, G. B., Kucherlapati, R., Mardis, E. R., Levine, D. A., and Network, C. G. A. R. (2013) Integrated genomic characterization of endometrial carcinoma. *Nature* **497**, 67-73
65. Kandoth, C., McLellan, M. D., Vandin, F., Ye, K., Niu, B., Lu, C., Xie, M., Zhang, Q., McMichael, J. F., Wyczalkowski, M. A., Leiserson, M. D., Miller, C. A., Welch, J. S., Walter, M. J., Wendl, M. C., Ley, T. J., Wilson, R. K., Raphael, B. J., and Ding, L. (2013) Mutational landscape and significance across 12 major cancer types. *Nature* **502**, 333-339
66. Bengoechea-Alonso, M. T., and Ericsson, J. (2010) The ubiquitin ligase Fbxw7 controls adipocyte differentiation by targeting C/EBPalpha for degradation. *Proc Natl Acad Sci U S A* **107**, 11817-11822
67. Busino, L., Millman, S. E., Scotto, L., Kyratsous, C. A., Basrur, V., O'Connor, O., Hoffmann, A., Elenitoba-Johnson, K. S., and Pagano, M. (2012) Fbxw7α- and GSK3-mediated degradation of p100 is a pro-survival mechanism in multiple myeloma. *Nat Cell Biol* **14**, 375-385
68. Cerami, E., Gao, J., Dogrusoz, U., Gross, B. E., Sumer, S. O., Aksoy, B. A., Jacobsen, A., Byrne, C. J., Heuer, M. L., Larsson, E., Antipin, Y., Reva, B., Goldberg, A. P., Sander, C., and Schultz, N. (2012) The cBio cancer genomics portal: an open platform for exploring multidimensional cancer genomics data. *Cancer Discov* **2**, 401-404
69. Gao, J., Aksoy, B. A., Dogrusoz, U., Dresdner, G., Gross, B., Sumer, S. O., Sun, Y., Jacobsen, A., Sinha, R., Larsson, E., Cerami, E., Sander, C., and Schultz, N. (2013) Integrative analysis of complex cancer genomics and clinical profiles using the cBioPortal. *Sci Signal* **6**, pl1
70. Bialkowska, A. B., Liu, Y., Nandan, M. O., and Yang, V. W. (2014) A colon cancer-derived mutant of Krüppel-like factor 5 (KLF5) is resistant to degradation by glycogen synthase kinase 3β (GSK3β) and the E3 ubiquitin ligase F-box and WD repeat domain-containing 7α (FBW7α). *J Biol Chem* **289**, 5997-6005
71. Olive, V., Sabio, E., Bennett, M. J., De Jong, C. S., Biton, A., McGann, J. C., Greaney, S. K., Sodir, N. M., Zhou, A. Y., Balakrishnan, A., Foth, M., Luftig, M. A., Goga, A.,

Speed, T. P., Xuan, Z., Evan, G. I., Wan, Y., Minella, A. C., and He, L. (2013) A component of the mir-17-92 polycistronic oncomir promotes oncogene-dependent apoptosis. *Elife* **2**, e00822
72. Wang, L., Ye, X., Liu, Y., Wei, W., and Wang, Z. (2014) Aberrant regulation of FBW7 in cancer. *Oncotarget* **5**, 2000-2015
73. Akhoondi, S., Lindström, L., Widschwendter, M., Corcoran, M., Bergh, J., Spruck, C., Grandér, D., and Sangfelt, O. (2010) Inactivation of FBXW7/hCDC4-β expression by promoter hypermethylation is associated with favorable prognosis in primary breast cancer. *Breast Cancer Res* **12**, R105
74. Gu, Z., Mitsui, H., Inomata, K., Honda, M., Endo, C., Sakurada, A., Sato, M., Okada, Y., Kondo, T., and Horii, A. (2008) The methylation status of FBXW7 beta-form correlates with histological subtype in human thymoma. *Biochem Biophys Res Commun* **377**, 685-688
75. Cheng, Y., Chen, G., Martinka, M., Ho, V., and Li, G. (2013) Prognostic significance of Fbw7 in human melanoma and its role in cell migration. *J Invest Dermatol* **133**, 1794-1802
76. Gu, Z., Inomata, K., Mitsui, H., and Horii, A. (2008) Promoter hypermethylation is not the major mechanism for inactivation of the FBXW7 beta-form in human gliomas. *Genes Genet Syst* **83**, 347-352
77. Kimura, T., Gotoh, M., Nakamura, Y., and Arakawa, H. (2003) hCDC4b, a regulator of cyclin E, as a direct transcriptional target of p53. *Cancer Sci* **94**, 431-436
78. Sancho, R., Blake, S. M., Tendeng, C., Clurman, B. E., Lewis, J., and Behrens, A. (2013) Fbw7 repression by hes5 creates a feedback loop that modulates Notch-mediated intestinal and neural stem cell fate decisions. *PLoS Biol* **11**, e1001586
79. Min, S. H., Lau, A. W., Lee, T. H., Inuzuka, H., Wei, S., Huang, P., Shaik, S., Lee, D. Y., Finn, G., Balastik, M., Chen, C. H., Luo, M., Tron, A. E., Decaprio, J. A., Zhou, X. Z., Wei, W., and Lu, K. P. (2012) Negative regulation of the stability and tumor suppressor function of Fbw7 by the Pin1 prolyl isomerase. *Mol Cell* **46**, 771-783
80. Kanatsu-Shinohara, M., Onoyama, I., Nakayama, K. I., and Shinohara, T. (2014) Skp1-Cullin-F-box (SCF)-type ubiquitin ligase FBXW7 negatively regulates spermatogonial stem cell self-renewal. *Proc Natl Acad Sci U S A* **111**, 8826-8831
81. Tetzlaff, M. T., Yu, W., Li, M., Zhang, P., Finegold, M., Mahon, K., Harper, J. W., Schwartz, R. J., and Elledge, S. J. (2004) Defective cardiovascular development and elevated cyclin E and Notch proteins in mice lacking the Fbw7 F-box protein. *Proc Natl Acad Sci U S A* **101**, 3338-3345
82. Tsunematsu, R., Nakayama, K., Oike, Y., Nishiyama, M., Ishida, N., Hatakeyama, S., Bessho, Y., Kageyama, R., Suda, T., and Nakayama, K. I. (2004) Mouse Fbw7/Sel-10/Cdc4 is required for notch degradation during vascular development. *J Biol Chem* **279**, 9417-9423
83. Grim, J. E., Knoblaugh, S. E., Guthrie, K. A., Hagar, A., Swanger, J., Hespelt, J., Delrow, J. J., Small, T., Grady, W. M., Nakayama, K. I., and Clurman, B. E. (2012) Fbw7 and p53 cooperatively suppress advanced and chromosomally unstable intestinal cancer. *Mol Cell Biol* **32**, 2160-2167
84. Hoeck, J. D., Jandke, A., Blake, S. M., Nye, E., Spencer-Dene, B., Brandner, S., and Behrens, A. (2010) Fbw7 controls neural stem cell differentiation and progenitor apoptosis via Notch and c-Jun. *Nat Neurosci* **13**, 1365-1372

85. Sancho, R., Gruber, R., Gu, G., and Behrens, A. (2014) Loss of Fbw7 reprograms adult pancreatic ductal cells into α, δ, and β cells. *Cell Stem Cell* **15**, 139-153
86. Onoyama, I., Suzuki, A., Matsumoto, A., Tomita, K., Katagiri, H., Oike, Y., Nakayama, K., and Nakayama, K. I. (2011) Fbxw7 regulates lipid metabolism and cell fate decisions in the mouse liver. *J Clin Invest* **121**, 342-354
87. Matsuoka, S., Oike, Y., Onoyama, I., Iwama, A., Arai, F., Takubo, K., Mashimo, Y., Oguro, H., Nitta, E., Ito, K., Miyamoto, K., Yoshiwara, H., Hosokawa, K., Nakamura, Y., Gomei, Y., Iwasaki, H., Hayashi, Y., Matsuzaki, Y., Nakayama, K., Ikeda, Y., Hata, A., Chiba, S., Nakayama, K. I., and Suda, T. (2008) Fbxw7 acts as a critical fail-safe against premature loss of hematopoietic stem cells and development of T-ALL. *Genes Dev* **22**, 986-991
88. Thompson, B. J., Jankovic, V., Gao, J., Buonamici, S., Vest, A., Lee, J. M., Zavadil, J., Nimer, S. D., and Aifantis, I. (2008) Control of hematopoietic stem cell quiescence by the E3 ubiquitin ligase Fbw7. *J Exp Med* **205**, 1395-1408
89. Reavie, L., Della Gatta, G., Crusio, K., Aranda-Orgilles, B., Buckley, S. M., Thompson, B., Lee, E., Gao, J., Bredemeyer, A. L., Helmink, B. A., Zavadil, J., Sleckman, B. P., Palomero, T., Ferrando, A., and Aifantis, I. (2010) Regulation of hematopoietic stem cell differentiation by a single ubiquitin ligase-substrate complex. *Nat Immunol* **11**, 207-215
90. Siu, K. T., Xu, Y., Swartz, K. L., Bhattacharyya, M., Gurbuxani, S., Hua, Y., and Minella, A. C. (2014) Chromosome instability underlies hematopoietic stem cell dysfunction and lymphoid neoplasia associated with impaired Fbw7-mediated cyclin E regulation. *Mol Cell Biol* **34**, 3244-3258
91. King, B., Trimarchi, T., Reavie, L., Xu, L., Mullenders, J., Ntziachristos, P., Aranda-Orgilles, B., Perez-Garcia, A., Shi, J., Vakoc, C., Sandy, P., Shen, S. S., Ferrando, A., and Aifantis, I. (2013) The ubiquitin ligase FBXW7 modulates leukemia-initiating cell activity by regulating MYC stability. *Cell* **153**, 1552-1566
92. Babaei-Jadidi, R., Li, N., Saadeddin, A., Spencer-Dene, B., Jandke, A., Muhammad, B., Ibrahim, E. E., Muraleedharan, R., Abuzinadah, M., Davis, H., Lewis, A., Watson, S., Behrens, A., Tomlinson, I., and Nateri, A. S. (2011) FBXW7 influences murine intestinal homeostasis and cancer, targeting Notch, Jun, and DEK for degradation. *J Exp Med* **208**, 295-312
93. Davis, H., Lewis, A., Behrens, A., and Tomlinson, I. (2014) Investigation of the atypical FBXW7 mutation spectrum in human tumours by conditional expression of a heterozygous propellor tip missense allele in the mouse intestines. *Gut* **63**, 792-799
94. Sancho, R., Jandke, A., Davis, H., Diefenbacher, M. E., Tomlinson, I., and Behrens, A. (2010) F-box and WD repeat domain-containing 7 regulates intestinal cell lineage commitment and is a haploinsufficient tumor suppressor. *Gastroenterology* **139**, 929-941
95. Kwon, Y. W., Kim, I. J., Wu, D., Lu, J., Stock, W. A., Liu, Y., Huang, Y., Kang, H. C., DelRosario, R., Jen, K. Y., Perez-Losada, J., Wei, G., Balmain, A., and Mao, J. H. (2012) Pten regulates Aurora-A and cooperates with Fbxw7 in modulating radiation-induced tumor development. *Mol Cancer Res* **10**, 834-844
96. Onoyama, I., Tsunematsu, R., Matsumoto, A., Kimura, T., de Alborán, I. M., Nakayama, K., and Nakayama, K. I. (2007) Conditional inactivation of Fbxw7 impairs cell-cycle exit during T cell differentiation and results in lymphomatogenesis. *J Exp Med* **204**, 2875-2888

97. Reavie, L., Buckley, S. M., Loizou, E., Takeishi, S., Aranda-Orgilles, B., Ndiaye-Lobry, D., Abdel-Wahab, O., Ibrahim, S., Nakayama, K. I., and Aifantis, I. (2013) Regulation of c-Myc ubiquitination controls chronic myelogenous leukemia initiation and progression. *Cancer Cell* **23**, 362-375
98. Takeishi, S., Matsumoto, A., Onoyama, I., Naka, K., Hirao, A., and Nakayama, K. I. (2013) Ablation of Fbxw7 eliminates leukemia-initiating cells by preventing quiescence. *Cancer Cell* **23**, 347-361
99. Davis, H., and Tomlinson, I. (2012) CDC4/FBXW7 and the 'just enough' model of tumourigenesis. *J Pathol* **227**, 131-135
100. Siu, K. T., Rosner, M. R., and Minella, A. C. (2012) An integrated view of cyclin E function and regulation. *Cell Cycle* **11**, 57-64
101. Hwang, H. C., and Clurman, B. E. (2005) Cyclin E in normal and neoplastic cell cycles. *Oncogene* **24**, 2776-2786
102. Chi, Y., Welcker, M., Hizli, A. A., Posakony, J. J., Aebersold, R., and Clurman, B. E. (2008) Identification of CDK2 substrates in human cell lysates. *Genome Biol* **9**, R149
103. Geng, Y., Lee, Y. M., Welcker, M., Swanger, J., Zagozdzon, A., Winer, J. D., Roberts, J. M., Kaldis, P., Clurman, B. E., and Sicinski, P. (2007) Kinase-independent function of cyclin E. *Mol Cell* **25**, 127-139
104. Matsumoto, Y., and Maller, J. L. (2004) A centrosomal localization signal in cyclin E required for Cdk2-independent S phase entry. *Science* **306**, 885-888
105. Ohtsubo, M., and Roberts, J. M. (1993) Cyclin-dependent regulation of G1 in mammalian fibroblasts. *Science* **259**, 1908-1912
106. Bester, A. C., Roniger, M., Oren, Y. S., Im, M. M., Sarni, D., Chaoat, M., Bensimon, A., Zamir, G., Shewach, D. S., and Kerem, B. (2011) Nucleotide deficiency promotes genomic instability in early stages of cancer development. *Cell* **145**, 435-446
107. Costantino, L., Sotiriou, S. K., Rantala, J. K., Magin, S., Mladenov, E., Helleday, T., Haber, J. E., Iliakis, G., Kallioniemi, O. P., and Halazonetis, T. D. (2014) Break-induced replication repair of damaged forks induces genomic duplications in human cells. *Science* **343**, 88-91
108. Smith, A. P., Henze, M., Lee, J. A., Osborn, K. G., Keck, J. M., Tedesco, D., Bortner, D. M., Rosenberg, M. P., and Reed, S. I. (2006) Deregulated cyclin E promotes p53 loss of heterozygosity and tumorigenesis in the mouse mammary gland. *Oncogene* **25**, 7245-7259
109. Moberg, K. H., Bell, D. W., Wahrer, D. C., Haber, D. A., and Hariharan, I. K. (2001) Archipelago regulates Cyclin E levels in Drosophila and is mutated in human cancer cell lines. *Nature* **413**, 311-316
110. Davis, R. J., Welcker, M., and Clurman, B. E. (2014) Tumor suppression by the Fbw7 ubiquitin ligase: mechanisms and opportunities. *Cancer Cell* **26**, 455-464
111. Xu, Y., Swartz, K. L., Siu, K. T., Bhattacharyya, M., and Minella, A. C. (2014) Fbw7-dependent cyclin E regulation ensures terminal maturation of bone marrow erythroid cells by restraining oxidative metabolism. *Oncogene* **33**, 3161-3171
112. Ekholm-Reed, S., Spruck, C. H., Sangfelt, O., van Drogen, F., Mueller-Holzner, E., Widschwendter, M., Zetterberg, A., Reed, S. I., and Reed, S. E. (2004) Mutation of hCDC4 leads to cell cycle deregulation of cyclin E in cancer. *Cancer Res* **64**, 795-800

113. Arnold, H. K., and Sears, R. C. (2006) Protein phosphatase 2A regulatory subunit B56alpha associates with c-myc and negatively regulates c-myc accumulation. *Mol Cell Biol* **26**, 2832-2844
114. Yeh, E., Cunningham, M., Arnold, H., Chasse, D., Monteith, T., Ivaldi, G., Hahn, W. C., Stukenberg, P. T., Shenolikar, S., Uchida, T., Counter, C. M., Nevins, J. R., Means, A. R., and Sears, R. (2004) A signalling pathway controlling c-Myc degradation that impacts oncogenic transformation of human cells. *Nat Cell Biol* **6**, 308-318
115. McCourt, P., Gallo-Ebert, C., Gonghong, Y., Jiang, Y., and Nickels, J. T. (2013) PP2A(Cdc55) regulates G1 cyclin stability. *Cell Cycle* **12**, 1201-1210
116. Shi, Y. (2009) Serine/threonine phosphatases: mechanism through structure. *Cell* **139**, 468-484
117. Wlodarchak, N., and Xing, Y. (2016) PP2A as a master regulator of the cell cycle. *Crit Rev Biochem Mol Biol* **51**, 162-184
118. Wurzenberger, C., and Gerlich, D. W. (2011) Phosphatases: providing safe passage through mitotic exit. *Nat Rev Mol Cell Biol* **12**, 469-482
119. Xu, Y., Chen, Y., Zhang, P., Jeffrey, P. D., and Shi, Y. (2008) Structure of a protein phosphatase 2A holoenzyme: insights into B55-mediated Tau dephosphorylation. *Mol Cell* **31**, 873-885
120. Xu, Y., Xing, Y., Chen, Y., Chao, Y., Lin, Z., Fan, E., Yu, J. W., Strack, S., Jeffrey, P. D., and Shi, Y. (2006) Structure of the protein phosphatase 2A holoenzyme. *Cell* **127**, 1239-1251
121. Ye, X., Nalepa, G., Welcker, M., Kessler, B. M., Spooner, E., Qin, J., Elledge, S. J., Clurman, B. E., and Harper, J. W. (2004) Recognition of phosphodegron motifs in human cyclin E by the SCF(Fbw7) ubiquitin ligase. *J Biol Chem* **279**, 50110-50119
122. Foley, E. A., Maldonado, M., and Kapoor, T. M. (2011) Formation of stable attachments between kinetochores and microtubules depends on the B56-PP2A phosphatase. *Nat Cell Biol* **13**, 1265-1271
123. Hughes, B. T., Sidorova, J., Swanger, J., Monnat, R. J., and Clurman, B. E. (2013) Essential role for Cdk2 inhibitory phosphorylation during replication stress revealed by a human Cdk2 knockin mutation. *Proc Natl Acad Sci U S A* **110**, 8954-8959
124. Swingle, M., Ni, L., and Honkanen, R. E. (2007) Small-molecule inhibitors of ser/thr protein phosphatases: specificity, use and common forms of abuse. *Methods Mol Biol* **365**, 23-38
125. Mitsuhashi, S., Matsuura, N., Ubukata, M., Oikawa, H., Shima, H., and Kikuchi, K. (2001) Tautomycetin is a novel and specific inhibitor of serine/threonine protein phosphatase type 1, PP1. *Biochem Biophys Res Commun* **287**, 328-331
126. Schmitz, M. H., Held, M., Janssens, V., Hutchins, J. R., Hudecz, O., Ivanova, E., Goris, J., Trinkle-Mulcahy, L., Lamond, A. I., Poser, I., Hyman, A. A., Mechtler, K., Peters, J. M., and Gerlich, D. W. (2010) Live-cell imaging RNAi screen identifies PP2A-B55alpha and importin-beta1 as key mitotic exit regulators in human cells. *Nat Cell Biol* **12**, 886-893
127. Cundell, M. J., Bastos, R. N., Zhang, T., Holder, J., Gruneberg, U., Novak, B., and Barr, F. A. (2013) The BEG (PP2A-B55/ENSA/Greatwall) pathway ensures cytokinesis follows chromosome separation. *Mol Cell* **52**, 393-405

128. Grallert, A., Boke, E., Hagting, A., Hodgson, B., Connolly, Y., Griffiths, J. R., Smith, D. L., Pines, J., and Hagan, I. M. (2015) A PP1-PP2A phosphatase relay controls mitotic progression. *Nature* **517**, 94-98
129. Geng, Y., Eaton, E. N., Picón, M., Roberts, J. M., Lundberg, A. S., Gifford, A., Sardet, C., and Weinberg, R. A. (1996) Regulation of cyclin E transcription by E2Fs and retinoblastoma protein. *Oncogene* **12**, 1173-1180
130. Tan, Y., Sun, D., Jiang, W., Klotz-Noack, K., Vashisht, A. A., Wohlschlegel, J., Widschwendter, M., and Spruck, C. (2014) PP2A-B55β antagonizes cyclin E1 proteolysis and promotes its dysregulation in cancer. *Cancer Res* **74**, 2006-2014
131. Tan, J., Lee, P. L., Li, Z., Jiang, X., Lim, Y. C., Hooi, S. C., and Yu, Q. (2010) B55β-associated PP2A complex controls PDK1-directed myc signaling and modulates rapamycin sensitivity in colorectal cancer. *Cancer Cell* **18**, 459-471
132. Mayr, D., Kanitz, V., Anderegg, B., Luthardt, B., Engel, J., Löhrs, U., Amann, G., and Diebold, J. (2006) Analysis of gene amplification and prognostic markers in ovarian cancer using comparative genomic hybridization for microarrays and immunohistochemical analysis for tissue microarrays. *Am J Clin Pathol* **126**, 101-109
133. Kuo, Y. C., Huang, K. Y., Yang, C. H., Yang, Y. S., Lee, W. Y., and Chiang, C. W. (2008) Regulation of phosphorylation of Thr-308 of Akt, cell proliferation, and survival by the B55alpha regulatory subunit targeting of the protein phosphatase 2A holoenzyme to Akt. *J Biol Chem* **283**, 1882-1892
134. Rundell, K., and Parakati, R. (2001) The role of the SV40 ST antigen in cell growth promotion and transformation. *Semin Cancer Biol* **11**, 5-13
135. Pallas, D. C., Shahrik, L. K., Martin, B. L., Jaspers, S., Miller, T. B., Brautigan, D. L., and Roberts, T. M. (1990) Polyoma small and middle T antigens and SV40 small t antigen form stable complexes with protein phosphatase 2A. *Cell* **60**, 167-176
136. Calin, G. A., di Iasio, M. G., Caprini, E., Vorechovsky, I., Natali, P. G., Sozzi, G., Croce, C. M., Barbanti-Brodano, G., Russo, G., and Negrini, M. (2000) Low frequency of alterations of the alpha (PPP2R1A) and beta (PPP2R1B) isoforms of the subunit A of the serine-threonine phosphatase 2A in human neoplasms. *Oncogene* **19**, 1191-1195
137. Wang, S. S., Esplin, E. D., Li, J. L., Huang, L., Gazdar, A., Minna, J., and Evans, G. A. (1998) Alterations of the PPP2R1B gene in human lung and colon cancer. *Science* **282**, 284-287
138. Chen, W., Arroyo, J. D., Timmons, J. C., Possemato, R., and Hahn, W. C. (2005) Cancer-associated PP2A Aalpha subunits induce functional haploinsufficiency and tumorigenicity. *Cancer Res* **65**, 8183-8192
139. Chang, C. H., Qiu, J., O'Sullivan, D., Buck, M. D., Noguchi, T., Curtis, J. D., Chen, Q., Gindin, M., Gubin, M. M., van der Windt, G. J., Tonc, E., Schreiber, R. D., Pearce, E. J., and Pearce, E. L. (2015) Metabolic Competition in the Tumor Microenvironment Is a Driver of Cancer Progression. *Cell* **162**, 1229-1241
140. Kerr, E. M., Gaude, E., Turrell, F. K., Frezza, C., and Martins, C. P. (2016) Mutant Kras copy number defines metabolic reprogramming and therapeutic susceptibilities. *Nature* **531**, 110-113
141. Hay, N. (2016) Reprogramming glucose metabolism in cancer: can it be exploited for cancer therapy? *Nat Rev Cancer* **16**, 635-649
142. Altman, B. J., Stine, Z. E., and Dang, C. V. (2016) From Krebs to clinic: glutamine metabolism to cancer therapy. *Nat Rev Cancer* **16**, 619-634

143. Röhrig, F., and Schulze, A. (2016) The multifaceted roles of fatty acid synthesis in cancer. *Nat Rev Cancer* **16**, 732-749
144. Locasale, J. W. (2013) Serine, glycine and one-carbon units: cancer metabolism in full circle. *Nat Rev Cancer* **13**, 572-583
145. Ying, H., Kimmelman, A. C., Lyssiotis, C. A., Hua, S., Chu, G. C., Fletcher-Sananikone, E., Locasale, J. W., Son, J., Zhang, H., Coloff, J. L., Yan, H., Wang, W., Chen, S., Viale, A., Zheng, H., Paik, J. H., Lim, C., Guimaraes, A. R., Martin, E. S., Chang, J., Hezel, A. F., Perry, S. R., Hu, J., Gan, B., Xiao, Y., Asara, J. M., Weissleder, R., Wang, Y. A., Chin, L., Cantley, L. C., and DePinho, R. A. (2012) Oncogenic Kras maintains pancreatic tumors through regulation of anabolic glucose metabolism. *Cell* **149**, 656-670
146. DeBerardinis, R. J., Mancuso, A., Daikhin, E., Nissim, I., Yudkoff, M., Wehrli, S., and Thompson, C. B. (2007) Beyond aerobic glycolysis: transformed cells can engage in glutamine metabolism that exceeds the requirement for protein and nucleotide synthesis. *Proc Natl Acad Sci U S A* **104**, 19345-19350
147. Yuneva, M., Zamboni, N., Oefner, P., Sachidanandam, R., and Lazebnik, Y. (2007) Deficiency in glutamine but not glucose induces MYC-dependent apoptosis in human cells. *J Cell Biol* **178**, 93-105
148. Handschin, C., and Spiegelman, B. M. (2006) Peroxisome proliferator-activated receptor gamma coactivator 1 coactivators, energy homeostasis, and metabolism. *Endocr Rev* **27**, 728-735
149. Hsieh, A. L., Walton, Z. E., Altman, B. J., Stine, Z. E., and Dang, C. V. (2015) MYC and metabolism on the path to cancer. *Semin Cell Dev Biol* **43**, 11-21
150. Stine, Z. E., Walton, Z. E., Altman, B. J., Hsieh, A. L., and Dang, C. V. (2015) MYC, Metabolism, and Cancer. *Cancer Discov* **5**, 1024-1039
151. Kishton, R. J., Barnes, C. E., Nichols, A. G., Cohen, S., Gerriets, V. A., Siska, P. J., Macintyre, A. N., Goraksha-Hicks, P., de Cubas, A. A., Liu, T., Warmoes, M. O., Abel, E. D., Yeoh, A. E., Gershon, T. R., Rathmell, W. K., Richards, K. L., Locasale, J. W., and Rathmell, J. C. (2016) AMPK Is Essential to Balance Glycolysis and Mitochondrial Metabolism to Control T-ALL Cell Stress and Survival. *Cell Metab* **23**, 649-662
152. Sundqvist, A., Bengoechea-Alonso, M. T., Ye, X., Lukiyanchuk, V., Jin, J., Harper, J. W., and Ericsson, J. (2005) Control of lipid metabolism by phosphorylation-dependent degradation of the SREBP family of transcription factors by SCF(Fbw7). *Cell Metab* **1**, 379-391
153. Tipping, M. E. (2001) Sparse Bayesian Learning and the Relevance Vector Machine. Journal of Machine Learning Research
154. Huang, d. W., Sherman, B. T., and Lempicki, R. A. (2009) Bioinformatics enrichment tools: paths toward the comprehensive functional analysis of large gene lists. *Nucleic Acids Res* **37**, 1-13
155. Huang, d. W., Sherman, B. T., and Lempicki, R. A. (2009) Systematic and integrative analysis of large gene lists using DAVID bioinformatics resources. *Nat Protoc* **4**, 44-57
156. Gonen, M., and Margolin, A. A. (2014) Kernelized Bayesian transfer learning. in *28th AAAI Conference on Artificial Intelligence 2014*, Quebec City, Canada
157. Langmead, B., Trapnell, C., Pop, M., and Salzberg, S. L. (2009) Ultrafast and memory-efficient alignment of short DNA sequences to the human genome. *Genome Biol* **10**, R25

158. Dai, Z., Sheridan, J. M., Gearing, L. J., Moore, D. L., Su, S., Wormald, S., Wilcox, S., O'Connor, L., Dickins, R. A., Blewitt, M. E., and Ritchie, M. E. (2014) edgeR: a versatile tool for the analysis of shRNA-seq and CRISPR-Cas9 genetic screens. *F1000Res* **3**, 95
159. Robinson, M. D., McCarthy, D. J., and Smyth, G. K. (2010) edgeR: a Bioconductor package for differential expression analysis of digital gene expression data. *Bioinformatics* **26**, 139-140
160. Landor, S. K., Mutvei, A. P., Mamaeva, V., Jin, S., Busk, M., Borra, R., Grönroos, T. J., Kronqvist, P., Lendahl, U., and Sahlgren, C. M. (2011) Hypo- and hyperactivated Notch signaling induce a glycolytic switch through distinct mechanisms. *Proc Natl Acad Sci U S A* **108**, 18814-18819
161. Shim, H., Dolde, C., Lewis, B. C., Wu, C. S., Dang, G., Jungmann, R. A., Dalla-Favera, R., and Dang, C. V. (1997) c-Myc transactivation of LDH-A: implications for tumor metabolism and growth. *Proc Natl Acad Sci U S A* **94**, 6658-6663
162. Possemato, R., Marks, K. M., Shaul, Y. D., Pacold, M. E., Kim, D., Birsoy, K., Sethumadhavan, S., Woo, H. K., Jang, H. G., Jha, A. K., Chen, W. W., Barrett, F. G., Stransky, N., Tsun, Z. Y., Cowley, G. S., Barretina, J., Kalaany, N. Y., Hsu, P. P., Ottina, K., Chan, A. M., Yuan, B., Garraway, L. A., Root, D. E., Mino-Kenudson, M., Brachtel, E. F., Driggers, E. M., and Sabatini, D. M. (2011) Functional genomics reveal that the serine synthesis pathway is essential in breast cancer. *Nature* **476**, 346-350
163. Locasale, J. W., Grassian, A. R., Melman, T., Lyssiotis, C. A., Mattaini, K. R., Bass, A. J., Heffron, G., Metallo, C. M., Muranen, T., Sharfi, H., Sasaki, A. T., Anastasiou, D., Mullarky, E., Vokes, N. I., Sasaki, M., Beroukhim, R., Stephanopoulos, G., Ligon, A. H., Meyerson, M., Richardson, A. L., Chin, L., Wagner, G., Asara, J. M., Brugge, J. S., Cantley, L. C., and Vander Heiden, M. G. (2011) Phosphoglycerate dehydrogenase diverts glycolytic flux and contributes to oncogenesis. *Nat Genet* **43**, 869-874
164. Kottakis, F., Nicolay, B. N., Roumane, A., Karnik, R., Gu, H., Nagle, J. M., Boukhali, M., Hayward, M. C., Li, Y. Y., Chen, T., Liesa, M., Hammerman, P. S., Wong, K. K., Hayes, D. N., Shirihai, O. S., Dyson, N. J., Haas, W., Meissner, A., and Bardeesy, N. (2016) LKB1 loss links serine metabolism to DNA methylation and tumorigenesis. *Nature*
165. Birsoy, K., Wang, T., Chen, W. W., Freinkman, E., Abu-Remaileh, M., and Sabatini, D. M. (2015) An Essential Role of the Mitochondrial Electron Transport Chain in Cell Proliferation Is to Enable Aspartate Synthesis. *Cell* **162**, 540-551
166. Sullivan, L. B., Gui, D. Y., Hosios, A. M., Bush, L. N., Freinkman, E., and Vander Heiden, M. G. (2015) Supporting Aspartate Biosynthesis Is an Essential Function of Respiration in Proliferating Cells. *Cell* **162**, 552-563
167. Toledo, C. M., Ding, Y., Hoellerbauer, P., Davis, R. J., Basom, R., Girard, E. J., Lee, E., Corrin, P., Hart, T., Bolouri, H., Davison, J., Zhang, Q., Hardcastle, J., Aronow, B. J., Plaisier, C. L., Baliga, N. S., Moffat, J., Lin, Q., Li, X. N., Nam, D. H., Lee, J., Pollard, S. M., Zhu, J., Delrow, J. J., Clurman, B. E., Olson, J. M., and Paddison, P. J. (2015) Genome-wide CRISPR-Cas9 Screens Reveal Loss of Redundancy between PKMYT1 and WEE1 in Glioblastoma Stem-like Cells. *Cell Rep* **13**, 2425-2439
168. Shalem, O., Sanjana, N. E., and Zhang, F. (2015) High-throughput functional genomics using CRISPR-Cas9. *Nat Rev Genet* **16**, 299-311
169. Evans, D. R., and Guy, H. I. (2004) Mammalian pyrimidine biosynthesis: fresh insights into an ancient pathway. *J Biol Chem* **279**, 33035-33038

170. White, R. M., Cech, J., Ratanasirintrawoot, S., Lin, C. Y., Rahl, P. B., Burke, C. J., Langdon, E., Tomlinson, M. L., Mosher, J., Kaufman, C., Chen, F., Long, H. K., Kramer, M., Datta, S., Neuberg, D., Granter, S., Young, R. A., Morrison, S., Wheeler, G. N., and Zon, L. I. (2011) DHODH modulates transcriptional elongation in the neural crest and melanoma. *Nature* **471**, 518-522
171. Sykes, D. B., Kfoury, Y. S., Mercier, F. E., Wawer, M. J., Law, J. M., Haynes, M. K., Lewis, T. A., Schajnovitz, A., Jain, E., Lee, D., Meyer, H., Pierce, K. A., Tolliday, N. J., Waller, A., Ferrara, S. J., Eheim, A. L., Stoeckigt, D., Maxcy, K. L., Cobert, J. M., Bachand, J., Szekely, B. A., Mukherjee, S., Sklar, L. A., Kotz, J. D., Clish, C. B., Sadreyev, R. I., Clemons, P. A., Janzer, A., Schreiber, S. L., and Scadden, D. T. (2016) Inhibition of Dihydroorotate Dehydrogenase Overcomes Differentiation Blockade in Acute Myeloid Leukemia. *Cell* **167**, 171-186.e115
172. Sharma, A., Janocha, A. J., Hill, B. T., Smith, M. R., Erzurum, S. C., and Almasan, A. (2014) Targeting mTORC1-mediated metabolic addiction overcomes fludarabine resistance in malignant B cells. *Mol Cancer Res* **12**, 1205-1215
173. Liu, Y. C., Li, F., Handler, J., Huang, C. R., Xiang, Y., Neretti, N., Sedivy, J. M., Zeller, K. I., and Dang, C. V. (2008) Global regulation of nucleotide biosynthetic genes by c-Myc. *PLoS One* **3**, e2722
174. Munier-Lehmann, H., Vidalain, P. O., Tangy, F., and Janin, Y. L. (2013) On dihydroorotate dehydrogenases and their inhibitors and uses. *J Med Chem* **56**, 3148-3167
175. Li, F., Wang, Y., Zeller, K. I., Potter, J. J., Wonsey, D. R., O'Donnell, K. A., Kim, J. W., Yustein, J. T., Lee, L. A., and Dang, C. V. (2005) Myc stimulates nuclearly encoded mitochondrial genes and mitochondrial biogenesis. *Mol Cell Biol* **25**, 6225-6234
176. Xu, J., Chi, F., Guo, T., Punj, V., Lee, W. N., French, S. W., and Tsukamoto, H. (2015) NOTCH reprograms mitochondrial metabolism for proinflammatory macrophage activation. *J Clin Invest* **125**, 1579-1590
177. Ji, S., Qin, Y., Liang, C., Huang, R., Shi, S., Liu, J., Jin, K., Liang, D., Xu, W., Zhang, B., Liu, L., Liu, C., Xu, J., Ni, Q., Chiao, P. J., Li, M., and Yu, X. (2016) FBW7 (F-box and WD Repeat Domain-Containing 7) Negatively Regulates Glucose Metabolism by Targeting the c-Myc/TXNIP (Thioredoxin-Binding Protein) Axis in Pancreatic Cancer. *Clin Cancer Res* **22**, 3950-3960
178. Zhao, X., Hirota, T., Han, X., Cho, H., Chong, L. W., Lamia, K., Liu, S., Atkins, A. R., Banayo, E., Liddle, C., Yu, R. T., Yates, J. R., Kay, S. A., Downes, M., and Evans, R. M. (2016) Circadian Amplitude Regulation via FBXW7-Targeted REV-ERBα Degradation. *Cell* **165**, 1644-1657
179. Sancho, P., Barneda, D., and Heeschen, C. (2016) Hallmarks of cancer stem cell metabolism. *Br J Cancer* **114**, 1305-1312
180. Vazquez, F., Lim, J. H., Chim, H., Bhalla, K., Girnun, G., Pierce, K., Clish, C. B., Granter, S. R., Widlund, H. R., Spiegelman, B. M., and Puigserver, P. (2013) PGC1α expression defines a subset of human melanoma tumors with increased mitochondrial capacity and resistance to oxidative stress. *Cancer Cell* **23**, 287-301
181. Salem, M. E., Hartley, M., Unger, K., and Marshall, J. L. (2016) Neoadjuvant Combined-Modality Therapy for Locally Advanced Rectal Cancer and Its Future Direction. *Oncology (Williston Park)* **30**, 546-562
182. Dobbelstein, M., and Sørensen, C. S. (2015) Exploiting replicative stress to treat cancer. *Nat Rev Drug Discov* **14**, 405-423

183. Takeishi, S., and Nakayama, K. I. (2014) Role of Fbxw7 in the maintenance of normal stem cells and cancer-initiating cells. *Br J Cancer* **111**, 1054-1059
184. Gilan, O., Diesch, J., Amalia, M., Jastrzebski, K., Chueh, A. C., Verrills, N. M., Pearson, R. B., Mariadason, J. M., Tulchinsky, E., Hannan, R. D., and Dhillon, A. S. (2015) PR55α-containing protein phosphatase 2A complexes promote cancer cell migration and invasion through regulation of AP-1 transcriptional activity. *Oncogene* **34**, 1333-1339
185. Jemal, A., Bray, F., Center, M. M., Ferlay, J., Ward, E., and Forman, D. (2011) Global cancer statistics. *CA Cancer J Clin* **61**, 69-90
186. Mullarky, E., Lucki, N. C., Beheshti Zavareh, R., Anglin, J. L., Gomes, A. P., Nicolay, B. N., Wong, J. C., Christen, S., Takahashi, H., Singh, P. K., Blenis, J., Warren, J. D., Fendt, S. M., Asara, J. M., DeNicola, G. M., Lyssiotis, C. A., Lairson, L. L., and Cantley, L. C. (2016) Identification of a small molecule inhibitor of 3-phosphoglycerate dehydrogenase to target serine biosynthesis in cancers. *Proc Natl Acad Sci U S A* **113**, 1778-1783
187. Pacold, M. E., Brimacombe, K. R., Chan, S. H., Rohde, J. M., Lewis, C. A., Swier, L. J., Possemato, R., Chen, W. W., Sullivan, L. B., Fiske, B. P., Cho, S., Freinkman, E., Birsoy, K., Abu-Remaileh, M., Shaul, Y. D., Liu, C. M., Zhou, M., Koh, M. J., Chung, H., Davidson, S. M., Luengo, A., Wang, A. Q., Xu, X., Yasgar, A., Liu, L., Rai, G., Westover, K. D., Vander Heiden, M. G., Shen, M., Gray, N. S., Boxer, M. B., and Sabatini, D. M. (2016) A PHGDH inhibitor reveals coordination of serine synthesis and one-carbon unit fate. *Nat Chem Biol* **12**, 452-458
188. Louis, P., Hold, G. L., and Flint, H. J. (2014) The gut microbiota, bacterial metabolites and colorectal cancer. *Nat Rev Microbiol* **12**, 661-672